# STRUCTURE-PROPERTY RELATIONSHIPS IN GAS-PHASE PROTONATED AND METALATED PEPTIDE IONS

A Dissertation

by

JAMES GARRETT SLATON

Submitted to the Office of Graduate Studies of
Texas A&M University
in partial fulfillment of the requirements for the degree of

DOCTOR OF PHILOSOPHY

May 2007

Major Subject: Chemistry

# STRUCTURE-PROPERTY RELATIONSHIPS IN GAS-PHASE PROTONATED AND METALATED PEPTIDE IONS

A Dissertation

by

JAMES GARRETT SLATON

Submitted to the Office of Graduate Studies
Texas A&M University
in partial fulfillment of the requirements for the degree of

DOCTOR OF PHILOSOPHY

Approved by:

| | |
|---|---|
| Chair of Committee, | David H. Russell |
| Committee Members, | Michael B. Hall |
| | Edward D. Harris |
| | Timothy R. Hughbanks |
| Head of Department, | David H. Russell |

May 2007

Major Subject: Chemistry

ABSTRACT

Structure-Property Relationships in Gas-Phase Protonated and Metalated Peptide Ions.

(May 2007)

James Garrett Slaton, B.S., Truman State University

Chair of Advisory Committee Dr. David H. Russell

Peptide synthesis and metal doping, combined with mass spectrometric and ion mobility spectrometric techniques, have provided a picture of the fragmentation behavior of a large field of homologous peptide ions, represented as XVGVAZG, where the X amino acid is either arginine, histidine, lysine, aspartic acid or tryptophan and the Z amino acid is proline, glycine, serine, or histidine. These homologous peptide ions have been carefully selected to probe the effects of charge site location and secondary interactions upon the fragmentation chemistry of peptides. Peptides were synthesized on solid support, doped with appropriate metal salts to attach $Li^+$, $Na^+$, $K^+$, $Cu^+$ and $Ag^+$, and then examined using ion mobility spectrometry, and tandem mass spectrometry, both high energy collision induced dissociation (CID) and photodissociation using 193-nm laser light. Molecular dynamics calculations enabled me to derive candidate structures for these ions that agree with the ion mobility data for the ions.

The fragmentation chemistry and structure selection of the first group of peptides, those that contain a proline residue, indicate that the presence of high proton and high metal ion affinity residues at the N-terminal position of the peptide direct the fragmentation of the highly charge-solvated ions according to a charge site directed

mechanism. Further examples of charge-solvated structures and charge-directed fragmentation are shown for peptides where the sixth amino acid residue has been replaced with glycine or serine, eliminating the influence of the proline residue in the sixth position. Photodissociation of the peptides indicates that the position of valine residues along the peptide backbone influences the types of abundant fragment ions observed and $a_i$ and $da_i$ ions are observed exclusively at the site of valine residues. This observation continued, even when the position of the valine residues were altered by synthesis, leading me to the conclusion that the fragmentation of these peptides. The study was expanded to include significantly more complex peptides, those containing second high proton and high metal ion affinity residues, and though the data are complex, the influence of charge solvation in those systems is strong as well, according to my analysis of the candidate structures obtained and the types of fragment ions observed.

# DEDICATION

I would like to dedicate this scientific work foremost to my parents and family. Their support and guidance have been the primary reasons why I am interested both in science and hard work. Without these twin interests, my chemistry graduate school experience would have been unpleasant. I would also like to dedicate my dissertation to my beautiful wife, Simona, without whom I would be lost and with whom I have the inspiration to write weighty sentences like this one.

# ACKNOWLEDGMENTS

I would like to thank my advisor, Professor David H. Russell, for providing an excellent environment for the study of molecules in the gas phase as well as making possible my attendance at scientific conferences. Also, I acknowledge The Laboratory for Biological Mass Spectrometry's numerous graduate students, postdocs, staff scientists and undergraduates, particularly Drs. Bill Russell and Kent Gillig and Brandon Ruotolo and Joseph Morgan, who contributed in measures both large and small to my success. Lisa M. Perez of the Laboratory for Molecular Simulation also provided support to my computational chemistry efforts. The Department of Energy, Division of Chemical Sciences, The Robert A. Welch Foundation, and the Texas A&M Supercomputing Center also generously funded a number of grants for photodissociation work, gas-phase ion studies, and supercomputer time, respectively. I would also like to acknowledge the tutelage of Professor F. A. Cotton, who taught me more about life than he did about chemistry, which is saying something.

TABLE OF CONTENTS

# LIST OF FIGURES

FIGURE Page

FIGURE Page

FIGURE Page

FIGURE Page

# LIST OF TABLES

# CHAPTER I

## INTRODUCTION

The mechanism of fragmentation for protonated and metalated gas-phase peptides is still under debate. The main unimolecular decay mechanisms that are proposed are charge-remote [1] and charge-local [2], which includes the mobile proton model. In the charge-remote case, the ionizing charge on the peptide is sequestered at one position, such as at the basic N-terminus or at the side chains of highly basic residues. In the charge-local case, protonation at a distribution of peptide backbone amide sites causes destabilization of the covalent bonds adjacent to the protonated amide carbonyl. Subsequent fragmentation occurs primarily through breakage of the amide bond to yield $b_i$- or $y_i$-type ions [3].

Much of the understanding of peptide ion fragmentation chemistry is based upon studies of tryptic peptides, i.e. those with R or K residues in the C-terminal position. There are many other types of peptides important in biological systems. These include products of proteolytic digests using other proteinases, such as chymotrypsin, Asp-N, Glu-C, or Lys-C [4-7]. In addition, naturally-occurring peptides are well studied in endocrinology [8,[9], the examination of non-ribosomal peptide synthesis [10,11], and the development of antibiotics [12,13].

---

This dissertation follows the style and format of the *Journal of the American Society for Mass Spectrometry*.

The work presented here is a direct comparison of the fragmentation patterns of a series of homologous peptides to which a series of six charge carriers ($H^+$, $Li^+$, $Na^+$, $K^+$, $Cu^+$ and $Ag^+$) are attached. This extends the previous studies of the effect of chemical modification upon the fragmentation chemistry of peptides, such as that from Keogh and co-workers [14] and Dikler et al. [15], and in particular, the charge derivatization study of Allison [16]. Our objectives are to 1) determine the location of the charge within the peptide ions, 2) assess differences in the fragmentation chemistry of the protonated and metalated peptides, 3) establish candidate structures which agree reasonably well with the empirical fragmentation and collision cross-section data and 4) draw comparisons to published data with regard to a fragmentation mechanism. It is our hypothesis that the fragmentation reactions of peptide ions are governed by 1) the location of the charge along the backbone of the peptide, 2) the chemical identity of that charge, and 3) the primary and secondary structures of the ions. In order to study this, we have developed a series of homologous peptides with affinities for metal ions at different locations along the peptide backbone.

In earlier work on cuprated peptide ions containing basic residues [17,18], a mechanism was presented for those cuprated species that follows a charge-local description of peptide fragmentation. Shields *et al.* claimed that the attachment of the $Cu^I$ displaces a proton, which then acts as the charge carrier, inducing fragmentation reactions throughout the peptide backbone [18]. Several systems were examined, though

these analytes were not homologous and ancillary factors related to the disparate peptide sequences may have contributed to the observed fragmentation chemistry.

VGVAPG was chosen as a scaffold upon which to begin our work because of its previous interest to the field [16-19] and its suitability for site replacement study. The peptide is ideal for this type of examination because 1) the size of the peptide is sufficient to yield meaningful information about peptide fragmentation chemistry, 2) the size of the peptide does not lead to prohibitive computational costs for the theoretical treatments necessary to understand the system, 3) the peptide does not possess additional side chain sites that would strongly affect the sequestration of the charge, and 4) it is non-tryptic so that understanding may be gained of other peptide ion types, such as those mentioned above.

The replacement of the internal residues of this peptide scaffold also yields significant utility in the study of gas-phase peptide ion fragmentation. These studies are part of a larger body of work within the mass spectrometric community aimed at elucidating the nature of gas-phase peptide ions for predictive power in terms of peptide mass fingerprinting and protein identification, as well as fundamental questions about the behavior of gas-phase polyfunctional ions, such as peptides and oligonucleotides. The replacement of internal residues in this series of peptides serves to isolate the effects of strongly-interacting residues such as arginine and aspartic acid (depending upon the adducted charge carrier) and the alteration of the secondary structure of the peptide ions, which can further affect the charge solvation and intramolecular interactions undergone

by the peptide ions. A systematic analysis of these factors is necessary owing to the complexity of the molecules studied.

Previous studies of the fragmentation chemistry of similar peptides have been carried out, but in many cases the similarity of the studied models was serendipitous rather than programmed. In one exemplary study from the Wysocki group, an homologous series of peptides was studied by surface-induced dissociation (SID). The similarity of fragmentation in the collisional activation cases and the surface-induced fragmentation is reasonable when viewed within the framework of the mobile proton model. Other interesting studies from Wysocki [20] have shown that in peptide ion systems with large charged derivatives, with lowest energy structures showing weak interaction with the peptide backbone, H/D exchange occurs to a small degree, suggesting that H/D exchange (and by extension, pre-fragmentation scrambling) can occur remote from the ionizing charge in a peptide.

In a recent communication by Harrison [21], it was shown that the sequence information of amidated peptide ion $[YAGFL\text{-}NH_2]^+$ was lost owing to the scrambling of sequence-informative fragments of the ion. In short, these systems are complex and more work is needed in order to understand the types of fragmentation processes at work based upon sequence, internal energy, charge carrier, activation method, and timescale of fragmentation. It is clear that additional work in this area is needed to develop a clearer understanding of factors that affect the fragmentation of peptide ions, in order to derive conclusions of the peptide sequence. Structural studies of peptides have been performed in order to better understand reactivity of these species.

Studies of native proteins/peptides in solution clearly illustrate that a delicate balance of multiple forces determines the secondary and tertiary structures of proteins/peptides. Forces such as those between the solvent and the protein/peptide as well as intra-molecular interactions such as hydrogen bonding, van der Waals interactions, hydrophobic forces and cation-π interactions have all been recognized for their key roles in determining protein/peptide structure. Perhaps the major factor influencing protein/peptide structure is the interaction between the protein/peptide and the solvent. Because structural characteristics of most intramolecular interactions in protein/peptide systems can be masked by solvent interactions, it is desirable to remove interactions of the solvent with the system. Gas-phase structural studies have the potential to further our understanding of the effects of intramolecular interactions on the conformation of protein/peptide systems due to the simplification already described, as well as the elimination of dynamic exchanges that these labile systems undergo in solution phase. The viability of ion mobility-mass spectrometry (IM-MS), a gas-phase technique, for the analysis of conserved structure for protonated peptides has been previously shown [22-24].

Numerous techniques may be applied in the study of the structure of peptides in condensed phases. The quality of x-ray diffraction crystallography for small molecules such as those presented here is typically low, due to the poor diffraction power of the first-row non-metals. Heavy atom methods may, of course be applied, as in the study of protein crystallography, but the throughput of those experiments is generally governed by factors such as the kinetics of the crystal formation and the availability of intense

light sources. In addition, the crystal structure of a protein may be considerably different from the structure of the same protein in solution phase, particularly if it is part of some functional assembly of numerous distinct proteins, though this is true of other techniques as well.

In addition, optical techniques such as circular dichroism (CD) spectroscopy is useful in the characterization of solution-phase peptide structure. The secondary structures of α-helices and β-hairpins give distinct signatures at 208/222 and 215 nm, respectively. Measurements of the CD behavior of peptides under different solvation conditions, from well-solvated to poorly-solvated can give an indication of the gas-phase (un-solvated) behavior of a peptide sequence.

Nuclear Magnetic Resonance (NMR) spectroscopy can give abundant and detailed information on the structures of condensed-phase samples, including adjacent functional groups and the strength of interactions between local nuclei, e.g. protons in an H-bonding array. 2-Dimensional $^{1}$H-NMR techniques have provided a wealth of information regarding the structures of biomolecules, particularly those which do not form good crystalline arrays or are not good targets for crystallography, i.e. those with functional forms that are either well-solvated or are docked with a reaction partner. An encouraging factor regarding NMR spectroscopy is the applicability of the technique to solid-phase samples as well, so in principle detailed studies regarding the structural evolution of a species upon dissolution may be carried out.

A useful technique in the mass spectrometric analysis of structure is Hydrogen/Deuterium (H/D) isotope exchange, either in solution or the gas phase. It can

be used as a titration of the exchangeable sites on the surface of a biomolecule. If the extent of H/D exchange is small, then the change in analyte mass is also small, and there are few exchangeable hydrogen atoms in the structure of the biomolecule. This can be used to gauge the openness or compactness of a particular specie. The technique may also be carried out in the gas-phase, by the introduction of a deuterated reagent gas to a population of the gas-phase analyte. After some reaction time, changes in the isotope envelope of the ion give the same type of information about available reactive sites, with the added data on the kinetics of the exchanges, useful for the analysis of the relative reactivity of the exchange sites, and potentially the structural dynamics of the analyte ion.

In addition to the methods already described, tandem mass spectrometry gives information regarding the structure of ions in the gas phase. The fragmentation patterns of peptides in particular are useful in the determination of the identity of the ion, and are used extensively in that capacity. The other main gas-phase structural technique used in the characterization of species is ion mobility (IM) spectrometry. Ion mobility-mass spectrometry (IM-MS) can be used to investigate the structure or conformation of gas-phase biomolecules and the data can be combined with molecular modeling (MM) data to determine peptide/protein 2° structural motifs and the stabilization of charge [23-26].

Metal ions play important roles in many biological systems (enzymes, protein shuttles, ion channels and chaperones). There are many examples, such as the $K^+$-ion channel is a structure formed of a peptide sequence rich in tyrosine residues [27]. The size-selectivity of the channel (discrimination between $Na^+$ and $K^+$ and other species) is

attributed to the level of interaction of ions passing through the channel with the amino acid residues that comprise it. The interactions between the cations and the ion channel may be studied from the behavior of model systems in the absence of solvent (i.e. in gas-phase ion mobility measurements). The large body of work in the area of metals in biology will not be delved into here, aside from the mention of one relevant system.

Elastin proteins, which form a significant portion of the connective tissues of mammals, have sequence homology in the main chain across several species. This is particularly so for the bovine, human and porcine forms, where the same peptide sequence (VGVAPG) repeats 2, 6, and 6 times, respectively [28-30]. The prevalence of that particular sequence indicates its importance in imparting the secondary structure (a putative helix) to that domain of the protein. Variants of this peptide have been chosen as model compounds of this structure. This model compound also has similarity to the copper-binding site of human β-2-microglobulin [31], a protein indicated in the formation of amyloid deposits in joints that occurs during kidney dialysis treatment [32,33]. Mass spectrometry has been used to determine metal ion binding sites [34], but the types of information available from gas-phase IM measurements give added dimensionality, as has been demonstrated [23-25]. In this report, modeling results (e.g. total energy, closeness of approach for non-covalent interactions, cross-sectional area) are compared with empirical values determined by IM-MS, gas-phase H/D exchange, and tandem MS experiments for both small (tyrosine-containing tripeptides) and large (aspartic acid- and arginine-containing septapeptides) systems.

The use of mass spectrometry in the analysis of biologically relevant species, including oligonucleotides, proteins, peptides, lipids and carbohydrates, was once very difficult. Electron ionization (EI) and chemical ionization (CI) were both used to produce telltale ions from volatilized biomolecules, but were limited to a mass of 1000 molecular weight due to volatility and thermal lability issues. These "hard" ionization techniques produced high fragment ion abundances and low abundances of the molecular or pseudomolecular ions peaks for the species studied, which could make identification difficult. For large biomolecules, this was a severe limitation. Analysis of thermally labile species has been aided a great deal by the development of soft ionization techniques such as electrospray ionization (ESI), fast-atom bombardment (FAB) and matrix-assisted laser desorption/ionization (MALDI). The development of what are termed "soft" ionization techniques has led to the use of mass spectrometric methods being used prominently in protein identification.

**Preparations**

The preparation of the analytes examined in this study consisted of assembling the primary sequence of the peptide, followed by doping and the generation of the ions using MALDI. The syntheses of all peptide species, listed here:

| | | | |
|---|---|---|---|
| RVGVAPG, **1** | RVGVAGG, **5** | KVGVAGG, **9** | HVGVAHG, **13** |
| HVGVAPG, **2** | RVGVASG, **6** | KVGVASG, **10** | KVGVAHG, **14** |
| KVGVAPG, **3** | HVGVAGG, **7** | RAVGVGG, **11** | WVGVAHG, **15** |
| DVGVAPG, **4** | HVGVASG, **8** | RVGVAHG. **12** | |

were carried out using solid-phase methods and fluorenyl-9-methoxycarbonyl (Fmoc) protecting group chemistry. In detail, the resin selected was polystyrene-based 2-chlortrityl chloride, mesh size 100 μm, with a total resin loading of 0.3 mmol $g^{-1}$ (Advanced Chemtech, Louisville, KY, USA). Prior to the use of each sample of resin, the material was swelled in a mixture of solvents. Without the swelling step, the reactivity of the resin is exceedingly low. Care must be taken to eliminate all water from the initial coupling step, as water will react readily and irreversibly with the trityl functional group. The swelled resin was then immersed in a freshly-prepared solution of the C-terminal Fmoc amino acid, in a 1:1 molar ratio with the resin active sites, with the added reagents O-benzotriazole-N,N,N′,N′-tetramethyluronium hexafluorophosphate (HBTU) to activate the incoming residue by the formation of an active ester and 1-hydroxybenzotriazole hydrate ($HOBt \cdot H_2O$) to suppress racemization of susceptible residues. After sufficient time for the coupling of the amino acid residue (ca. 5 h), the resin was drained and rinsed with 5 volumes of dimethyl formamide (DMF) and 5 volumes of dichloromethane (DCM).

At this stage of the synthesis, a Kaiser test would be meaningless, so none is performed. The resin sites that remain after the coupling are then capped first by suspending the resin in a 19:1 (vol.) mixture of dichloromethane:methanol for 30 minutes, then by suspension of the resin in pure methanol for 30 minutes. The capping procedure is applied to decrease the likelihood of side reactions, important to maintain the highest possible purity. The resin is then rinsed with 5 volumes of DMF and drained.

Next, the removal of the Fmoc group from the growing chain is performed with the immersion of the beads in a solution of 20% piperidine in DMF, which was carried out a total of 4-5 times, each lasting 10 minutes until the Kaiser test for the presence of a primary amine was positive (yielded a strong blue color). Note that for some residues, such as histidine, the color change for a Kaiser test is sometimes wine-colored or even red. The test is performed by extracting an aliquot of beads (kept small to keep the overall yield high) and adding to them a few drops each of the following reagents. Reagent A is a mixture of 2% (vol.) 1 mM KCN in pyridine, Reagent B is 80% (vol.) liquefied phenol in ethanol and Reagent C is 5% (vol.) ninhydrin in ethanol. The test is developed by heating to roughly 130 °C for 5-20 minutes, depending upon the length and the identity of sequence of the growing peptide. The same test is performed in order to establish that the coupling of a fresh Fmoc amino acid is complete.

Couplings to a peptide are carried out under more forcing conditions, in which the incoming carboxylic acid (4 equivalents) is activated by HBTU (4 equivalents), and 10 equivalents of diisopropylethylamine (DIPEA). The incoming acid, $HOBt \cdot H_2O$, and HBTU are dissolved in a mixture of DCM and DMF. After the reagents dissolve, DIPEA is added; the mixture is quickly and thoroughly mixed and then introduced into the reaction flask. The beads are then agitated gently to ensure good mixing.

After the initial capping of trityl chloride sites with methanol, the capping step is performed using a 1:1 mixture of acetic anhydride and pyridine. This prevents deletion errors in the growing peptide which can often necessitate lengthy separations steps to

remove due to their similar sequence to the target peptide. Typically the coupling step is performed once for every few residues, rather than once per residue.

Once the primary sequence of the peptide is present on the beads, the deprotection of each amino acid residue is preformed. As Fmoc chemistry is acid labile and base-inert, the protecting groups which are used in the synthesis of polypeptides are acid-labile to ease their use. The pentamethylchroman substituent for arginine, trityl for histidine, n-butyl for serine, etc., are all cleaved as is the peptide, upon treatment with 95:2.5:2.5 trifluoroacetic acid(TFA):water:triisopropylsilane (TIS). For the oxidation-sensitive residue, tryptophan, the cleavage cocktail was changed to 88:5:5:2 TFA:dithiothreitol(DTT):water:TIS, which must be used immediately after preparation, as insoluble material begins to form rapidly and the efficacy of the reagent begins to fail. The DTT serves as a reducing agent for the Trp residue, and is washed away with the rest of the cleavage reagent.

The oil that is formed from the cleavage of the peptide from the resin is highly acidic and strongly yellow. Caution must be used in handling the oil. Collection of the material is done by copious rinsing, first with small volumes of TFA and then with small volumes of dichloromethane. The resin, which darkens to a purple color during the cleavage step, is rinsed with dichloromethane until the resin color disappears. The product oil is then concentrated to dryness and triturated from diethyl ether with a single drop of methanol. The precipitated peptide is then washed twice more with cold diethyl ether and dried prior to lyopholysis in water. Lyopholysis produces a highly flocculent white powder which is easily collected and is of high purity.

**Measurements**

The identity and purity of each peptide is checked by analysis using the Applied Biosystems DE-STR MALDI-time-of-flight (TOF) mass spectrometer. The peptide solutions are combined with methanolic solutions of the MALDI matrix, α-cyano-4-hydroxycinnamic acid in a roughly 1000:1 matrix:analyte ratio. 1 μL Aliquots of the sample mixtures are spotted onto a MALDI sample plate and dried under forced, heated air before introduction into the mass spectrometer.

The instrument is equipped with a delayed-extraction source and has a high-mass capability of roughly 3000 m/z in reflected mode and theoretically unlimited in linear mode. The instrument routinely (with internal calibration) achieves mass measurement accuracy in the single ppm range and resolution of 15000, which is more than sufficient for the clear identification of the peptide analytes and the observation of detectable impurities.

To prepare the metalated peptide ions, aqueous solutions of the peptide ions are incubated with solutions of the appropriate salts. For the cuprated salts, 1 mg $ml^{-1}$ aqueous peptide solution is combined in equal measure with 20 mM $Cu_2SO_4$ (aq) and allowed to stand at room temperature for 30 minutes. "Blank" or un-metalated peptides are treated with an equal volume of distilled, deionized water to ensure that the final concentration of peptide is the same in each case. From this point, the sample preparation is the same as for the confirmatory analyses.

After the confirmation of the peptide identity and the assessment of the sample purity, the tandem mass spectrometry of the peptides is performed in order to understand

the unimolecular reactivity of the ions. The Applied Biosystems Model 4700 Proteomics Analyzer (ABM 4700) is a tandem time-of-flight (TOF-TOF) instrument with a collision cell between the two mass analyzers. An ion of interest is selected in the first TOF and activated in the collision cell. Collision-induced dissociation is a very widespread method for activating ions in the gas-phase to observe the fragments of the ions to obtain more mass information about the analytes. The fragments of that ion are then analyzed in the second TOF region and detected. The nomenclature for peptide fragment ions is well-established and the scheme followed here is that established by Roepstorff and Fohlman [3] as modified by Biemann [35], with the addition of "+ metal" to indicate that a particular fragment is metal-bearing, *ex*. $[b_3 + Na]^+$. The types of peptide fragment ions discussed here are shown in Figure 1.

The ABM 4700 is an outstanding instrument for the analysis of proteomics samples, that is: protonated peptide ions. It has been designed with high throughput proteomics analyses in mind rather than investigations of the chemistry of metalated peptide ions. It has a permanent low mass cutoff of 69 daltons, which is higher than the mass of any of the metal ions used in this study, with the exception of $Ag^+$.

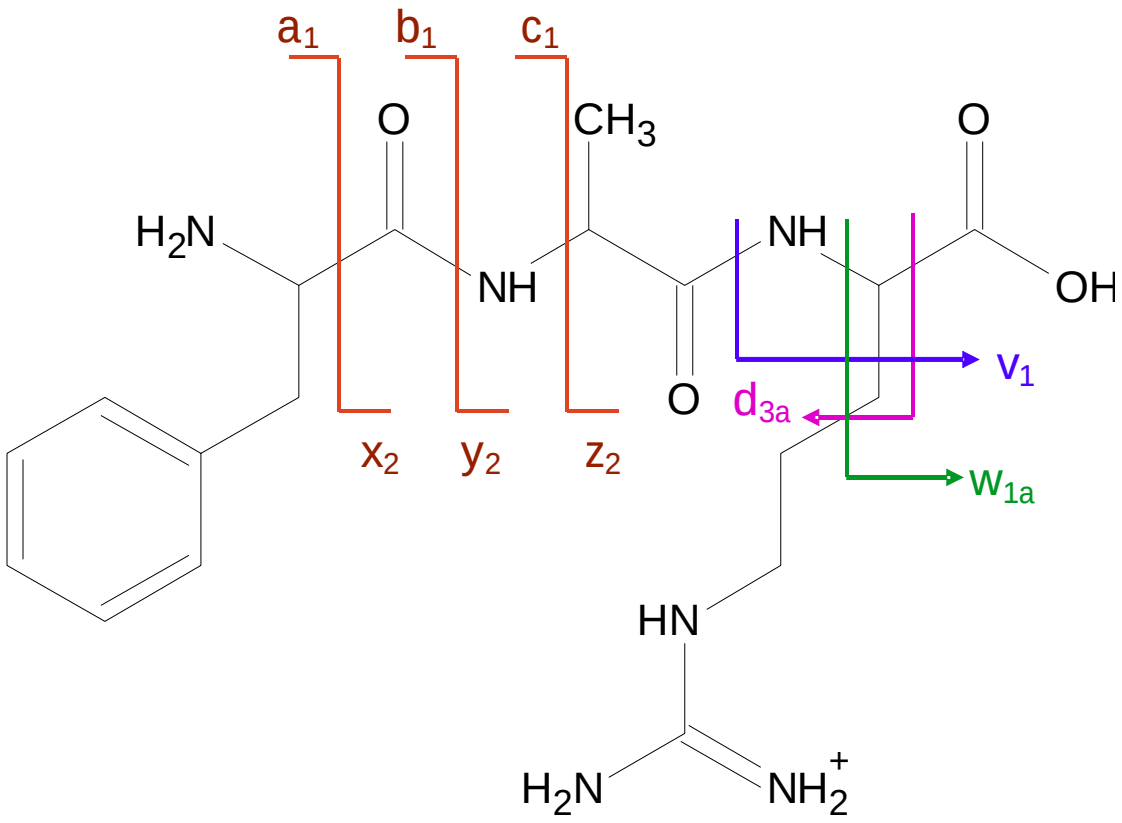


**Figure 1**. Nomenclature for peptide fragment ions, using $[FAR+H]^+$ as an example. Fragment ions are shown with arrows depicting the location of the charge of the fragment ion. Sequence informative ions corresponding to backbone cleavages are shown in red, whereas side chain loss ions are in other colors.

In fragmentation experiments performed on the ABM 4700 of some alkali-metalated ions, fragments corresponding to the protonated species were observed, which was puzzling. To determine the origin of these fragments, another type of experiment was conducted to compare the fragmentation of metalated and protonated peptide ions using a triple-quadrupole mass spectrometer.

The MDS Sciex QSTAR Pulstar was used to study the fragmentation chemistry of protonated and metalated ions, $[RVGVAPG+H]^+$ and $[RVGVAPG+Na]^+$ for a precursor ions scan. The two ions were prepared from the same solution, owing to the large amount of adventitious sodium present in laboratory solvents, reagents and glassware. 15 sequence-informative fragments were examined by a precursor ion scan, where the detection quadrupole is set to analyze for the fragment ion of interest and the selection quadrupole is scanned through a range of m/z. When a signal is read, it clearly establishes the identity of the parent ion of a particular fragment. In no case were there two different parent ions that yielded the same fragment, i.e. $[M+H]^+$ and $[M+Na]^+$ fragmenting to yield the same ion.

In addition to collision-induced dissociation, which is used to activate ions in both of the previously-described instruments, photodissociation was also used. This technique differs significantly from CID, in that there is no gas collision or corresponding transfer of momentum to the analyte of interest, but rather absorption of a high-energy photon (213 nm, 646 eV). This wavelength of light is well-suited to the study of peptide ions, as the amide bonds present in the peptide backbone absorb well at that wavelength, as well as the tryptophan and phenylalanine side chains, and to a lesser

extent, the arginine side chain. The ions are generated in a MALDI experiment and directed to an observation cell, where a pulse of 213 nm light irradiates the ion packet. Post-activation, the precursor ion dissociates and the fragments are analyzed in a second TOF mass spectrometer and detected. This experiment will be discussed in more detail in Chapter III.

The mass spectrometry of these peptide ions yields information about the mass of the precursor ions and what fragments they produce, but only limited information about the structures of the ions in the gas phase, Ion mobility has been used to characterize ions in the gas phase for a long time, and it has a very strong theoretical footing. The technique of ion mobility spectrometry is also known by other names, such as plasma chromatography. There is no partitioning occurring in ion mobility, however, which makes that description a misnomer. From first principles, the gas-phase mobility of an ion is governed by a number of external factors, such as the field acting on the ion, (voltage, E, divided by length, L ), the temperature and pressure of the separation medium (T, P), the mass ($m_g$) and number density ($N_0$)of the separation medium. Internal factors affecting the mobility of ions are the mass ($m_i$) and charge (z) of the analyte, the rotationally-averaged cross-sectional area of the ion and strength of the interaction of the analyte and the separation medium, which are the kinds of information we want. The relationship between these quantities can be better shown in the Equation 1, shown below. The relation has been arranged in terms of the most useful quantity, the thermally-averaged cross-section, $\Omega_{(1,1)}$, which gives us a way to analyze the structures of the intact species in the gas phase by measuring the drift time of the ion, $t_d$.

(1) $$\Omega_{(1,1)} = \frac{(18\pi)^{1/2}}{16}\frac{ze}{k_B T}\left[\frac{1}{m_i}+\frac{1}{m_g}\right]^{1/2}\frac{t_d E}{L}\frac{760}{P}\frac{T}{273.15}\frac{1}{N_0}$$

For a more thorough discussion of ion mobility theory, see the works of Mason and McDaniel [36,37].

In our laboratory was developed a new type of drift cell which does not have a linear field acting on the ions in the mobility cell. The field is a combination of linear and periodic fields which give a net focusing of the ions transiting through the cell relative to a purely linear field. The periodic component acts on the ions in the packet, inducing motion that alternates between focusing and defocusing the ions.

**Theoretical Treatment**

The data from the ion mobility measurements are used to identify each ion of interest and the collision cross-section for those ions. To get further information for the peptides, a theoretical analysis of the structures of the peptides mush be performed. The conformation of the peptide ions is assessed by a comparative method. Reasonable starting structures for the peptide ions of interest are generated using first the program InsightII (Accelrys, San Diego, CA, USA). Insight$^{II}$ has a biomolecule builder function which allows one to give a peptide any secondary structural elements that are desired. The secondary structures that are most prevalent in peptides, especially those based upon the elastin repeat unit VGVAPG are α-helical or β-strands/turns. These two secondary

structures as well as globular ones (somewhat ad hoc H-bonding structure) were generated in Insight$^{II}$.

The biopolymer builder in Insight$^{II}$ is quite useful, but it introduces errors at the termini of polypeptides because it is a biopolymer builder, not a peptide ion builder. The termini are corrected to be amine and carboxylate rather than amide and aldehyde in Cerius$^{II}$ (Accelrys, San Diego, CA, USA ). Additionally, the charge location and identity can be altered in this program, which is necessary to cover as much of the chemically-reasonable isomer and conformer space as possible. The last function of import in the generation of the ion models is the application of a force field to the ions in order that they might be further processed. The force field CFF 1.02 (described below) is loaded and each atom in the structure is given an appropriate set of parameters for use of the force field. After the atom parameterization, the ion is processed by a simulated annealing algorithm in order to reach a low energy conformation.

The force field used in this work is CFF 1.02. It is a Class 2 Force Field, which means that it has parameters for the atoms in the field that have been compared with empirical data from a number of methods, like X-ray crystallography, IR spectroscopy and $^{1}$H-NMR measurements in order to correct bond distances and angles for atoms in a wide variety of bonding modes and types of molecules. The force field calculations are semi-empirical, rather than simply molecular mechanics methods.

The development of Class II force fields began with the consistent force field, and led to more well-known fields such as Amber and CHARMM. Though the number of available force fields has grown, the force field selected for our work is CFF 1.02

force field because it has demonstrated significant utility in the analysis of peptide ions in the past. In addition, we had some familiarity with the field based upon prior work by the Russell Group and we had access to two licenses for the field, so expense was also an issue. It was chosen to handle the most important part of the theoretical processing of the peptide ions: the simulated annealing.

Simulated annealing is needed to overcome the strong intramolecular interactions present in a peptide ion. In vacuum, the solvation interactions between a peptide ion and its solvent dominate, but in the gas phase, there are not solvent molecules, so the peptide ion develops a series of intramolecular contacts in order to lower the overall energy of the system and to solvate the charges, such as ammonium, guanidinium or imidazolium groups and metal ions.

Simulated annealing is a computational method by which the temperature of a species is quickly ramped up and down to give sufficient energy to surmount small barriers to reorganization within the molecule, which may prevent the system from reaching a lowest energy conformation. This is particularly useful in the analysis of peptides, as they have quite-strong intramolecular interactions to overcome, such as salt bridges, cation-$\pi$ interactions, and arrays of hydrogen bonds.

To be certain that the energetics of the systems are reasonable, the simulated annealing runs for every ion were repeated and the results of each run compared. In more that 95% of the cases, the characteristics (average energy, standard deviation of the energy, etc.) of the two runs were highly reproducible and the decrease in potential energy was smooth over the course of the simulated annealing. For the remaining less

than 5%, the reproducibility of the two runs was low, and there was a significant and abrupt drop in overall energy of the system in one of the simulated annealing courses, which seems to indicate a barrier being overcome. For those species, an additional simulated annealing course was performed until the energy of the ions decreased smoothly and reproducibly during the simulated annealing course. For more detail on the simulated annealing of these ions, see Appendix A.

The free program MOBCAL [38,39], takes the Cartesian coordinates of the atoms in a structure and simulates the collision of a gas atom with that structure 10,000 time to determine an average value of the cross section, which estimates the collision cross-section value for that ion. The program was primarily designed to handle simple organics, so additional atomic parameters for K and Cu were added to the program libraries to accommodate my research. The program was used to analyze test structures generated through the simulated annealing process.

The selection of candidate structures is performed by plotting the calculated collision cross section and the total calculated enthalpy for each structure in and using the experimental cross section values as a selection criterion. The other selection criteria applied are whether the candidate structure, in the case of metalated ions particularly, displays IM contacts between the metal ion functional groups belonging to the residue with which it forms the most preferential interaction. Whether the structure makes good chemical sense is also assessed. Often, there are numerous structures that are present in the area of the plot that fits the measured values within uncertainty. The lowest energy

structures that are found to pass all checks are analyzed and a consensus structure is chosen. For more details on the selection of candidate structures, see Appendix B.

How do the candidate structures for the peptide ions relate to the fragmentation behavior of the peptide ions? The effects of primary structure on fragmentation have been well-studied. Effects of the presence of proline, or residues with extremes of proton affinity at the termini or along the peptide backbone, have been studied. As for the effects of secondary structure and intramolecular forces, this is less well understood, though work from Glish, Beauchamp, Gaskell, and Wysocki [40-42] have sought to further our understanding of these influences on fragmentation. Understanding the relationships between the structures of peptide ions, both protonated and metalated, upon the fragment ions one ultimately derives from the activated ions is the crux of the work presented here, with the peptide sequences and charge carriers carefully chosen to attempt to understand these effects in a systematic way.

# CHAPTER II

# FACTORS AFFECTING GAS-PHASE PEPTIDE ION FRAGMENTATION: N-TERMINAL RESIDUE, CHARGE CARRIER, AND CONFORMATION

## Introduction

The chemistry of gas-phase peptide ions is an active area of mass spectrometry research [43-46], ranging in scope from studies of the unimolecular dissociation reactions of protonated ions ($[M+H]^+$), to the binding sites and bond energies of metal ions to peptides [17,18,47], to intramolecular (IM) interactions (2°/3° structure) and how such interactions influence chemistry [24,48,49]. The main unimolecular decay mechanisms that have been proposed to describe peptide ion fragmentation chemistry include both charge-remote [1] and charge-directed [2] fragmentation, which includes the mobile proton model [50]. Charge-remote fragmentation is important when the ionizing charge on the peptide is sequestered to an isolated region of the peptide, such as at the basic N-terminus or at the side chains of highly basic (R, K and H) residues [18,47]. On the other hand, charge-directed fragmentation is the result of charge delocalization over the peptide backbone amide sites which weakens the amide bond and fragmentation occurs primarily through breakage of the amide bond to yield $b_i$- or $y_i$-type ions [3,50].

Much of our understanding of peptide ion fragmentation chemistry is based upon studies of tryptic peptides, *i.e.* peptides with R or K residues in the C-terminal position; however, there are many important non-tryptic biological peptides, which include

products of proteolytic digests using other proteases, such as chymotrypsin, Asp-N, Glu-C, or Lys-C [4-7], and naturally-occurring peptides important in endocrinology [8,9], insect peptidomics [51,52], non-ribosomal peptide synthesis [10,11], and peptide antibiotics [12,13].

We present a comparison of the fragmentation patterns of a series of homologous non-tryptic peptides to which five different charge carriers ($H^+$, $Li^+$, $Na^+$, $K^+$, and $Cu^+$) are attached. We also use ion mobility-mass spectrometry to determine the collision cross-sections of the ions and semi-empirical molecular dynamics simulations to derive plausible ion conformations based on the cross-sections. To restate from the Introduction, our objectives in this work are to: 1) determine the location of the charge within the peptide ions, 2) assess differences in the fragmentation chemistry owing to differences in the charge carrier, 3) establish candidate structures which agree with the empirical fragmentation and collision cross-section data, and 4) evaluate the role of charge-remote fragmentation reactions for these systems. Our hypothesis is that the fragmentation reactions of peptide ions are governed by: 1) the location of the charge along the backbone of the peptide, 2) the relative binding energies of the charge carrier to the peptide, and 3) the 2°/3° structures (IM interactions, including charge solvation) of the ions. To facilitate these studies, we have synthesized a series of homologous peptides with amino acids having known metal ion affinities at specific sites within the peptides.

The peptide sequence VGVAPG is a flexible scaffold with which to probe several effects on peptide fragmentation. This scaffold is desirable because: 1) the size of the

peptide is sufficient to yield meaningful information about peptide fragmentation chemistry, 2) the peptide is in the size range that can be examined in-depth using computational methods to better understand the system, 3) the peptide does not possess additional polar functional groups that would strongly affect the sequestration of the charge, and 4) it is non-tryptic so that understanding may be gained of other less-studied peptide ion types.

This extends our previous studies of the effects of chemical modification upon the fragmentation chemistry of peptides [15,53], as well as that from Keogh [14], Cotter [54], and in particular the phosphonium acetyl charge-derivatization studies of Allison [16]. Allison suggested that attachment of a phosphonium acetyl charge derivative promotes remote-site fragmentation. Macfarlane also suggested that metal-cationized peptides dissociate via charge-remote reactions [55], however we prefer to describe the fragmentation in terms of charge-localized reactions [17,18]. For example, on the basis of experimental and computational studies, we suggested that attachment of the $Cu^+$ to peptides containing Arg, Lys, and His residues can displace a proton, which mobilizes, inducing fragmentation reactions involving bond cleavage at various sites along the peptide backbone [18].

**Experimental**

The peptides used for these studies were all synthesized using standard peptide synthesis techniques. All syntheses and the cation-doping procedures were carried out in clean glassware or in single-use plastic ware. Water was obtained from a Barnstead Nanopure Model 4741 filtration system (Dubuque, Iowa, USA) and other solvents were

obtained from EM Science (Gibbstown, New Jersey, USA). HPLC-grade dichloromethane, ether and methanol were distilled in glass over appropriate drying agents and stored over freshly-activated 4-Å molecular sieves. HPLC-grade DMF was distilled under reduced pressure, stored over activated 4-Å molecular sieves, and degassed immediately before use. α-Cyano-4-hydroxycinnamic acid (Aldrich, Milwaukee, Wisconsin, USA) was recrystallized twice from hot methanol. Other materials were from recognized commercial sources and were used as received.

Peptides were prepared using Fmoc chemistry on 2-chlorotrityl chloride resin (Novabiochem, San Diego, California, USA) and were purified using serial precipitation from ether and lyopholysis. The identity and purity of each peptide was confirmed by MALDI-TOF-MS before other analyses were done. Peptides were metalated by incubating the peptides at 1 mg $mL^{-1}$ concentration in a 1:1 (v:v) ratio with 20-mM aqueous (for $CuSO_4$) or saturated methanolic (for $Li_2CO_3$, $Na_2CO_3$, or $K_2CO_3$) solutions for 30 minutes. For copper, this yielded a dopant-to-analyte concentration ratio of roughly 15. Then, the peptide/dopant solutions were combined with 30 mg $mL^{-1}$ α-cyano-4-hydroxycinnamic acid in MeOH which yielded a matrix-to-analyte ratio of *ca*. 1000. Each sample was prepared with approximately 150 pmol of analyte, mixed thoroughly and spotted onto a MALDI plate for analysis.

Tandem mass spectra were acquired in positive ion mode using a Model 4700 Proteomics Analyzer (Applied Biosystems, Framingham, Massachusetts, USA). The CID acceleration was 1 kV and the collision gas was atmosphere. The mass spectra obtained in these experiments were first handled using Data Explorer™, histogrammed

using Microsoft Excel™, and imported into PSI-Plot™ for 3-dimensional visualization. Fragment ions are labeled using nomenclature suggested by Roepstorff and Fohlman [3] as modified by Biemann [35]. The peptide-metal ion adducts are labeled with the addition of "+ metal" to indicate that a fragment ion is metal-bearing, (e.g. $[b_3+\text{Na-H}]^+$).

Measurements of the gas-phase collision cross-sections for $[M+H]^+$, $[M+Na]^+$ and $[M+Cu]^+$ ions were performed using methods previously described [[24]]. Briefly, the ions were generated by MALDI using a high-repetition rate frequency-tripled Nd:YAG laser (355 nm, JDS Uniphase, San Jose, California, USA) operated at 200 Hz. The ions entered a series of concentric ring electrodes which guided the ions through a 30.5 cm mobility cell operated at roughly 1 torr of helium via an applied periodic focusing field [56]. After exiting the mobility cell, the ions entered a differential-pumping region where they were focused into a plane. The ions then passed into a high-vacuum chamber where they were pulsed into an orthogonal two-stage reflectron time-of-flight mass analyzer and detected.

Candidate structures were generated using Insight$^{II}$ and Cerius$^2$ (Accelrys, San Diego, California, USA) [57,58] followed by two stages of simulated annealing in the CFF 1.02 force field [59] of each starting structure. The simulated-annealing algorithm applied a stepwise temperature program from 300 to 1000 K and back over a period of 280 ps. Three hundred ramp/relaxation cycles were made, with the resultant structures retained for further analysis. The results of the first and second simulated annealing runs for each structure were compared for consistency. 95% of the structures examined from the first two runs produced structure populations with potential energies within one

standard deviation (0.6 kcal $mol^{-1}$), while the remaining *ca*. 5% were reannealed and the energy differences between cycles dropped to within one standard deviation, which indicated convergence to low energy structures.

Calculations of the collision cross-sections were done using a modified version of MOBCAL, a Cartesian coordinate cross-section averaging program developed by Jarrold [38], with an expanded atomic parameter list. Dynamics simulation and the collision cross section calculation output were examined in cluster plot form and candidate structures were selected on the basis of their agreement with experiment and their low potential energy. Models for the cuprated ions were generated as the neutral peptide with a $Cu^{2+}$ ion attached, as the $Cu^{+}$ ion is not parameterized in the CFF 1.02 force field. The copper ions were typed as the $Cu^{2+}$ ion, and their charge was explicitly set to $1^{+}$. Dynamics simulations were run also using the $Cu^{2+}$ ions, and the structural agreement between $Cu^{+}$ and $Cu^{2+}$ structures was good in terms of the IM interactions observed. The $[M+Cu^{2+}]^{2+}$ structures were contracted and lower in energy relative to the $[M+Cu^{+}]^{+}$ structures by an average of *ca*. 10 $Å^2$ and *ca*. 170 kcal $mol^{-1}$, respectively. Retyping the atoms with a charge of +1 more accurately reflects the charge state of the peptide ion, which is irrefutable based upon the observed mass-to-charge ratio and isotopic envelope for the peptide ion. The smallness of structural changes are attributed to the total contribution of intramolecular interactions dominating over Coulombic effects.

**Results and Discussion**

**Figure 2a-c** contains the high energy CID tandem MS spectra for $[\mathbf{1}+H]^{+}$, $[\mathbf{1}+Na]^{+}$, and $[\mathbf{1}+Cu]^{+}$, respectively. The $[\mathbf{1}+H]^{+}$ ion yields abundant $a_i$ and $b_i$ fragment

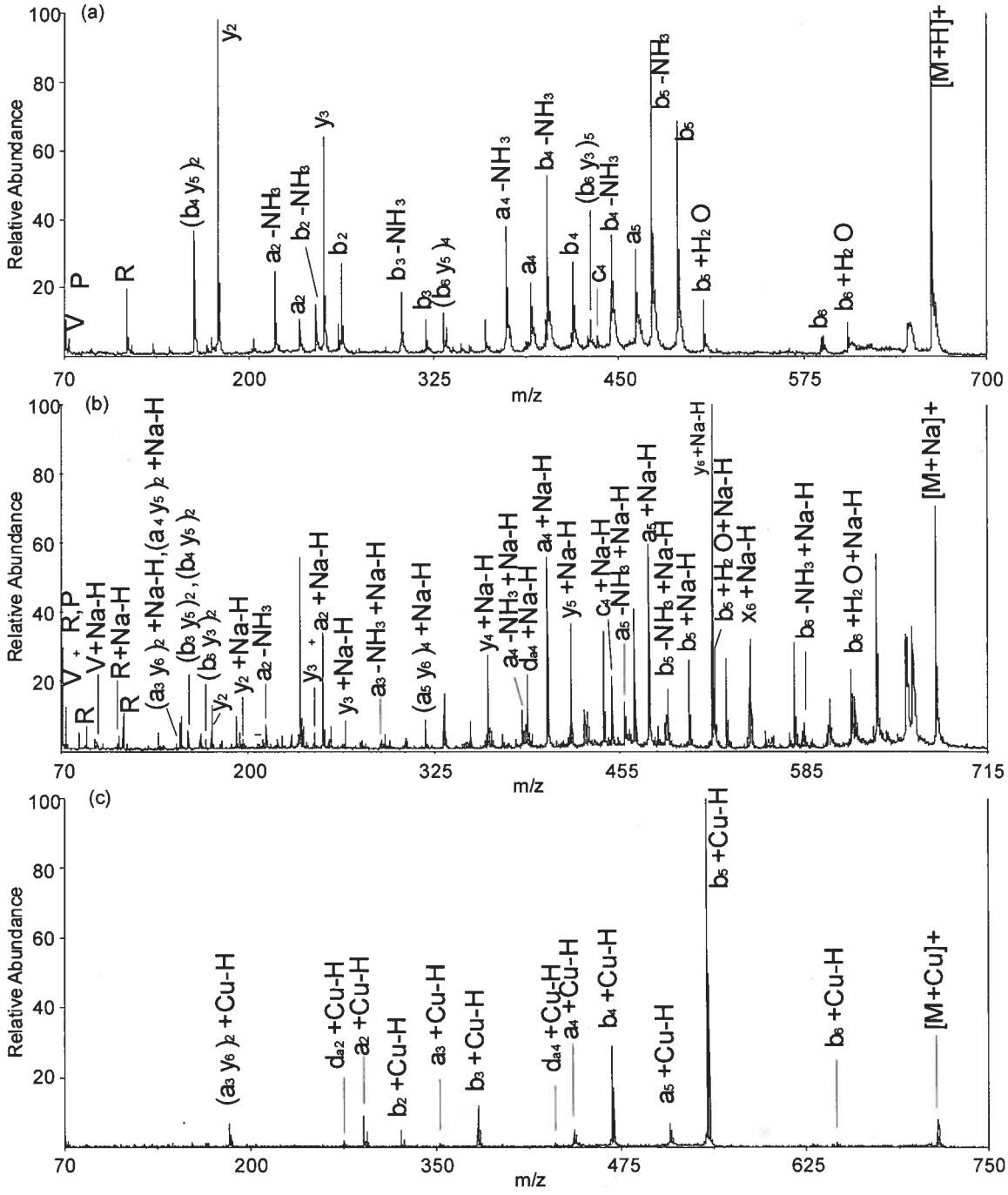


**Figure 2.** Tandem mass spectra for (a) $[RVGVAPG+H]^+$, (b) $[RVGVAPG+Na]^+$ and (c) $[RVGVAPG+Cu]^+$.

ions and low-abundance $y_i$ fragment ions, which suggests a preference for charge retention by the high proton affinity (PA) N-terminal arginine side chain, the PA for R = 251.2 kcal $^{-}$ mol $^{1}$; 30 kcal mol$^{-1}$ greater than any side chain of Val$^{2}$-Gly$^{7}$ as well as the N-terminus and backbone amide groups [60] . The spectrum of [**1**+Na]$^{+}$ ion (**Figure 2b**) contains both N- and C-terminal fragment ions, consistent with less-specific binding of $Na^{+}$ ions ($Na^{+}$ affinities range from 54 kcal mol$^{-1}$ to 38 kcal mol$^{-1}$ for the amino acid residues in the peptide [61]). The spectra for [M+Li]$^{+}$ and [M+K]$^{+}$ ions are not shown, however, these ions yield fragment ions which are similar to the [M+Na]$^{+}$ spectrum. Generally, [M+Li]$^{+}$ or [M+K]$^{+}$ precursor ions and fragment ions are of lower abundance, but the spectra appear to be similar to those for [M+Na]$^{+}$ ions. For comparison of spectra, metal affinities are reported in **Table 1**. Alkali metal affinities were calculated from the method of Lau et al. [62] based upon the amino acid $Na^{+}$ affinities reported by Kish et al. [61]. For [**1**+Cu]$^{+}$ (**Figure 2c**), the $y_i$ ion series is lower than the reduce due to the large $Cu^{+}$ binding energy of 136.1 kcal mol$^{-1}$ by the N-terminal arginine residue [47].

**Figure 3a-c** contains high energy CID tandem MS spectra for [**2**+H]$^{+}$, [**2**+Na]$^{+}$, and [**2**+Cu]$^{+}$, respectively. The chemistry of the [M+Cu]$^{+}$ and [M+H]$^{+}$ ions of **2** are similar to that of peptide **1**; however, the high energy CID tandem MS spectrum of the [**2**+Na]$^{+}$ ions contains a higher abundance of N-terminal fragments ions than [**1**+Na]$^{+}$, including high abundance $Na^{+}$ containing histidine immonium ions. This observation is consistent with a high $Na^{+}$ ion affinity for the imidazole ring; 52 kcal mol$^{-1}$, second only to that for the side chain of Arg (54 kcal mol$^{-1}$) [61,63].

**Table 1**. Proton and metal ion affinities for relevant amino acid residues.

| | | Binding Energies, kcal $mol^{-1}$ | | | |
|---|---|---|---|---|---|
| Residue | $H^{+a}$ | $Li^{+b}$ | $Na^{+b}$ | $K^{+c}$ | $Cu^{+d}$ |
| Arg | 251.2 | 77 | 54 | 43 | 136.1 |
| His | 236 | 75 | 52 | 42 | 110 |
| Lys | 238 | 73 | 51 | 41 | 120.4 |
| Gln | 224.1 | 73 | 51 | 41 | 102.6 |
| Trp | 226.8 | 72 | 50 | 40 | |
| Asn | 222 | 71 | 49 | 39 | 90.2 |
| Glu | 218.2 | 70 | 49 | 39 | 87.4 |
| Asp | 217.2 | 70 | 49 | 39 | 84.3 |
| Tyr | 221 | 69 | 48 | 38 | |
| Phe | 220.6 | 68 | 47 | 38 | |
| Thr | 220.5 | 68 | 47 | 38 | |
| Pro | 220.0 | 68 | 47 | 37 | |
| Ser | 218.6 | 66 | 46 | 36 | |
| Ile | 219.3 | 61 | 42 | 33 | |
| Cys | 215.9 | 61 | 42 | 33 | |
| Leu | 218.6 | 61 | 42 | 33 | |
| Val | 217.6 | 60 | 41 | 33 | |
| Ala | 215.5 | 58 | 40 | 31 | |
| Gly | 211.9 | 56 | 38 | 30 | |

[a]Values for $Na^+$ affinities were converted from the kJ $mol^{-1}$ values reported by Hunter et al. [60]

[b]Values for $Na^+$ affinities were converted from the kJ $mol^{-1}$ values reported by Kish et al. [61]

[c]Values for the $Li^+$ and $K^+$ affinities were estimated using the empirical relation developed by Lau et al. [62]

[d]Values for the $Cu^+$ affinities were taken from the binding energies calculated by Bluhm et al. [47]

**Figure 4a-c** contains the high energy CID tandem MS spectra for [**3**+H]$^+$, [**3**+Na]$^+$, and [**3**+Cu]$^+$, respectively. The pattern of abundances of *N*-terminal fragment ions of [**3**+H]$^+$ relative to [**3**+Cu]$^+$ differ significantly from the patterns of fragment ion abundances for the corresponding ions of **1** and **2**. The fragment ions of [**3**+Cu]$^+$ indicate that $Cu^+$ is not bound with specificity as great as in the case of **1** and **2**. The PAs of the *N*-terminal residues in **1-4** follow the order Arg>His>Lys>Asp [64]. The lysine side chain retains a high PA (238 kcal mol$^{-1}$) [60] , the B3LYP binding energies for monodentate binding of $Cu^+$ to the N-terminal residues in **1-3** show a decrease from 80.1 to 72.2 to 62.3 kcal mol$^{-1}$, and the bidentate binding energies are 136.1, 110.0, 120.4, and 84.3 kcal mol$^{-1}$, for the N-terminal residue in **1-4**, respectively [47]. The peptides **1-3** all contain a basic residue in the N-terminal position, and in order to examine a peptide sequence that did not, we prepared DVGVAPG (**4**) as well. This peptide does not retain the specific metal-binding behavior at the *N*-terminal residue that **1-3** possess.

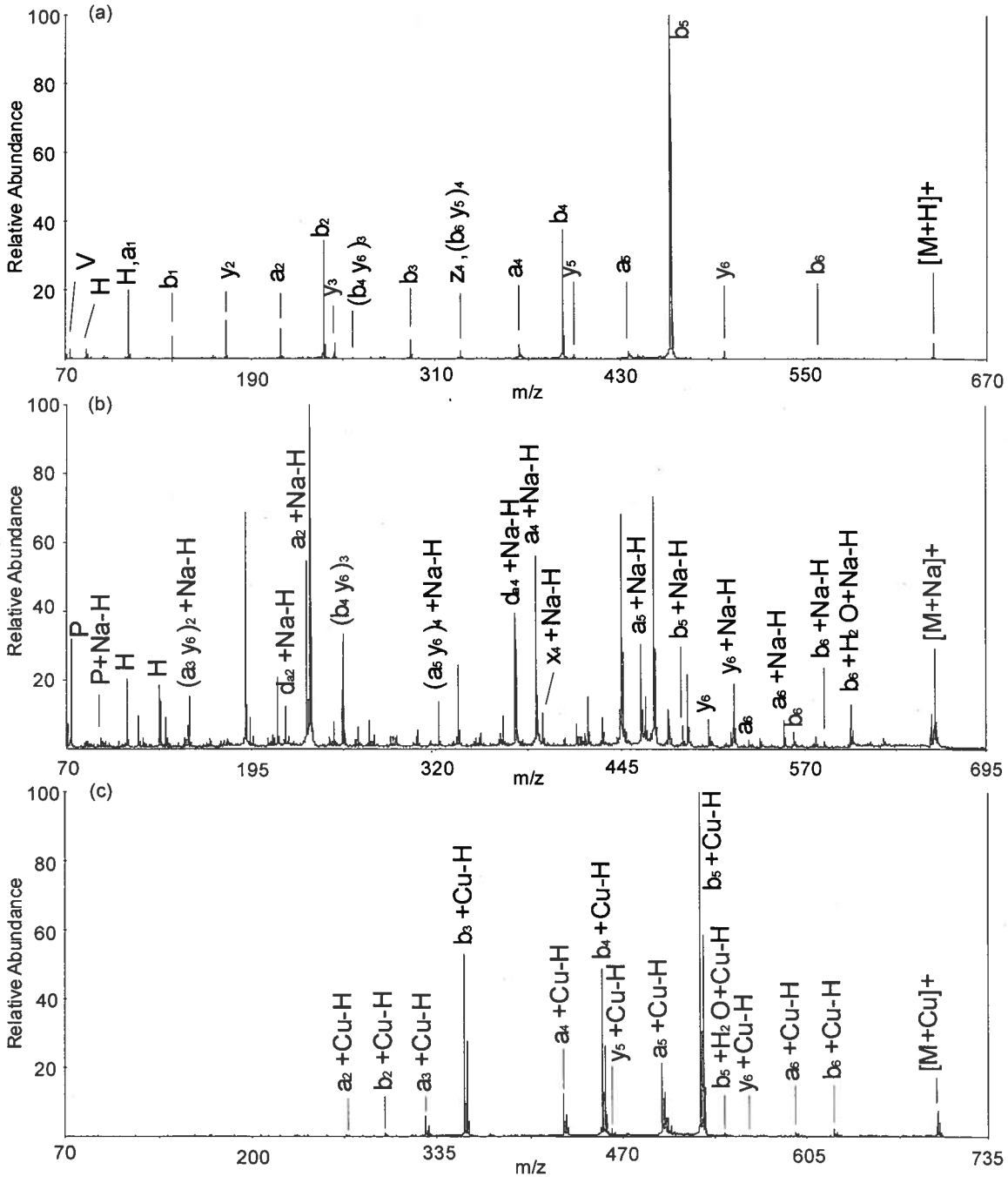


**Figure 3**. Tandem mass spectra for (a) $[HVGVAPG+H]^+$, (b) $[HVGVAPG+Na]^+$ and (c) $[HVGVAPG+Cu]^+$.

**Figure 5a-c** contains the high energy CID tandem MS spectra for [**4**+H]$^+$, [**4**+Na]$^+$, and [**4**+Cu]$^+$, respectively. The fragmentation chemistry of [**4**+H]$^+$, [**4**+Na]$^+$, and [**4**+Cu]$^+$ are similar in observed fragments and fragment abundance than the same charge carriers applied to **1**–**3**, consistent with the thermochemistry listed in **Table 1**. The charge carriers in [**4**+H]$^+$, [**4**+Na]$^+$, and [**4**+Cu]$^+$ are not sequestered with specificity, leading to broad distributions of fragment ions observed in the tandem mass spectra.

The normalized relative abundance of sequence-informative fragment ions for the [M+H]$^+$, [M+Li]$^+$, [M+Na]$^+$, [M+K]$^+$ and [M+Cu]$^+$ ions of each peptide are summarized in **Table 2**. The abundance values give more detail on the classes of fragments observed from each peptide with each charge carrier in the study. For example, the most abundant fragment ions in all cases are $a_i$, $b_i$, and $y_i$ ions, however, the [M+Na]$^+$ ions (as well as [M+Li]$^+$ and [M+K]$^+$) contain higher abundances of C-terminal fragments, i.e. $x_i$ and $z_i$.

It appears that this is the result of a lack of specific binding of the alkali metal ions to specific sites, carbonyl or amide electron pairs, along the peptide backbone, which results in a broader distribution of fragment ion types. This is similar to observations based upon the mobile proton model, but we are not saying that the charges are mobile, but delocalized. This is supported by the distribution of individual fragment abundance in each class (e.g. $y_1$ to $y_7$) within particular alkali metalated peptide fragment ion spectra becoming broader (data not shown).

**Table 2**. Normalized fragment ion abundances by type for all ions of peptides **1**-**4** given in percent of total sequence ion abundance with N- and C-terminal fragment ion sums.

| Peptide | Fragments | Charge Carrier | | | | |
|---|---|---|---|---|---|---|
| RVGVAPG, **1** | | $Cu^+$ | $H^+$ | $Li^+$ | $Na^+$ | $K^+$ |
| | $a_i$ | 15.7 | 29.8 | 44.5 | 35.3 | 16.1 |
| | $b_i$ | 83.6 | 46.2 | 29.3 | 16.9 | 9.7 |
| | $c_i$ | 0.0 | 0.7 | 2.1 | 4.4 | 0.0 |
| | $x_i$ | 0.5 | 0.1 | 7.0 | 8.0 | 6.5 |
| | $y_i$ | 0.2 | 23.2 | 17.1 | 35.4 | 24.2 |
| | $z_i$ | 0.0 | 0.0 | 0.0 | 0.0 | 43.5 |
| | $N_t$ | 99.3 | 76.7 | 75.9 | 56.6 | 25.8 |
| | $C_t$ | 0.7 | 23.3 | 24.1 | 43.4 | 74.2 |
| HVGVAPG, **2** | | | | | | |
| | $a_i$ | 20.3 | 7.6 | 39.6 | 48.9 | 27.6 |
| | $b_i$ | 78.0 | 83.7 | 22.2 | 15.5 | 17.3 |
| | $c_i$ | 0.5 | 0.1 | 8.1 | 5.2 | 5.5 |
| | $x_i$ | 0.1 | 0.0 | 1.3 | 3.4 | 5.2 |
| | $y_i$ | 1.1 | 8.6 | 24.9 | 24.5 | 30.1 |
| | $z_i$ | 0.0 | 0.0 | 3.9 | 2.5 | 14.3 |
| | $N_t$ | 98.8 | 91.4 | 69.9 | 69.6 | 50.4 |
| | $C_t$ | 1.2 | 8.6 | 30.1 | 30.4 | 49.6 |
| KVGVAPG, **3** | | | | | | |
| | $a_i$ | 22.7 | 15.7 | 25.7 | 47.0 | 17.7 |
| | $b_i$ | 73.4 | 64.7 | 33.3 | 22.0 | 3.7 |
| | $c_i$ | 0.0 | 0.0 | 7.1 | 0.7 | 2.3 |
| | $x_i$ | 0.0 | 0.2 | 4.4 | 1.4 | 0.0 |
| | $y_i$ | 3.9 | 19.4 | 29.1 | 28.4 | 24.6 |
| | $z_i$ | 0.0 | 0.0 | 0.4 | 0.5 | 51.7 |
| | $N_t$ | 96.1 | 80.4 | 66.1 | 69.7 | 23.7 |
| | $C_t$ | 3.9 | 19.6 | 33.9 | 30.3 | 76.3 |
| DVGVAPG, **4** | | | | | | |
| | $a_i$ | 7.8 | 26.5 | 7.4 | 6.4 | 7.9 |
| | $b_i$ | 67.3 | 57.3 | 3.5 | 3.7 | 8.6 |
| | $c_i$ | 0.0 | 0.5 | 0.4 | 2.5 | 4.9 |
| | $x_i$ | 0.0 | 0.0 | 1.0 | 0.6 | 0.0 |
| | $y_i$ | 24.9 | 14.3 | 87.1 | 86.2 | 59.5 |
| | $z_i$ | 0.0 | 1.4 | 0.6 | 0.6 | 19.1 |
| | $N_t$ | 75.1 | 84.3 | 11.3 | 12.6 | 21.4 |
| | $C_t$ | 24.9 | 15.7 | 88.7 | 87.4 | 78.6 |

To more fully examine this topic and gain some structural insight into the fragmentation, we employed ion mobility measurements and computational chemistry methods to determine plausible structures for these ions. In the best-fit structures, the metal ions are complexed by numerous ligands in the form of amide and carbonyl electron pairs, which supports our assumption of low metal binding specificity along the peptide backbone.

*Best-Fit Ion Structures*

From our analysis of the ion mobility spectra for the precursor ions of [**1-4**+H]$^+$, [**1-4**+Na]$^+$ and [**1-4**+Cu]$^+$, and our computer simulations of the lowest energy structures of the ions, we have developed a picture of structures for these ions that match the empirical data. **Table 3** lists the experimental and calculated collision cross-sections for the [M+H]$^+$, [M+Na]$^+$, and [M+Cu]$^+$ ions; the "best-fit" structures are shown in **Figures 6a-9c**. Representative structures of [M+H]$^+$ and [M+Na]$^+$ ions that agree best with the measured collision cross sections do not always correlate with the lowest energy structure, but in all cases the best-fit structures are within *ca*. 5 kcal mol$^{-1}$ of the lowest energy conformer.

**Table 3**. Collision cross sections of XVGVAPG peptide ions.

| Collision cross sections of chosen ions, Å$^2$ | | | |
|---|---|---|---|
| Peptide | $H^+$ | $Na^+$ | $Cu^+$ |
| RVGVAPG, **1** | 192 | 201 | 205 |
| HVGVAPG, **2** | 188 | 191 | 192 |
| KVGVAPG, **3** | 185 | 192 | 189 |
| DVGVAPG, **4** | 180 | 185 | 200 |

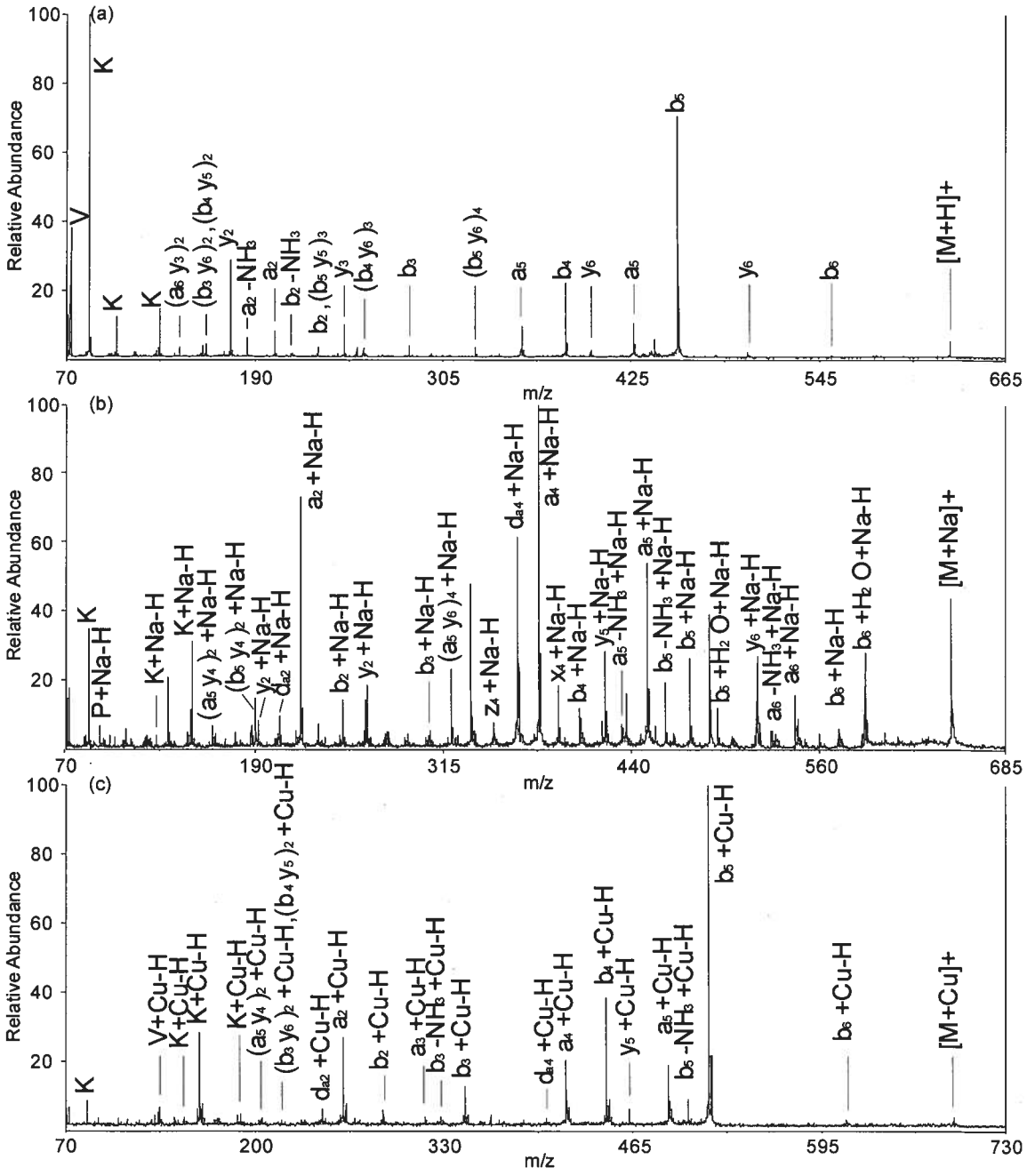


**Figure 4**. Tandem mass spectra for (a) $[KVGVAPG+H]^+$, (b) $[KVGVAPG+Na]^+$ and (c) $[KVGVAPG+Cu]^+$.

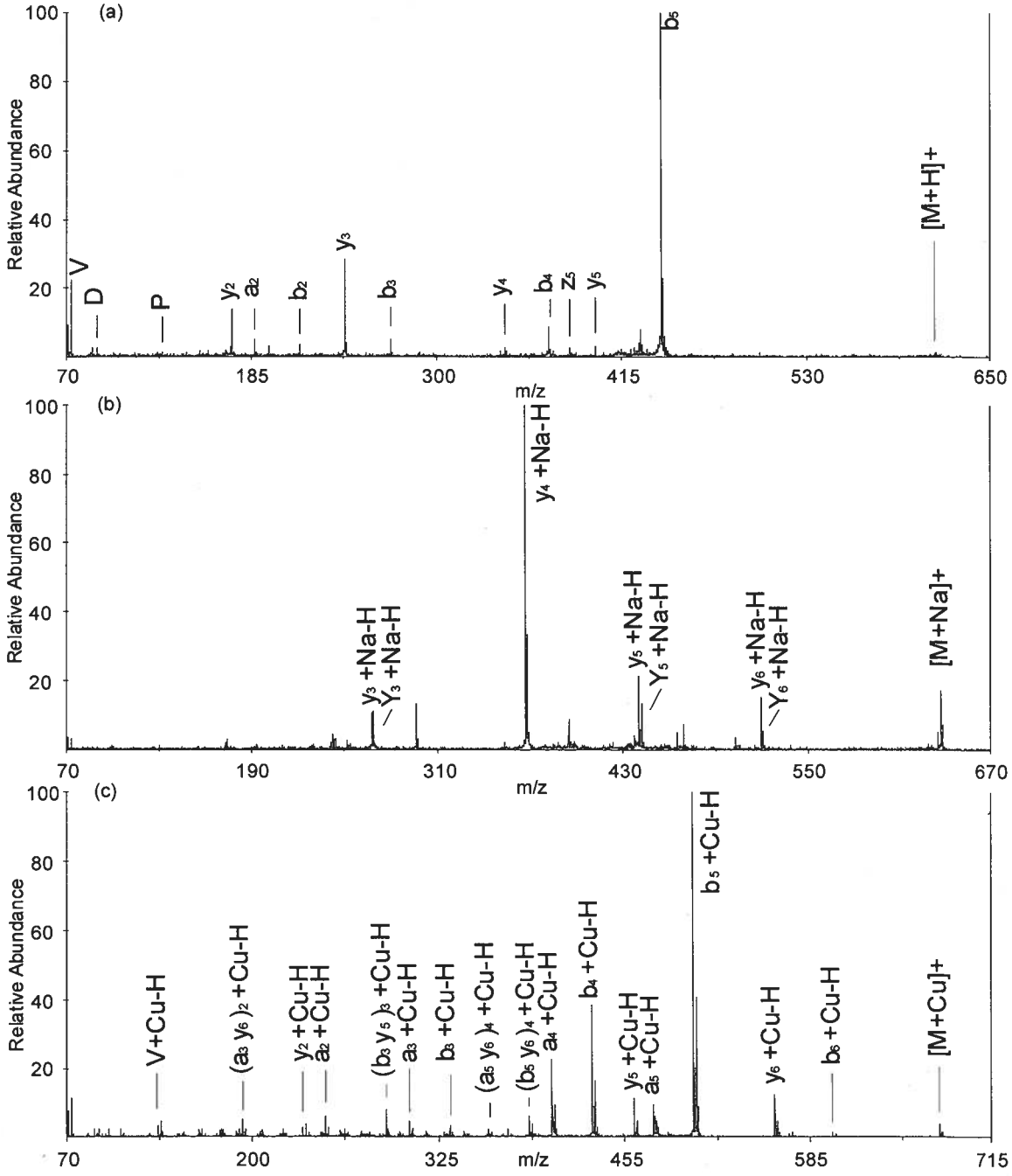


**Figure 5**. Tandem mass spectra for (a) $[DVGVAPG+H]^+$, (b) $[DVGVAPG+Na]^+$ and (c) $[DVGVAPG+Cu]^+$.

The gross structural elements and types of intramolecular interactions observed in the best-fit structures were similar to those of the lowest energy structures and the most dramatic changes were remote from the charge site (e.g. interatomic distances and bond angles). Each peptide adopted a structure where the $H^+$ or $M^+$ was solvated as much as possible given the steric requirements of each peptide backbone. These structures resemble a set a ligands coordinating a metal center, akin to an EDTA complex. Although there were small differences in absolute bond distances and angles between structures, the best-fit structures indicate that the individual amino acid residues along the peptide backbone matter less than the presence of electron pairs, similar to the results obtained by Sawyer [49]. Absolute bond distances are a less important metric of agreement than are the collision cross sections, the relative energy scale, and the types of intramolecular interactions present.

Although the $Na^+$ affinities of Arg and His are similar, in the compact oxygen cage structure that the $[M+Na]^+$ ions adopt, only monodentate binding from the N-terminal side chain occurs which more strongly favors interaction with the imidazole ring in **1** rather than the guanidino group of **2**. This type of structure, with a metal center surrounded by an oxygen-rich coordination sphere is similar to the structures of transition metal complexes described by Martell [65]. Although the calculated bidentate binding energy for Lys is higher than for His, other $Cu^+$ complexation schemes may result for **3** owing to the flexibility of the Lys side chain. Both monodentate and bidentate binding energies must be considered in this case; we attribute the lower

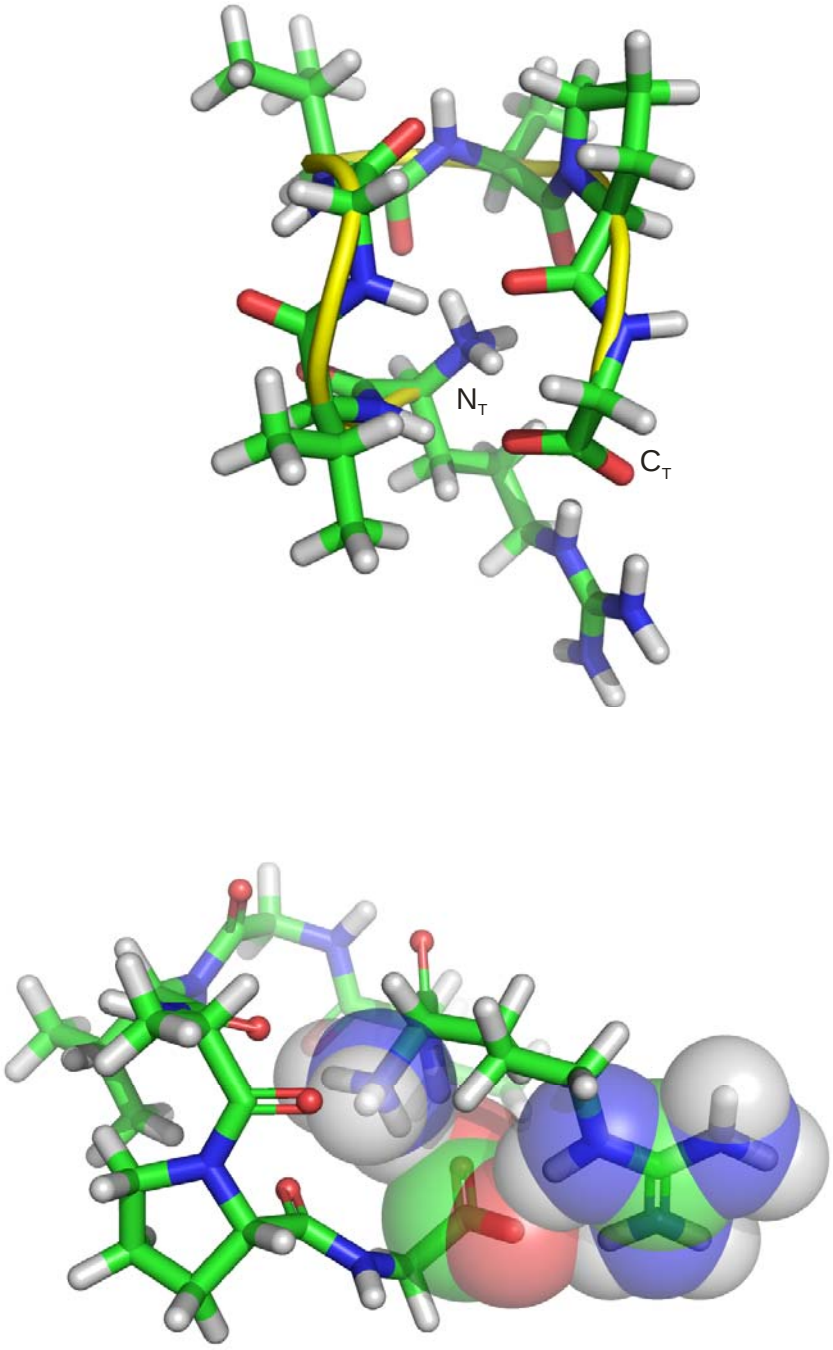


**Figure 6a**. Representations of the candidate structures obtained for $[RVGVAPG+H]^+$

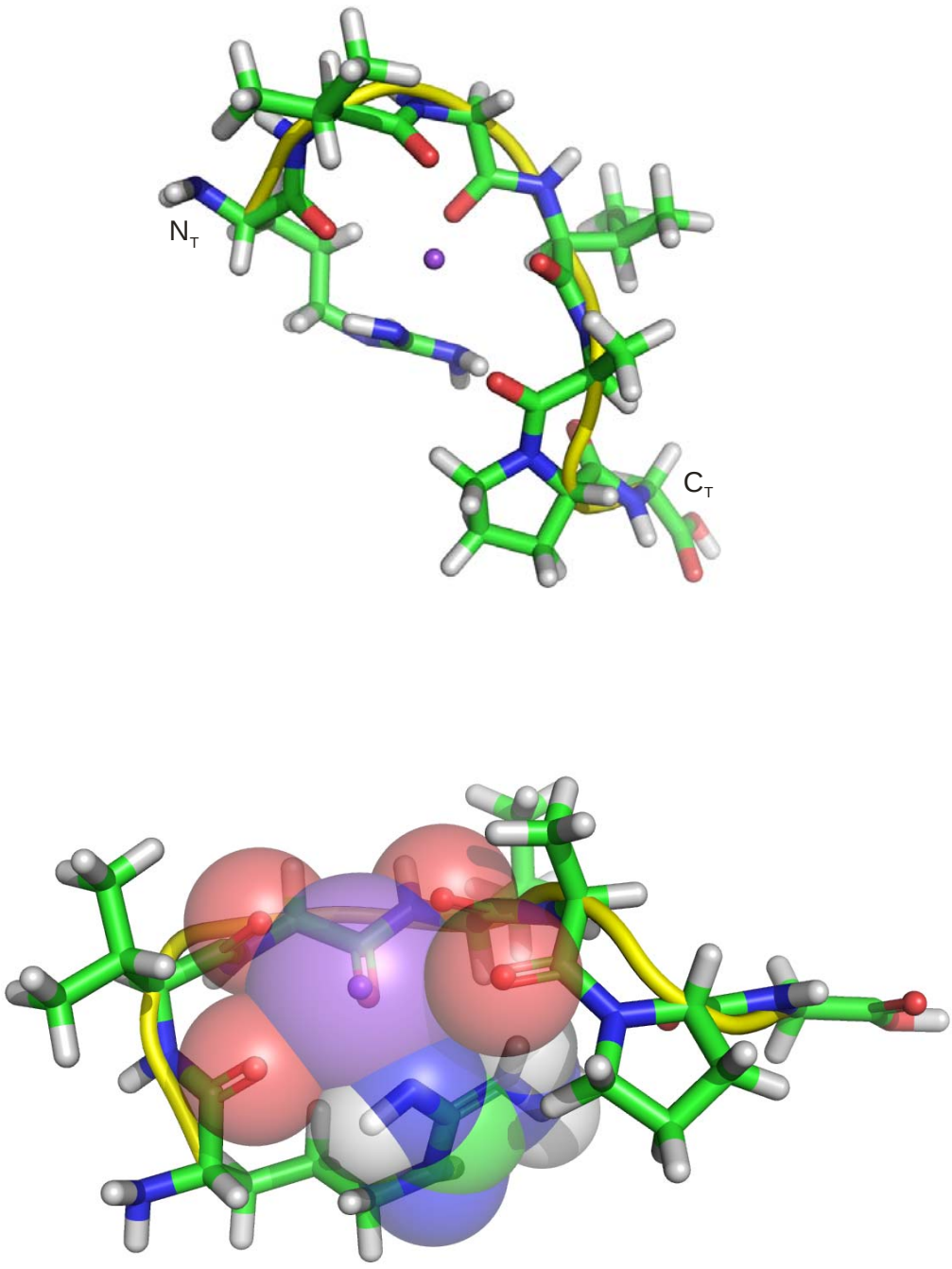


**Figure 6b**. Representations of the candidate structures obtained for $[RVGVAPG+Na]^+$

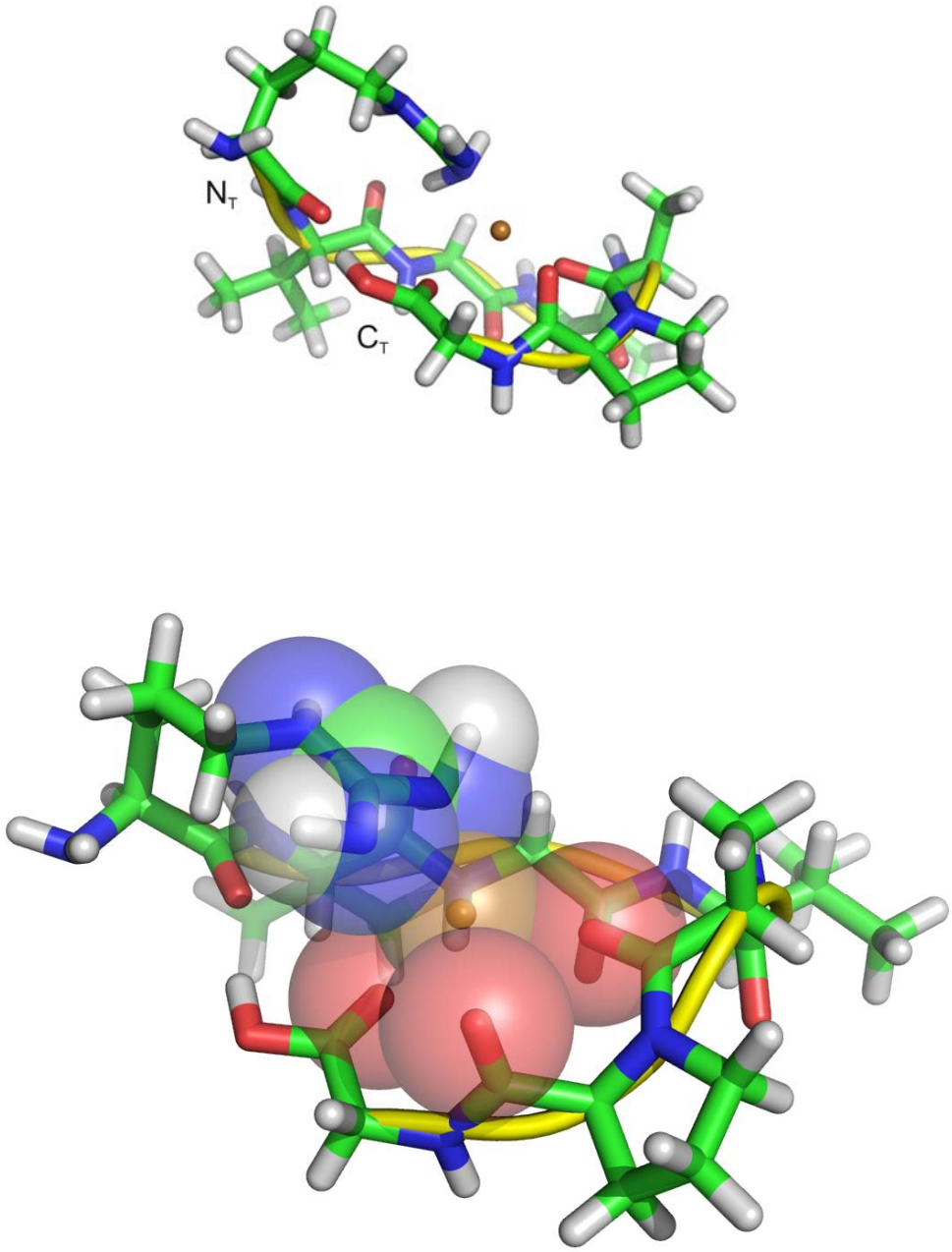


**Figure 6c**. Representations of the candidate structures obtained for $[RVGVAPG+Cu]^+$

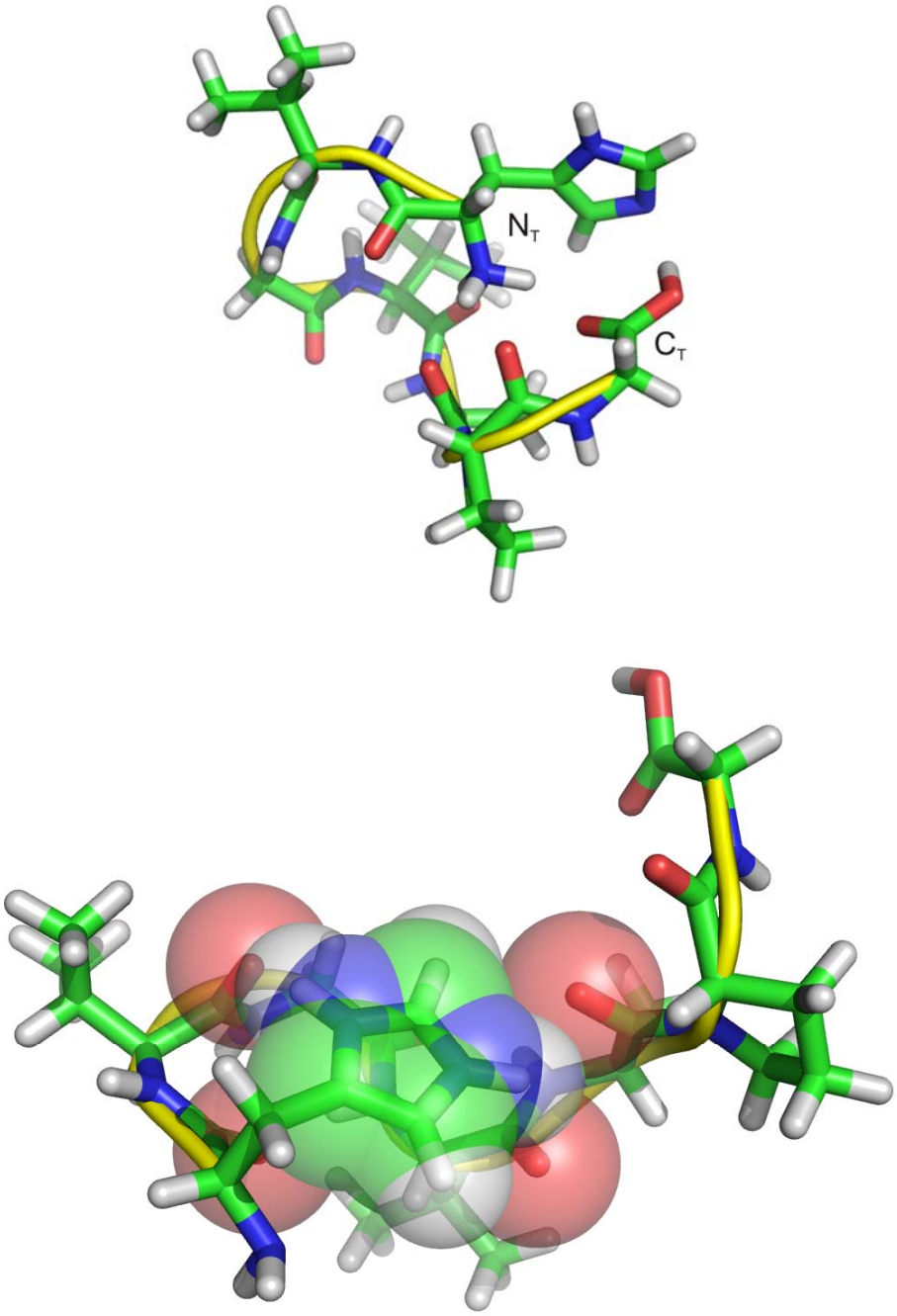


**Figure 7a**. Representations of the candidate structures obtained for $[HVGVAPG+H]^+$.

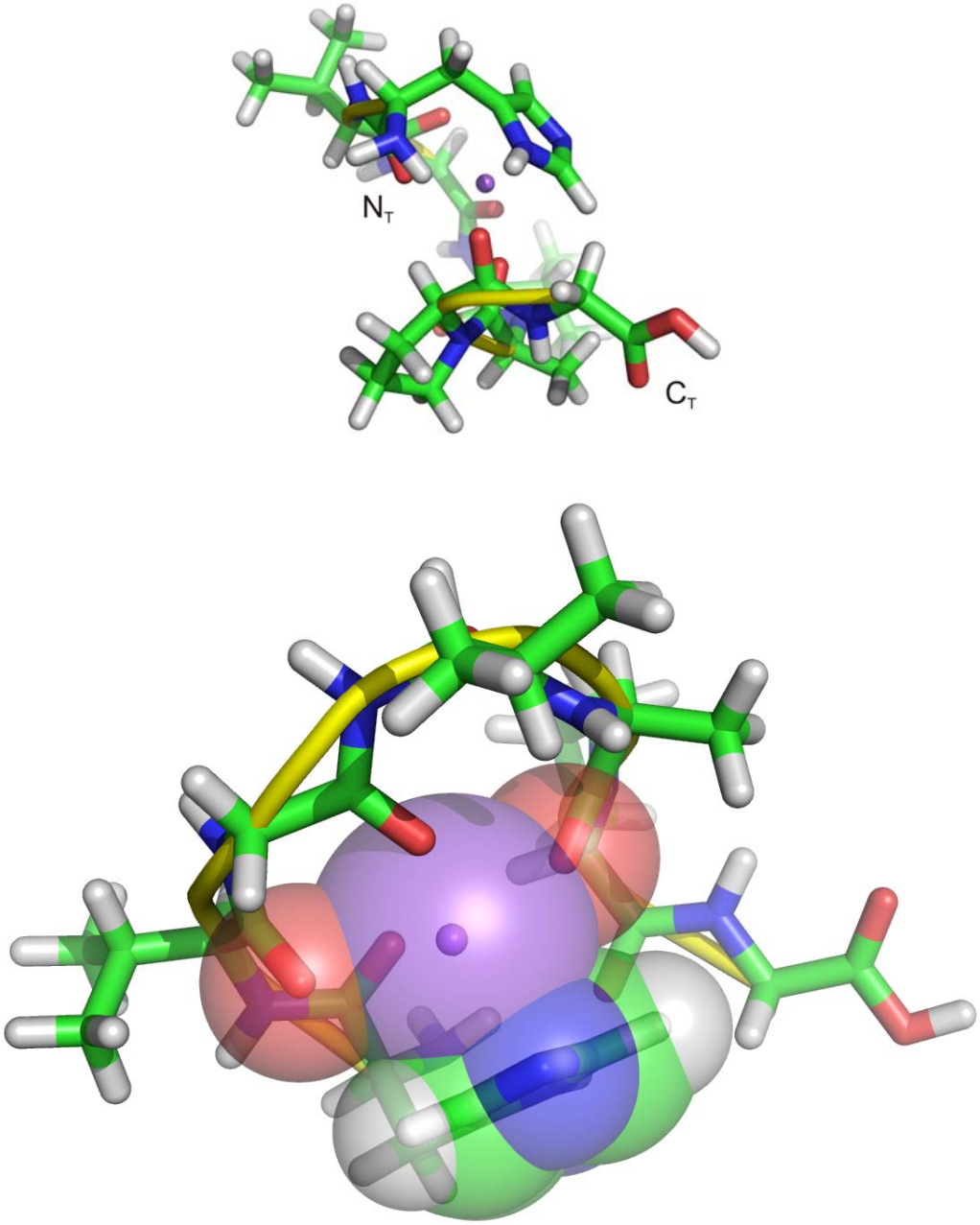


**Figure 7b**. Representations of the candidate structures obtained for $[HVGVAPG+Na]^+$.

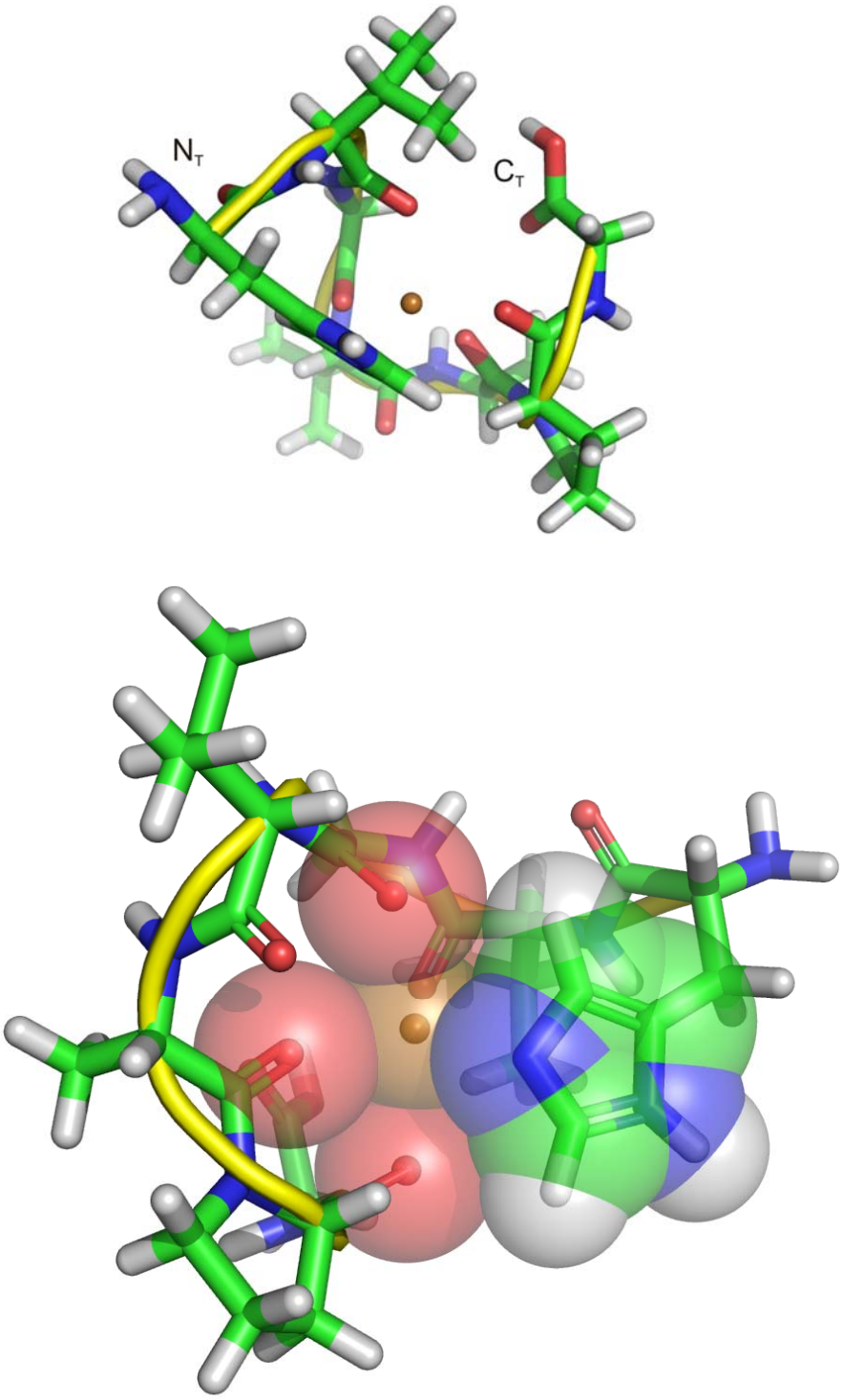


**Figure 7c**. Representations of the candidate structures obtained for $[HVGVAPG+Cu]^+$.

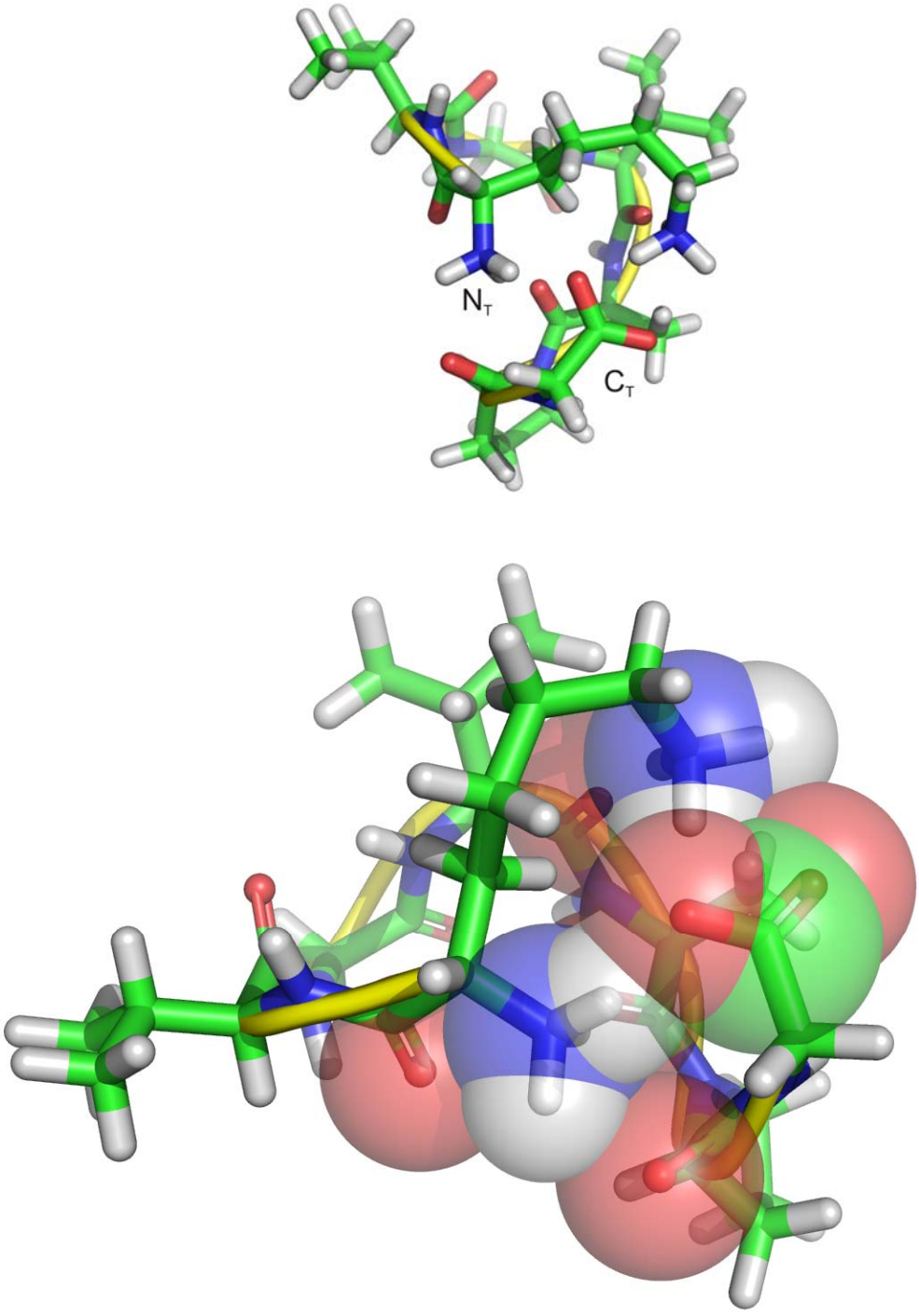


**Figure 8a**. Representations of the candidate structures obtained for $[KVGVAPG+H]^+$.

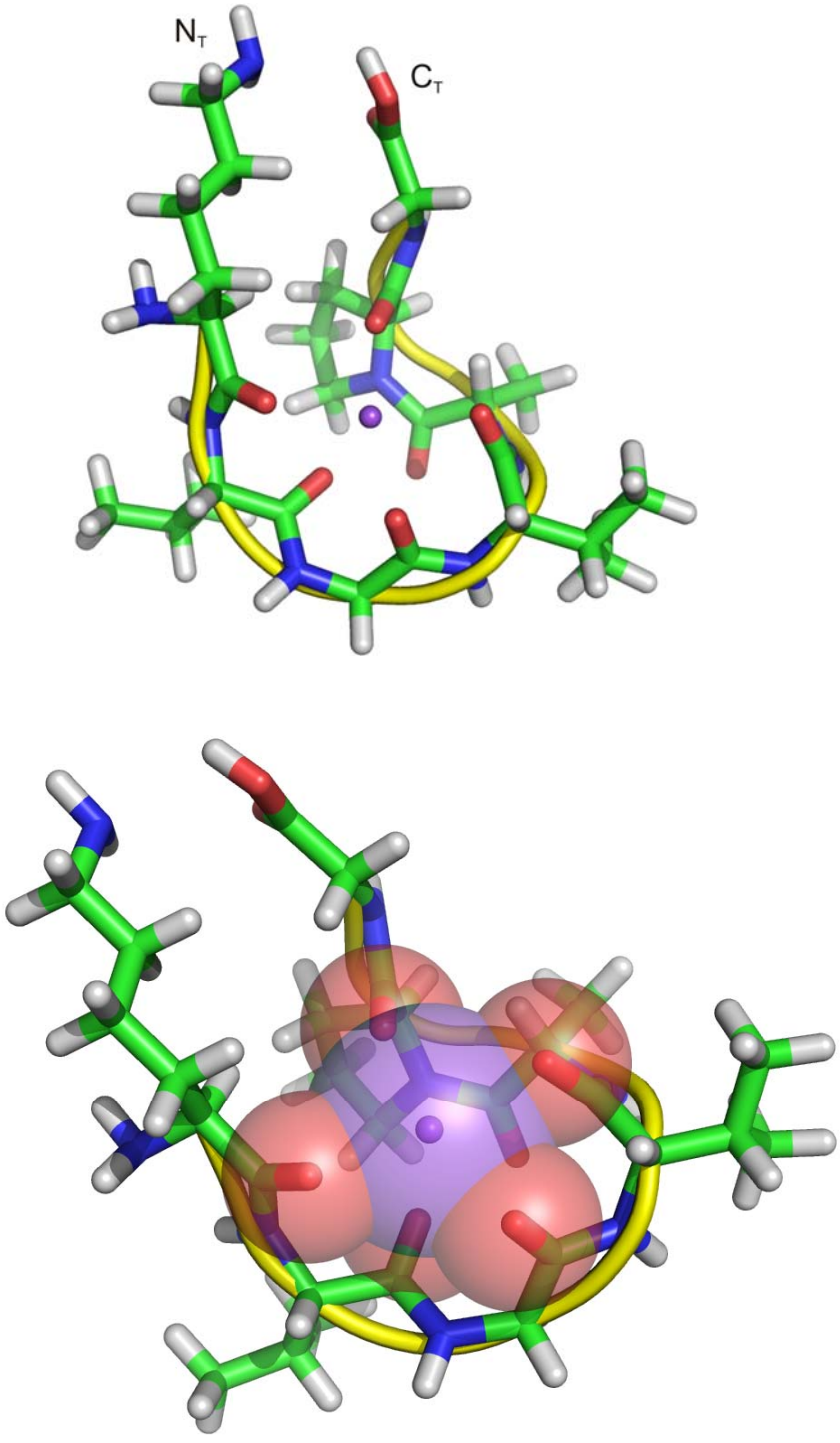


**Figure 8b**. Representations of the candidate structures obtained for $[KVGVAPG+Na]^+$.

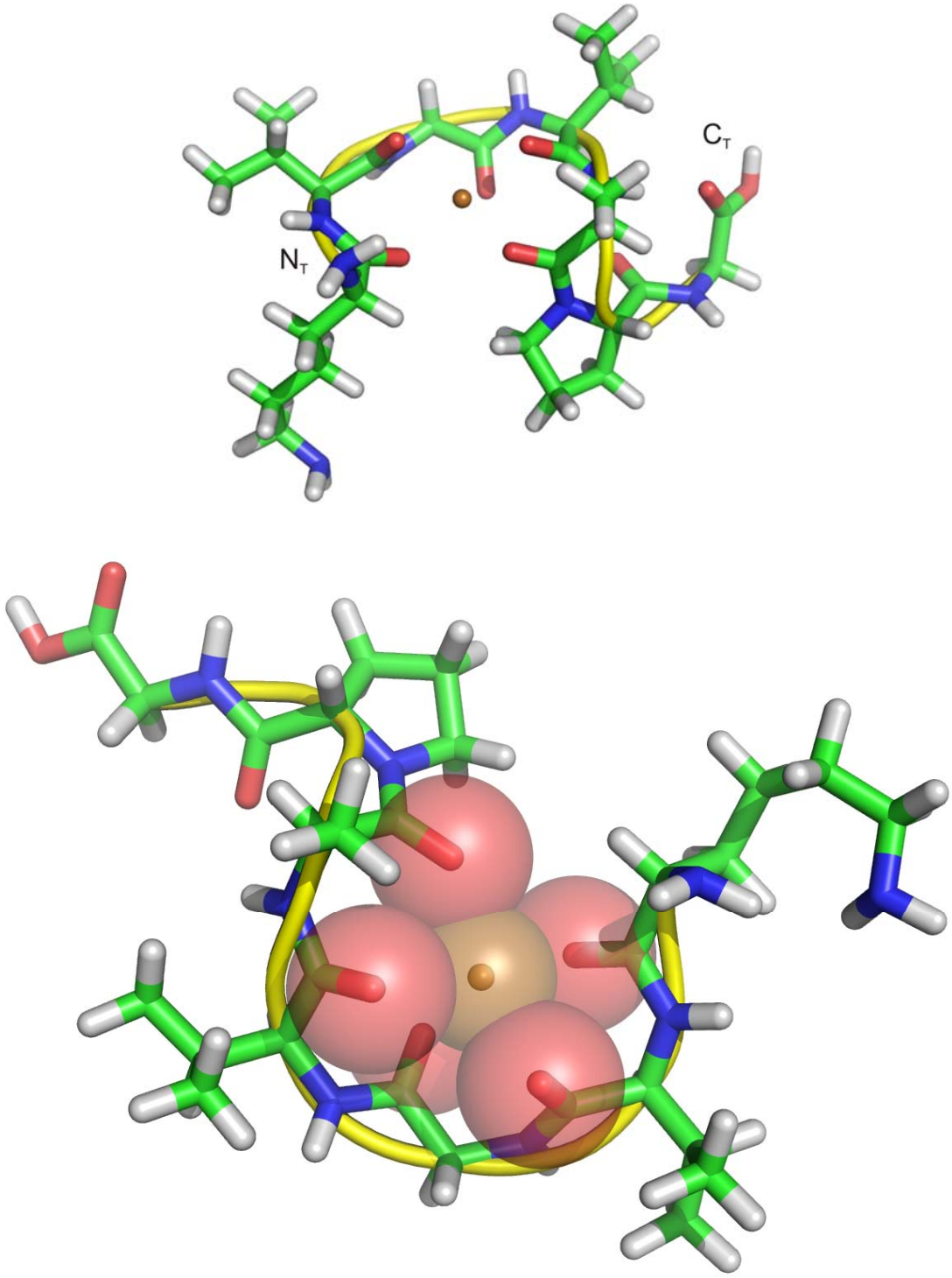


**Figure 8c**. Representations of the candidate structures obtained for $[KVGVAPG+Cu]^+$.

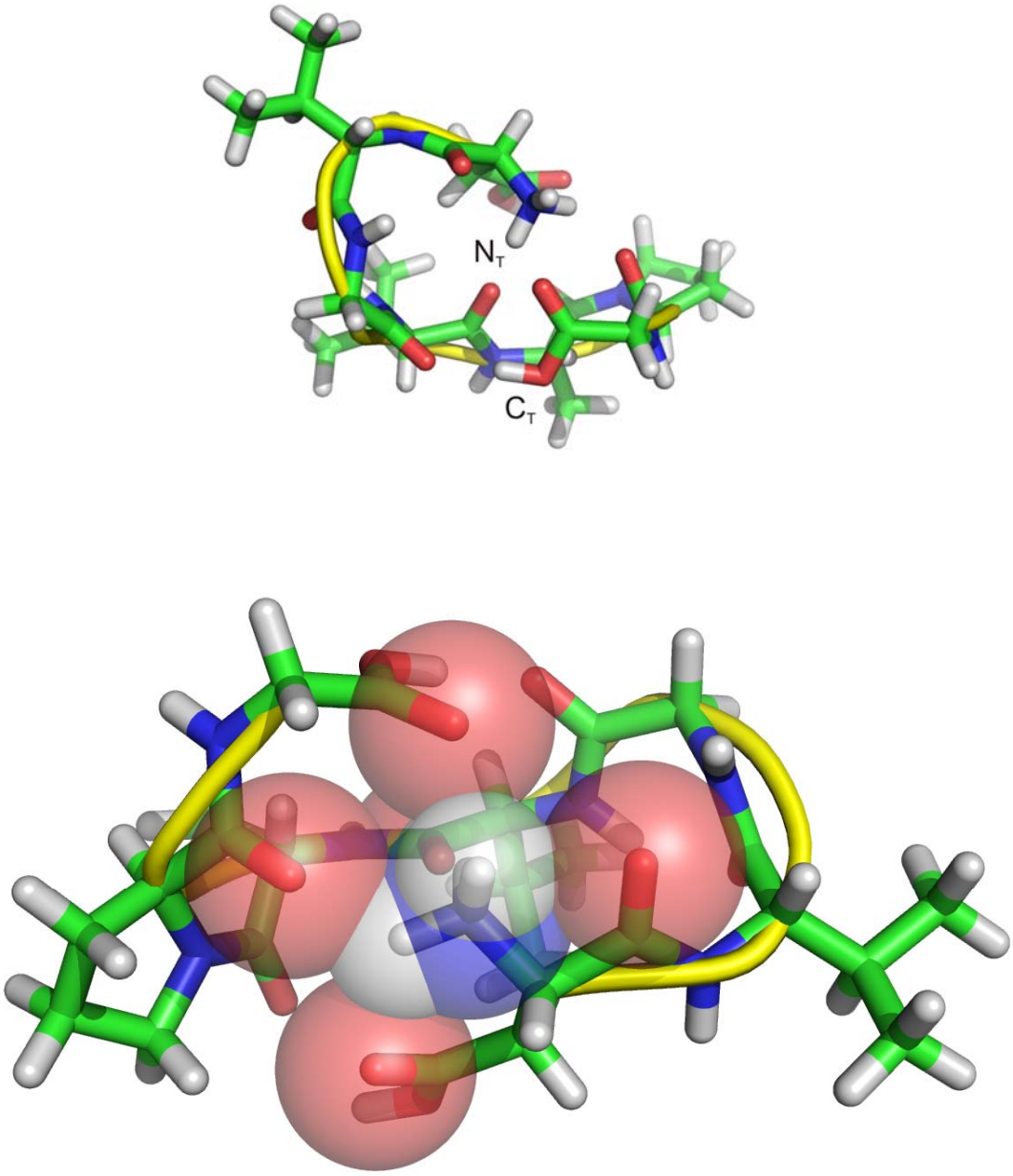


**Figure 9a**. Representations of the candidate structures obtained for $[DVGVAPG+H]^+$.

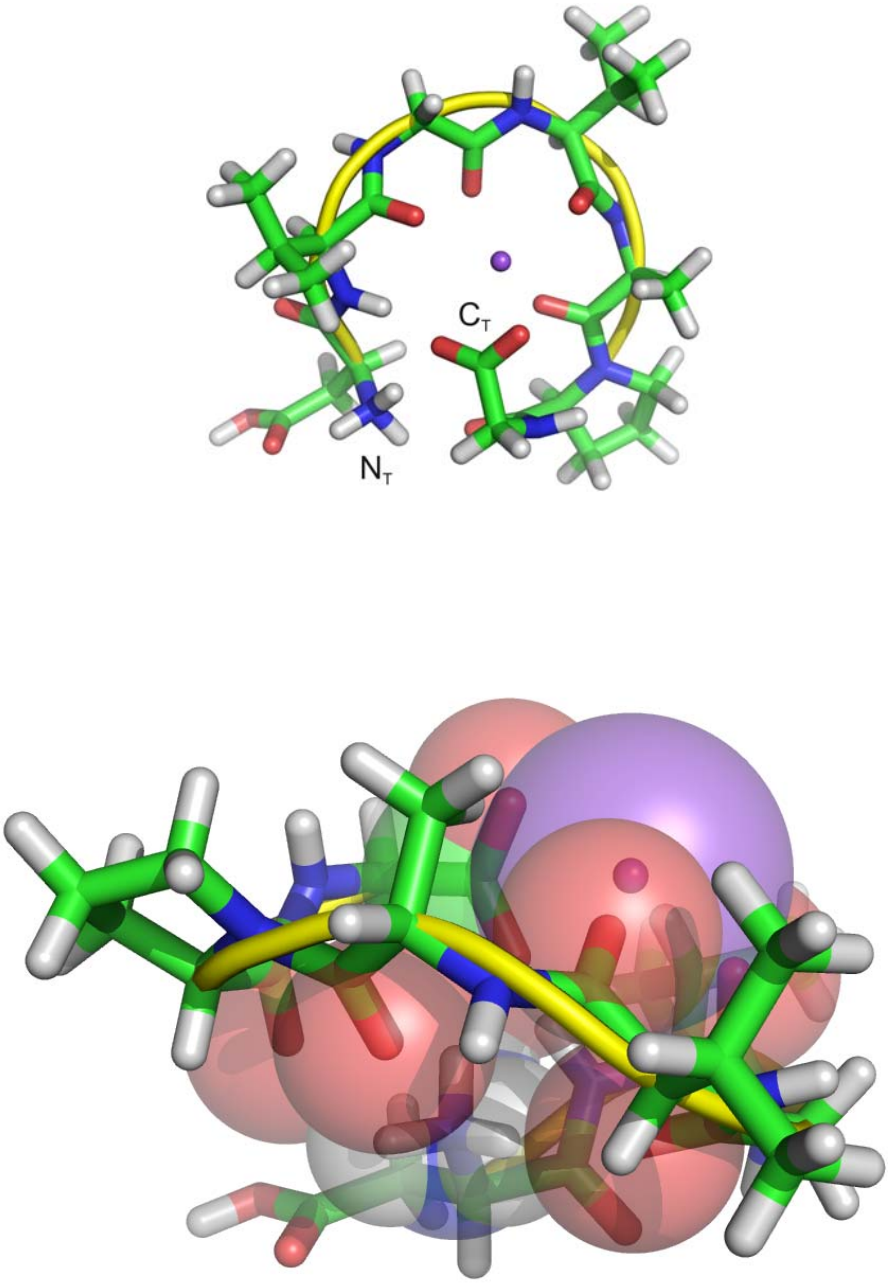


**Figure 9b**. Representations of the candidate structures obtained for $[DVGVAPG+Na]^+$.

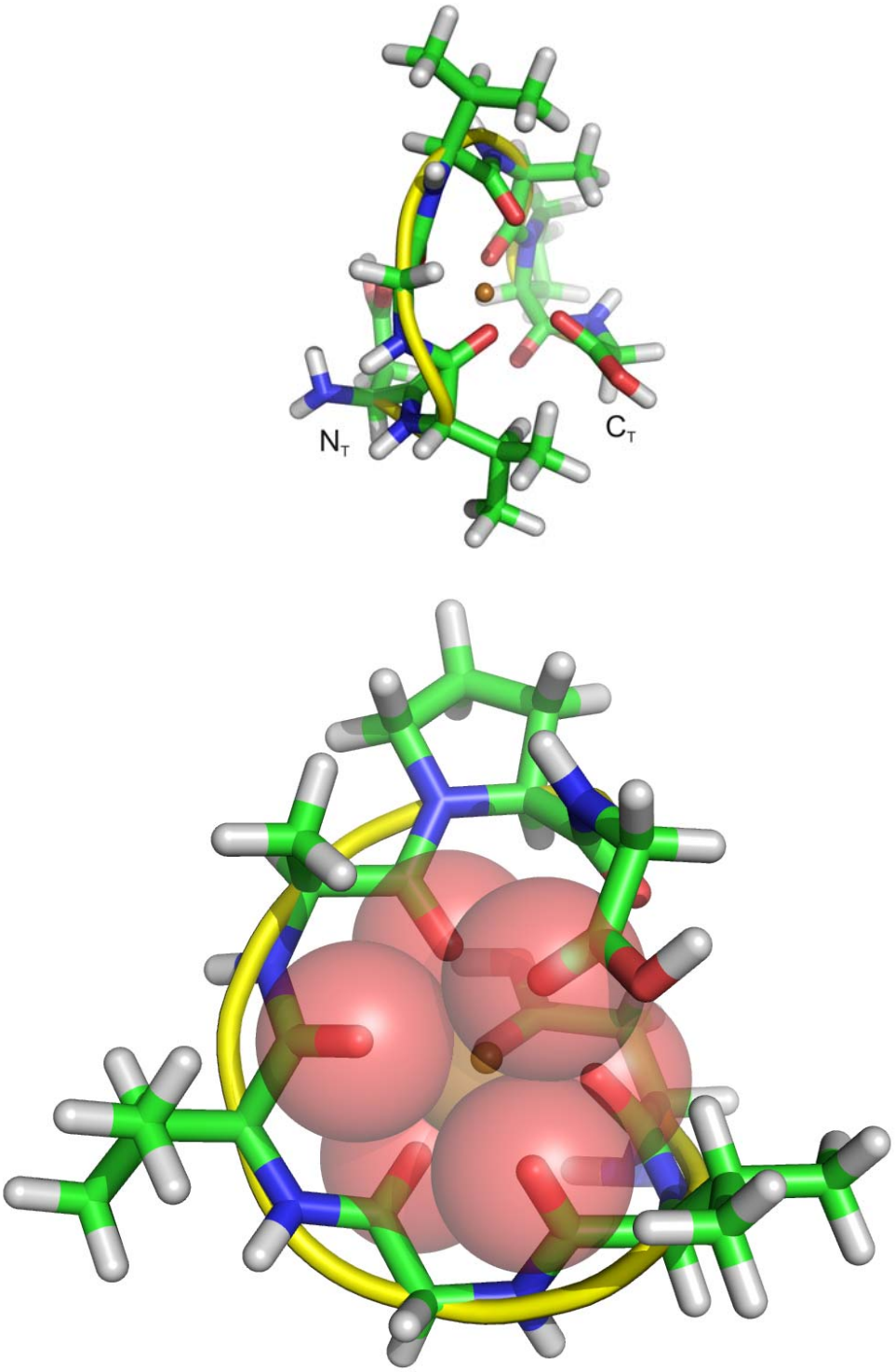


**Figure 9c**. Representations of the candidate structures obtained for $[DVGVAPG+Cu]^+$.

abundance of N-terminal fragment ions from [**3**+Cu]$^+$ to the reduced composite $Cu^+$ affinity of the lysine side chain relative to the N-terminal residues in **1** and **2**

It is interesting to compare our fragmentation results for [M+Cu]$^+$ of **1**-**3** to Allison's in order to draw conclusions about the fragmentation mechanism because the systems appear at first to be similar, based upon the peptide sequences used and the presence of a charged derivative fixed at the N-terminus of Allison's system [16]. The derivative in our case was a residue with a high PA or metal binding affinity which directed the location of the charge in [M+H]$^+$ or [M+metal]$^+$. It should be noted that the charge derivative used by Allison is large, approaching the size of the peptide to which it is attached, whereas our derivative is much smaller and subject to more and stronger IM interactions. The phosphonium acetyl peptides may be otherwise flexible, but consistent with Allison's mechanism, the most important component of a charge-local mechanism (charge proximity) is missing. Allison observed that $a_i$ ions are the most abundant fragment ions for the phosphonium acetyl ions; [M+Cu]$^+$ ions of **1**-**3** yielded a nearly-complete $a_i$ series and a complete and higher-abundance $b_i$ series. For both the phosphonium acetyl peptides and for the [M+Cu]$^+$ ions of **1**-**3**, N-terminal fragments dominate. In our [M+Cu]$^+$ ions and Allison's phosphonium acetyl ions, no ammonia loss fragments were observed as the N-terminus in the phosphonium ion and the arginine side chain in **1** are chemically altered and do not eliminate $NH_3$.

Allison proposed that the phosphonium acetyl peptide ions fragment by a charge-remote mechanism. We extend the mechanism suggested by Shields [18] (shown in Scheme 1) to explain the formation of [fragment+Cu–H]$^+$ for N-terminal Arg peptide

**Scheme 1**. Representation of Shields et al mechanism for the most abundant fragment ions observed for (a) [**1**-**3**+Cu]$^+$: [$a_i$+Cu-H]$^+$ fragment ion formation by direct cleavage from N-terminal cuprated peptide ions and (b) of [$b_i$+Cu-H]$^+$ fragment ions from N-terminal cuprated peptide ions, similar to that proposed by Yalcin [66]. Other possible mechanisms are described in Shields [18].

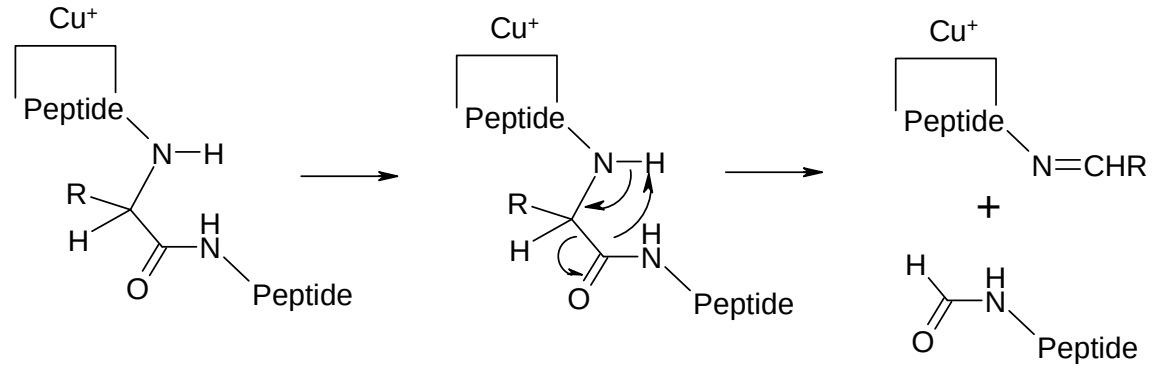


a

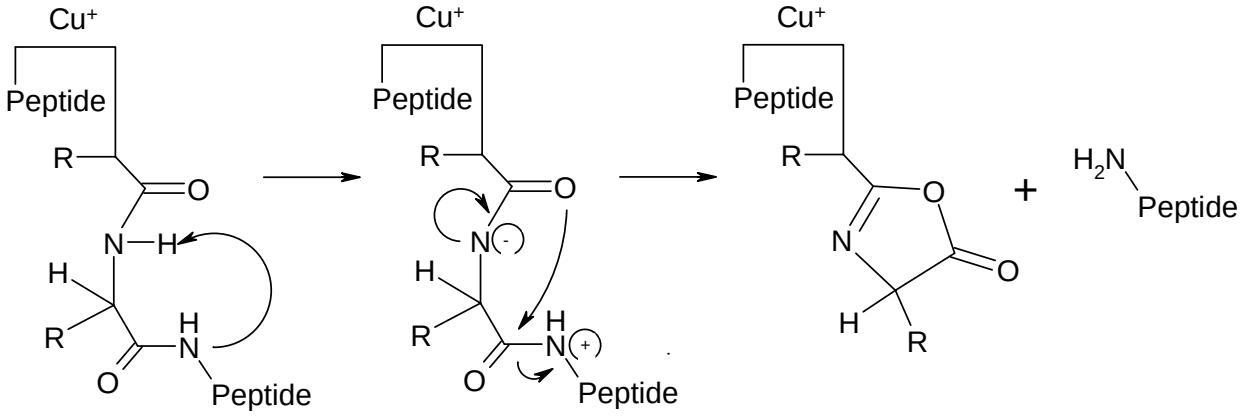


b

ions to [**2**+Cu]$^+$ and [**3**+Cu]$^+$, based upon the favorable energetics of $Cu^+$ binding to His and Lys. Ongoing studies of the nature of the arginine side chain in protonated peptides by this research group indicate that the protonated side chain resembles a carbocation and through resonance, is quite stable [67]. As such, fragmentation of [**1**+H]$^+$ does not adhere to the mobile proton model. The proton transfers inherent in our mechanism may be facilitated by efficient charge-solvation in the peptide ions, examples of which are shown in our candidate structure images. Though the effects of IM interactions and peptide conformation on fragmentation chemistry are not entirely understood, efforts to understand the connections between structure and reactivity of peptide ions are ongoing [42,43,46,49]. These effects are very important as the strengths of peptide backbone bonds are within 10% of each other [68].

**Conclusions**

The results presented here support our earlier charge-directed mechanism for fragmentation of [M+Cu]$^+$ ions [18]. Although we initially believed that our studies would provide an excellent test of Allison's mechanism for fragmentation of phosphonium acetylated VGVAPG, the model peptides possessed significantly different capacities for charge solvation, owing to the steric bulk of the charged group used by Allison. The product ion distributions of [M+H]$^+$, [M+Na]$^+$ and [M+Cu]$^+$ ions give an indication as to the nature of the interaction of the metal ions with the peptide. Candidate structures obtained from the ion mobility measurements and theoretical treatment of these data emphasized the effects of charge location and solvation within a peptide ion upon its fragmentation chemistry, which are not completely understood.

# CHAPTER III

# SECONDARY STRUCTURE AND CHARGE-SOLVATION EFFECTS UPON PEPTIDE FRAGMENTATION VIA PROMPT 193-NM PHOTODISSOCIATION AND HIGH-ENERGY CID TOF-TOF-MS

## Introduction

The relation of structure and reactivity in gas-phase peptide ions continues to be an area of interest to mass spectrometrists. Although most applications of peptide/protein mass spectrometry are aimed at determination of primary structure (*e.g.*, amino acid sequence or site-specific determination of post-translational modifications), techniques such as H/D exchange and ion mobility-mass spectrometry (IM-MS) have made it possible to extract detailed information related to secondary and tertiary structure. We recently initiated a series of studies aimed at delineating the effects of secondary structure on the fragmentation of gas-phase peptide ions [69,70]. For example, we have designed and synthesized a series of peptides having specific charge carriers, basic amino acids or side-chains having high metal ion affinities. We begin by determining candidate ion structure(s) by using IM-MS and molecular dynamics and then examine the effects of various experimental parameters on the product ions of fragmentation reactions. Here, we report results from ion mobility-mass spectrometry (IM-MS) and molecular dynamics simulations on a series of model peptide ions, specifically $[M + H]^+$ ions of XVGVAZG, where X is R, K, or H and Z is G, S, or P, and this information is then used to rationalize differences between prompt photofragment ion spectra and TOF-TOF collision-induced dissociation (CID) spectra. The prompt

photofragmentation technique is used to measure the product ions formed by photoexcited ions with lifetimes of less than 1 μs [70], whereas the product ions contained in CID TOF-TOF are formed by collisionally activated ions dissociating with a broad range of ion lifetimes, extending to 10-20 μs, depending on the instrument geometry.

Our level of understanding of peptide ion fragmentation is based on results from experiments utilizing a variety of activation methods, *e.g.*, collision-induced dissociation (CID) [34,71], surface-induced dissociation (SID) [50,72,73], and photodissociation [74,75], but the product ions measured in these experiments are formed over a broad range of ion lifetimes. Signal integration over a long time period is advantageous for analytical studies, because this increases the total abundances of product ions; however, for mechanistic studies it is advantageous to select a relatively narrow range of ion lifetimes or relatively narrow range of internal energies. Specific details of the fragmentation pathways and the influence of various experimental parameters are presented in a number of excellent reviews and papers [46,76-81]. On the other hand, with the exception of our earlier work, where we showed that ion lifetimes have a dramatic effect on the fragmentation reactions of poly-amino acid radical cations, the effects of ion lifetimes has been largely ignored.

The effects of intramolecular interactions on peptide ion fragmentation have also received very little attention, in part because of difficulties associated with assigning structure to gas-phase ions. Keough demonstrated that incorporation of N-terminal charge carrying groups increased the yield of N-terminal fragment ions while reducing

the yield for C-terminal ions, with the end result being reduced spectral congestion of tandem mass spectra [14]. Allison used a similar derivatization scheme to study charge-remote site fragmentation reactions of model peptide ions [16], and Wysocki used this same approach [20] to examine the effects of intramolecular interactions on both fragmentation and H/D exchange reactions of singly and doubly-charged gas-phase peptide ions (amino acid sequence LDIFSDF) derivatized with a tris(trimethoxyphenyl)phosphonium acetyl group using H/D exchange mass spectrometry [82]. H/D exchange data was interpreted in terms of two populations: (i) ions that did not undergo H/D exchange and (ii) ions that exchanged a range of 6-11 protons. They suggested that the non-exchanging population contained an ionizing proton that is immobilized by IM interactions, which prevents exchange with the deuterating reagent. The authors suggested that multiple reacting conformations were being probed in the experiment; however, they did not provide candidate structures for the different ions. Wysocki also suggested that the degree of lability of specific hydrogen atoms may indicate preferred sites of fragmentation even in the absence of a proximal charge. For example, the electrostatic potential map suggests that the phosphonium acetyl derivative does not interact strongly with the peptide backbone to which it is attached, thus charge is localized on the derivative.

We have examined a number of model peptides containing N-terminal charge carrying amino acids and found that the fragmentation reactions of these ions share similarities with the N-terminal charge carrying model peptides discussed above. Here, we report results of fragmentation studies on a specific set of N-terminal charge carrying

peptide ions and the results are both similar and dissimilar to those obtained reported above. That is, the CID TOF-TOF spectra share many similarities to CID spectra of N-terminal charge carriers; however, prompt dissociation of photoexcited $[M + H]^+$ ions yield quite different fragment ions. That is, prompt photofragment ion spectra contain abundant $a_i$ and side chain cleavage product ions, similar to those reported by Allison. We interpret these data as evidence for remote charge-site fragmentations.

**Experimental**

Reagents for peptide synthesis were purchased from Advanced Chemtech (Louisville, KY, USA) and used without further purification. The series of homologous peptides described here were prepared on solid support using Fmoc chemistry. A more detailed description of the peptide synthesis is provided elsewhere [83]. α-Cyano-4-hydroxycinnamic acid (CHCA) was obtained from Sigma-Aldrich (St. Louis, MO, USA) and re-crystallized prior to use. Stock solutions of peptides were prepared at 50 μg/mL concentration using distilled, deionized water and then mixed 1:1 with 12 mg/mL CHCA. 0.5 μL droplets of the resultant solution were spotted onto a stainless steel MALDI stage and dried under forced air at room temperature.

The homebuilt instrument used to measure the collision cross-sections of each peptide ion has been described previously [84]. The ions are formed by MALDI (337-nm $N_2$ laser) using CHCA. The ions are accelerated from the sample plate and then injected into a 30.5-cm drift tube maintained at *ca.* 1 torr of He gas. Ions exiting the drift tube are guided using a 5-element Einzel lens into an o-TOF source and mass analyzed.

High energy CID spectra were acquired using the ABM 4700 [85,86]. Collision gas pressure was set to medium, and 1 keV of laboratory frame collision energy was used. The prompt 193-nm photodissociation studies were carried out using a homebuilt TOF-TOF instrument that has been described elsewhere [87]. Briefly, MALDI-formed ions are accelerated via delayed extraction to 15 keV into a 0.52-m linear TOF. Ions of interest are selected via a parallel plate timed-ion-selector and then decelerated to 8 keV as they enter a biases photodissociation cell [70]. Selected ions are irradiated at the center of the cell with a 17-ns pulse from an ArF excimer laser (Model LPX100i, Lambda Physik, Acton, MA, USA). The laser fluence was adjusted to achieve *ca.* 10-20% beam attenuation in an effort to minimize multi-photon dissociation. Under these conditions, a fraction of photoactivated ions dissociate prior to exiting the cell. The ions spend less than 1 μs in the photoactivation cell subsequent to irradiation, therefore the observed ions decay with rate constants greater than $10^6$ $s^{-1}$, are reaccelerated and mass analyzed in the 2.9-m reflectron TOF.

Generation of candidate structures was performed using Insight$^{II}$ and Cerius$^2$ (Accelrys, San Diego, California, USA) [57,58] and the CFF 1.02 force field [59]; two stages of simulated annealing were then applied to each starting structure. The annealing algorithm simulates a series of 280 ps-duration symmetric 1000 K temperature ramp/relaxation cycles. Three hundred of these cycles are performed, with each resultant structure retained for further analysis. The results of the first and second simulated annealing runs for each structure were compared; additional simulations were deemed unnecessary as the average change in potential energies for the confirmatory

simulations (*ca*. 0.6 kcal $mol^{-1}$) were within one standard deviation (*ca*. 5 kcal $mol^{-1}$) of a single simulation.

Calculations of the collision cross-sections were performed using a modified version of MOBCAL [38], a Cartesian coordinates collision cross-section averaging program developed by Jarrold, that had been given an expanded atomic parameter list. Energetics and cross-section output were examined as cluster plots. Structure candidates were selected according to their agreement with measured cross section and low potential energy; representative structures for each ion are presented.

**Results and Discussion**

The XVGVAZG peptides were designed to examine the effects of various N-terminal charge carriers on peptide fragmentation reactions. The N-terminal charge carriers used by Wysocki and Allison are bulky and inhibit intramolecular interactions between the charge site and polar functional groups. On the other hand, the X group of the XVGVAZG peptides is relatively small and can easily interact with peptide backbone as well as polar side chains. On the basis of previous ion mobility-mass spectrometry (IM-MS) studies of model peptides containing basic N-terminal amino acids as well as IMS studies of the XVGVAZG peptides it appears that the $[M + H]^+$ ions adopt highly charge-solvated structures. That is, the N-terminus of X (R, K, or H) as well as the basic side chain groups are protonated and solvated by the anionic carboxylate group. This type of structure has been proposed previous to explain both fragmentation reaction chemistry as well as products formed by H/D exchange reactions [88]. The carboxylate group inserts between the two cationic sites, shielding the

Coulombic repulsion between the positively-charged groups and lending structural rigidity to the ions [49]. Although these types of salt-bridged structures are generally more energetic than charge-solvated structures, based upon the sequence of the peptide, the difference in energy may become small relative to the energy of intramolecular interactions [89].

In comparing the structures of the glycine peptides (**5**, **7**, **9**) to their serine-containing analogs (**6**, **8**, **10**), it is noteworthy that the serine side chains are not involved in the intramolecular H-bonding scheme. This is due to a combination of factors. First, the serine hydroxyl group is neither flexible nor large relative to the peptide backbone. Also, the strength of the interaction of serine with the backbone carbonyl groups is much weaker that the ion-dipole interactions that the peptide undergoes in the adopted low-energy structures [90]. In addition, for the serine hydroxyl group to participate in the IM interaction shown in our model, the residue would have to undergo a disfavored *cis-trans* isomerization [91]. It is interesting to note that the serine hydroxyl group is unsolvated in all low-energy structures obtained in the cluster analysis, regardless of the pre-annealing structure. These initial structures included right-handed α-helices, β-hairpins, and fully extended populations.

The CID spectrum of [**1**+H]$^+$ (**Figure 10a)** contains abundant $b_i$- and $y_i$-type ions, conversely, the photofragment ion spectrum (**Figure 10b**) contains primarily $a_i$ and $d_{ai}$ fragment ions and fragment ions resulting from the loss of small neutrals. It is also apparent that the S/N ratios in the photodissociation data are not as high as in the high-energy CID data, likely owing to the sampling of only the fragment ions formed within 1 μs of activation and the better-optimized ion focusing optics of the commercial instrument. The presence of mostly $a_i$-ions in the photofragment ion spectrum indicates that the fragmentation pathway favors charge retention at the N-terminus, which is intuitive based upon the peptide sequence. For the other peptides examined, this trend is also observed, as will be discussed. There are also notable differences in the tandem mass spectra of [**5**+H]$^+$ (**Figure 11**). For example, the abundances of $y_i$ ions in the CID spectrum for **2** is lower than that for the CID spectrum of [**1**+H]$^+$, and $y_i$ ions are not observed in the prompt photofragment ion spectrum.

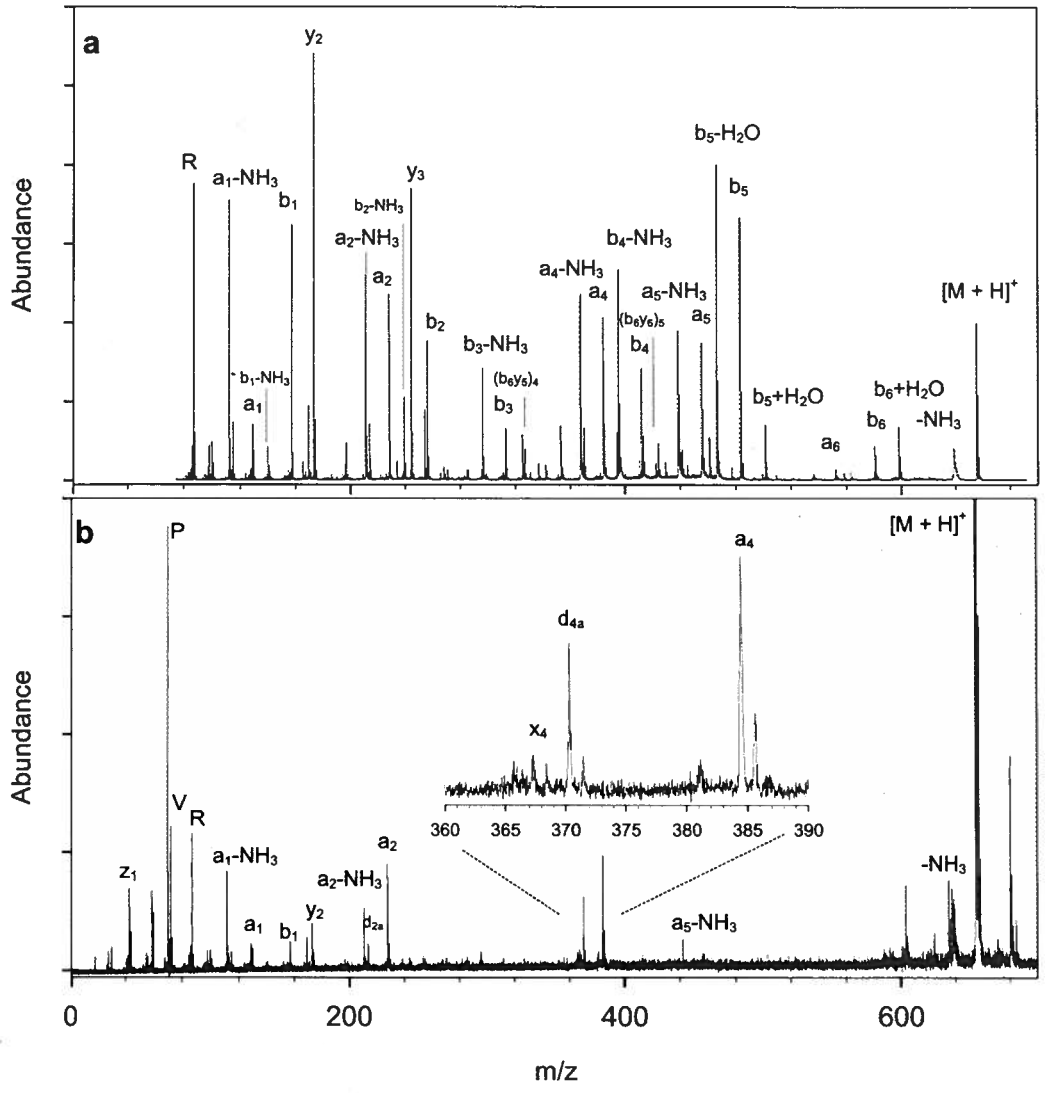


**Figure 10**. Tandem mass spectra for $[RVGVAPG+H]^+$.using (a) high-energy CID TOF-TOF and (b) photodissociation TOF-TOF.

In addition, $d_{ia}$ ions are observed in both fragment ion spectra and the abundance of small neutral loss fragments in the CID spectrum is nearly the same as for the intact backbone cleavage product ions. Collision cross sections for all relevant ions are contained in **Table 4**.

**Table 4**. Collision cross sections of XVGVAGG and XVGVASG ions.

| Collision cross sections of ions, $Å^2$ | | | |
|---|---|---|---|
| Peptide | $H^+$ | $Na^+$ | $Cu^+$ |
| RVGVAGG, **5** | 177.8 | 181.4 | 206.3 |
| RVGVASG, **6** | 184.8 | 191.5 | 200.2 |
| HVGVAGG, **7** | 169.9 | 176.4 | 186.5 |
| HVGVASG, **8** | 180.4 | 187.2 | 197.5 |
| KVGVAGG, **9** | 172.4 | 179.2 | 187 |
| KVGVASG, **10** | 177.7 | 181.8 | 193.8 |

A structural representation for $[\mathbf{5}+H]^+$ is shown for reference in **Figure 12**. For peptide ions $[\mathbf{6\text{-}10}+H]^+$, the tandem mass spectra and ionic structure representations, shown in **Figures 13-22**, show similar properties to those discussed for the arginine peptides. The most notable feature of the remaining ions is the flexibility of the lysine side chain in ions **9** and **10** which allows for efficient packing about the carboxylate group and the formation of a stable structure.

For each of the ions examined, the photofragmentation and CID of the peptide ions yield different results. Though the ions observed in the photofragment ion spectra are explainable by the single low-energy conformation determined by ion mobility measurements and molecular dynamics simulations, the same cannot be said for the fragment ions observed in the CID spectra for the same ions. The CID-formed fragment ions are the result of internal reorganization of the ion, either by charge migration via the mobile proton model, or the formation of a distribution of reactive structures, where subsequent fragmentation produces a large number of fragment ions. For the above-mentioned reasons, we can say that the conformation of a gas-phase peptide ion determines, to some degree, the types of fragments observed. In addition, the type of intramolecular interactions adopted by the ions is important. In peptide ions without a tendency to form stable low-energy conformations (i.e. those without salt bridges), the ion of interest may exist in several accessible conformations, and the differences in observed fragment ions may be minimized.

A survey of published photodissociation data for protonated peptides with an N-terminal basic residue [74,75,79,87,92], suggests that the position of valine residues within the activated peptide ions often directs the fragmentation to favor $a_i$ and $d_{ai}$ ions at the valine residue. This effect is observed for both 157-nm and 193-nm light and for a large number of peptides. Though, in the surveyed literature, no two peptides were homologs, so other contributing factors to the fragmentation could not be eliminated.

In order to more completely understand the effects of valine position on the fragmentation patterns observed in the photodissociation of peptide ions, we fragmented the isomer ions $[RVGVAGG+H]^+$ and $[RAVGVGG+H]^+$ under the same conditions. As can be observed in **Figure 5**, the $a_5/d_{a5}$ and $a_3/d_{a3}$ fragment ion pairs appear, whereas the $a_4/d_{a4}$ and $a_2/d_{a2}$ fragment ion pairs disappear. The formation of a stable $a_i$ ion terminated with a valine residue is the explanation. This indicates that the fragmentation mechanism at work in these peptides is charge-directed. If there were no influence from the residue itself, as in a charge-remote mechanism, then these strong isomeric effects would not be observed.

**Conclusions**

For our systems, the influence of intramolecular charge solvation plays a strong role in the fragment ions observed in the prompt photodissociation experiments. In those experiments, the types of fragments observed (high $a_i$ and $d_{ai}$ ion current and little else), correspond to a mechanism where the charge is sequestered at the N-terminal residue [93] and the position of valine residues directs the formation of abundant fragment ions. Alternatively, in CID experiments performed on the same ions, the initial conformation and intramolecular interactions are less important. Collisional activation mobilizes the ionizing proton and the experiment allows sufficient time for the reorganization of the gas-phase conformation, decreasing the influence of initial charge solvation schemes according to a charge-directed mechanism. For the photodissociation experiments upon these peptides, the fragmentation is rationalized in terms of a remote charge-site mechanism.

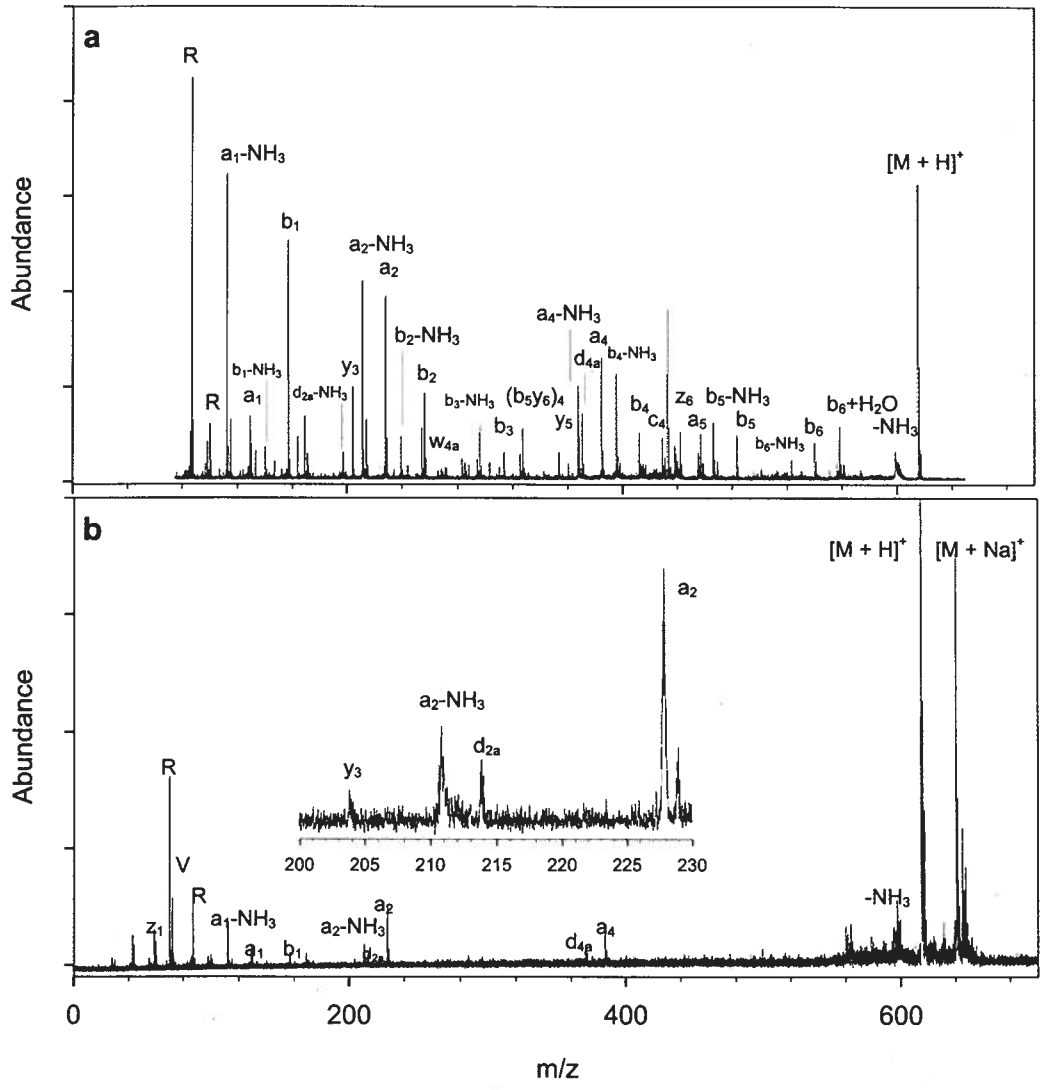


**Figure 11**. Tandem mass spectra for $[RVGVAGG+H]^+$.using (a) high-energy CID TOF-TOF and (b) photodissociation TOF-TOF.

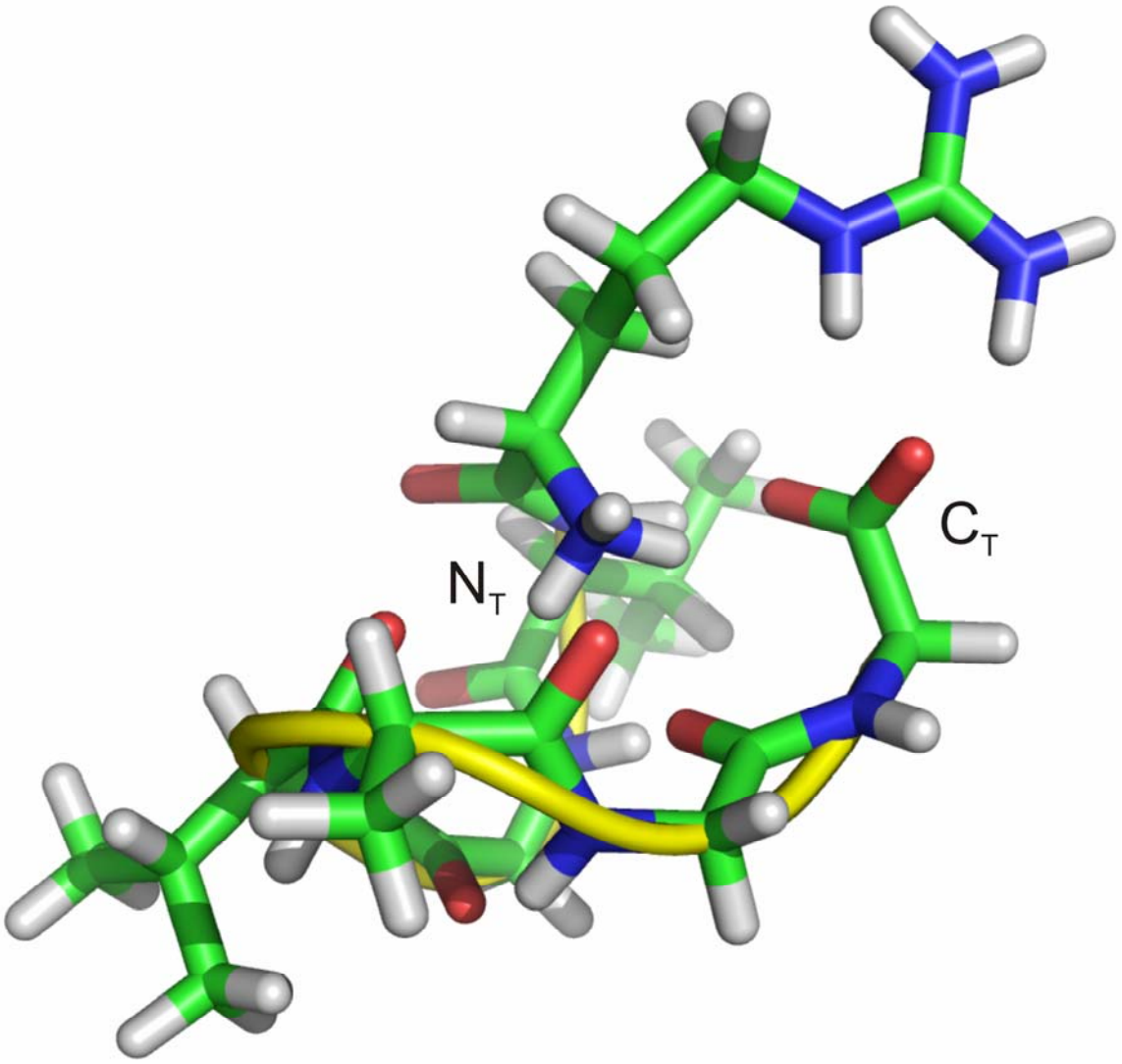


**Figure 12**. Candidate structure obtained for $[RVGVAGG+H]^+$.

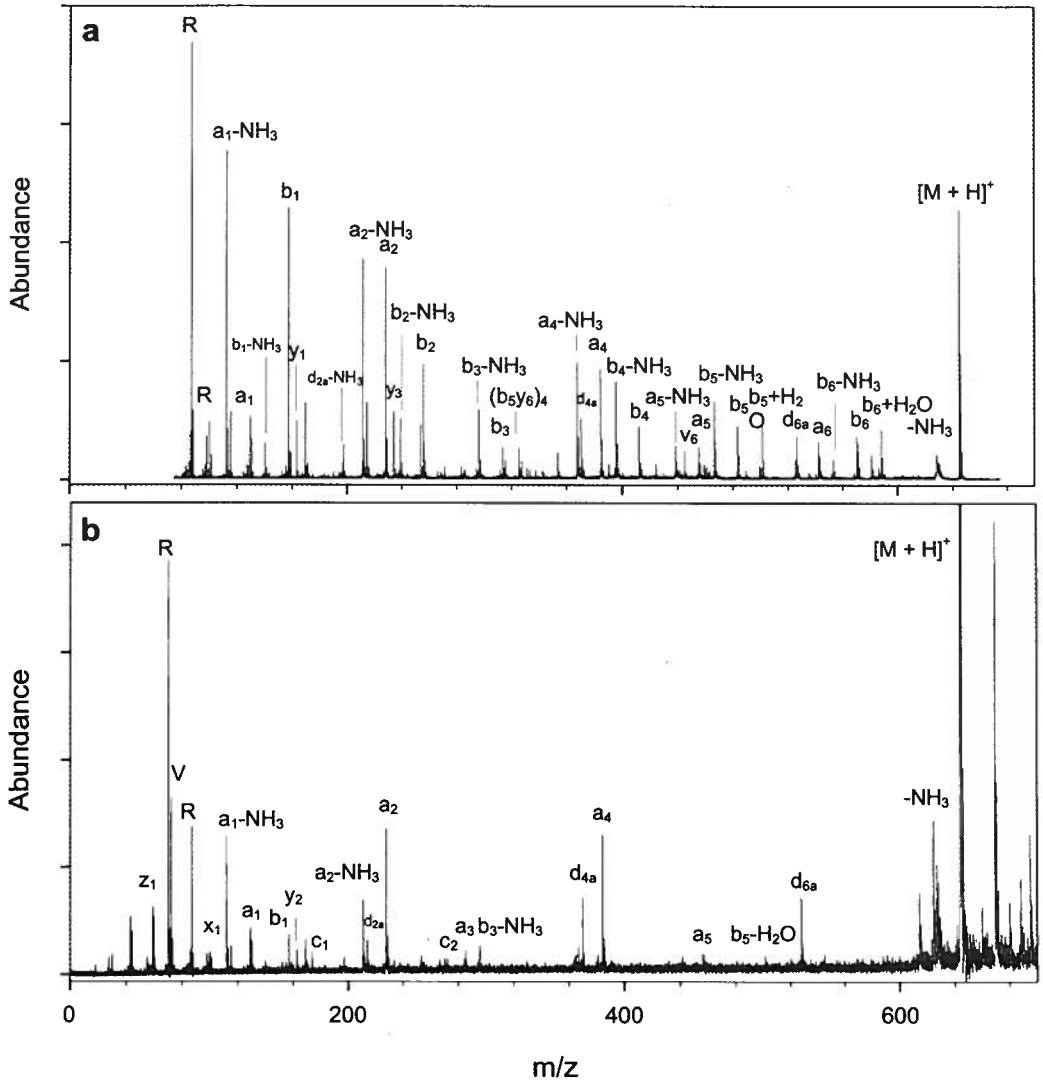


**Figure 13**. Tandem mass spectra for $[RVGVASG+H]^+$.using (a) high-energy CID TOF-TOF and (b) photodissociation TOF-TOF.

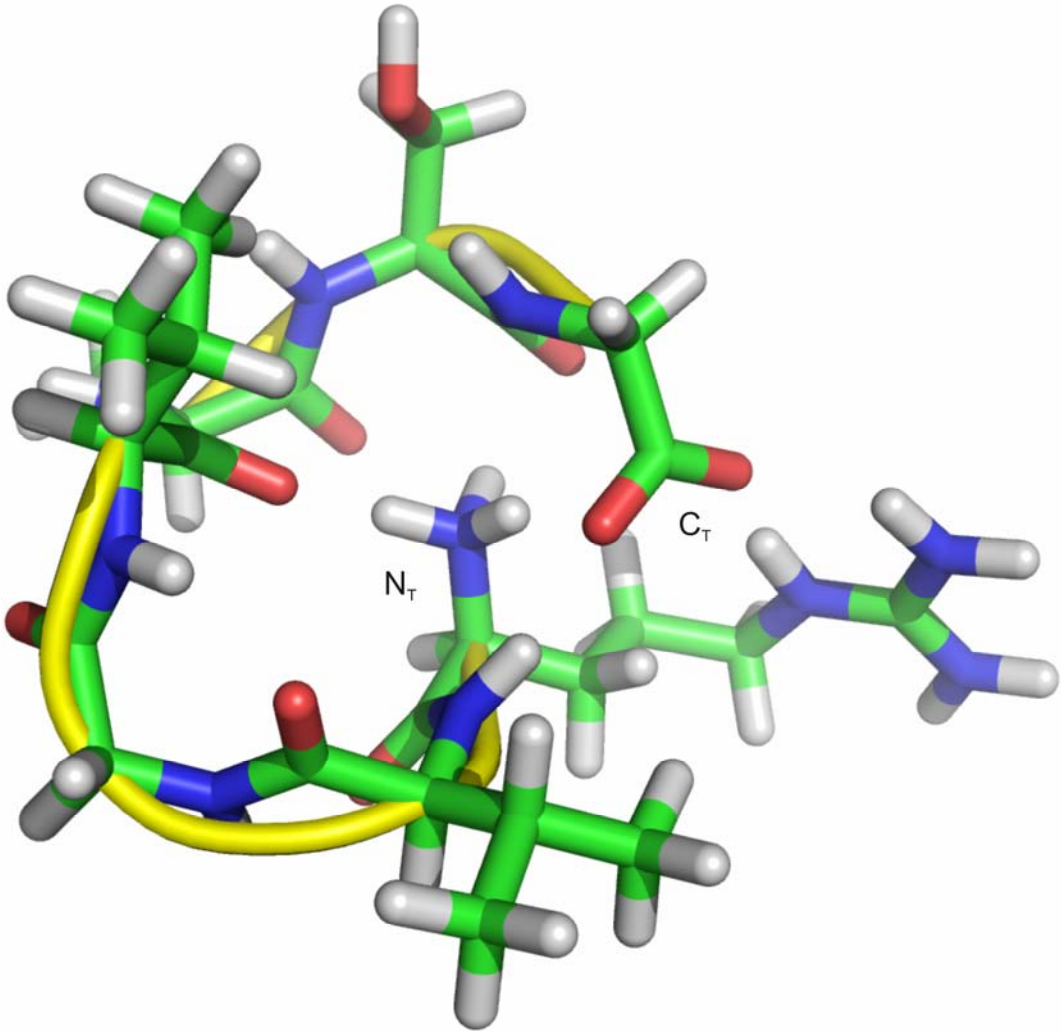


**Figure 14**. Candidate structure obtained for $[RVGVASG+H]^+$.

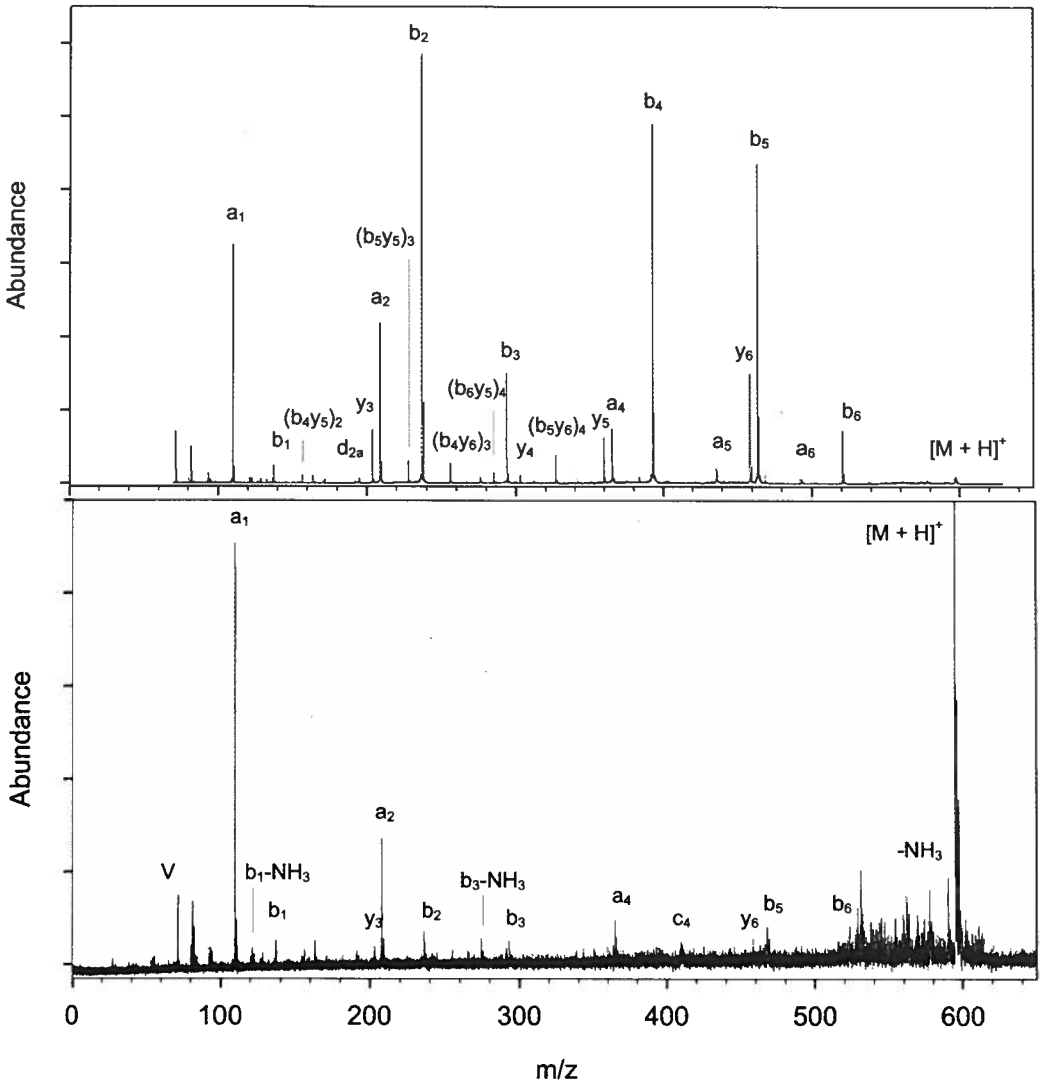


**Figure 15**. Tandem mass spectra for $[HVGVAGG+H]^+$.using (a) high-energy CID TOF-TOF and (b) photodissociation TOF-TOF.

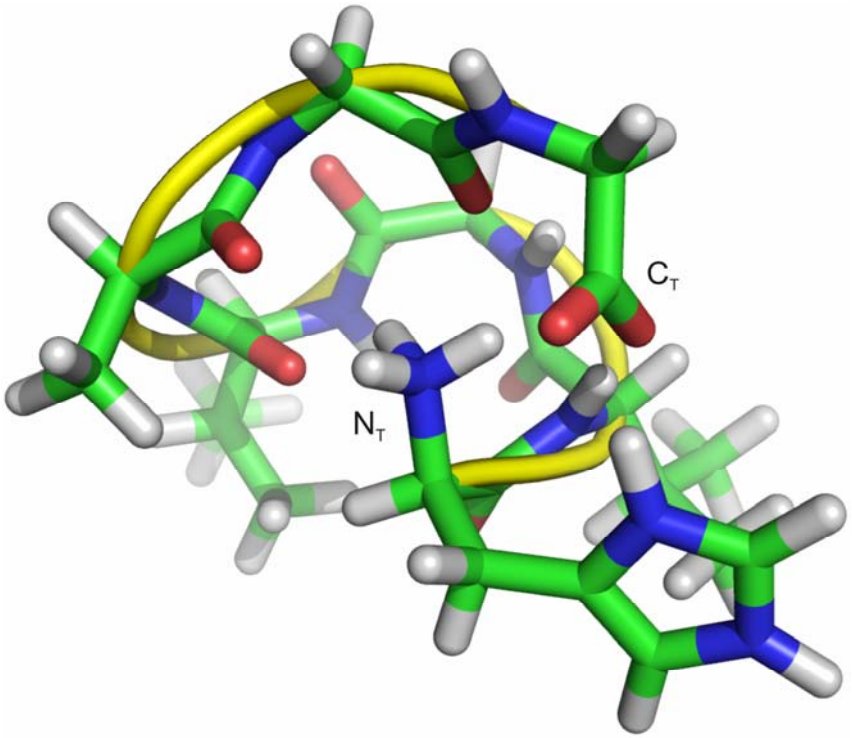


**Figure 16**. Candidate structure obtained for $[HVGVAGG+H]^+$.

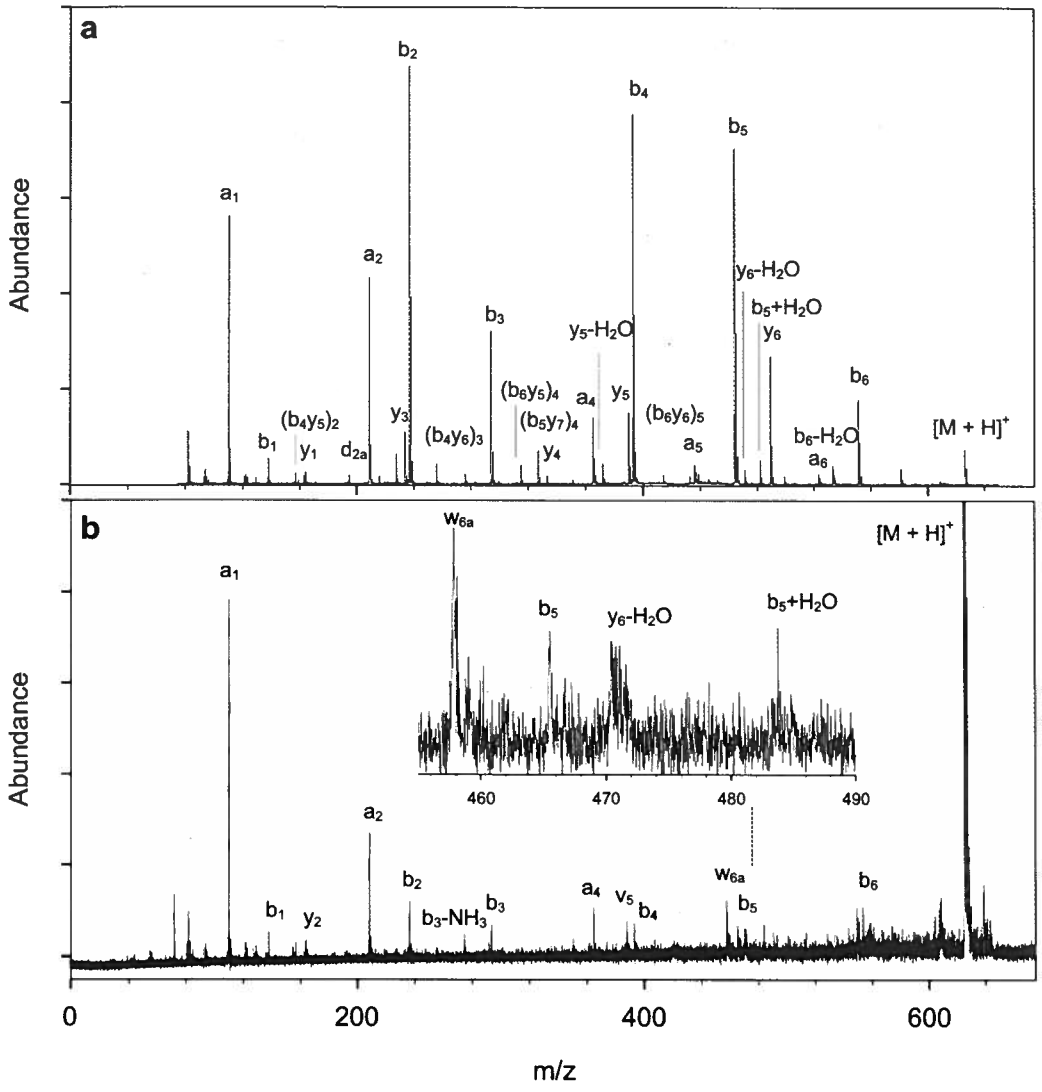


**Figure 17**. Tandem mass spectra for $[HVGVASG+H]^+$.using (a) high-energy CID TOF-TOF and (b) photodissociation TOF-TOF.

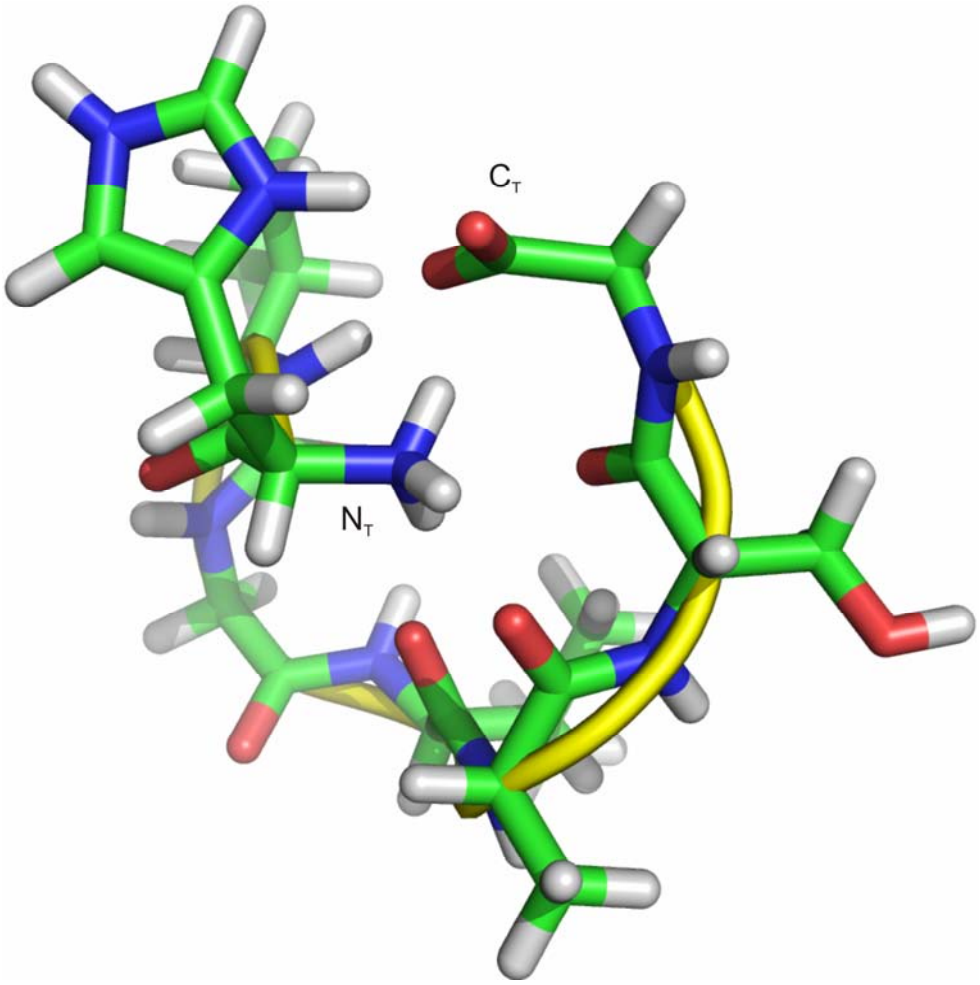


**Figure 18**. Candidate structure obtained for $[HVGVASG+H]^+$.

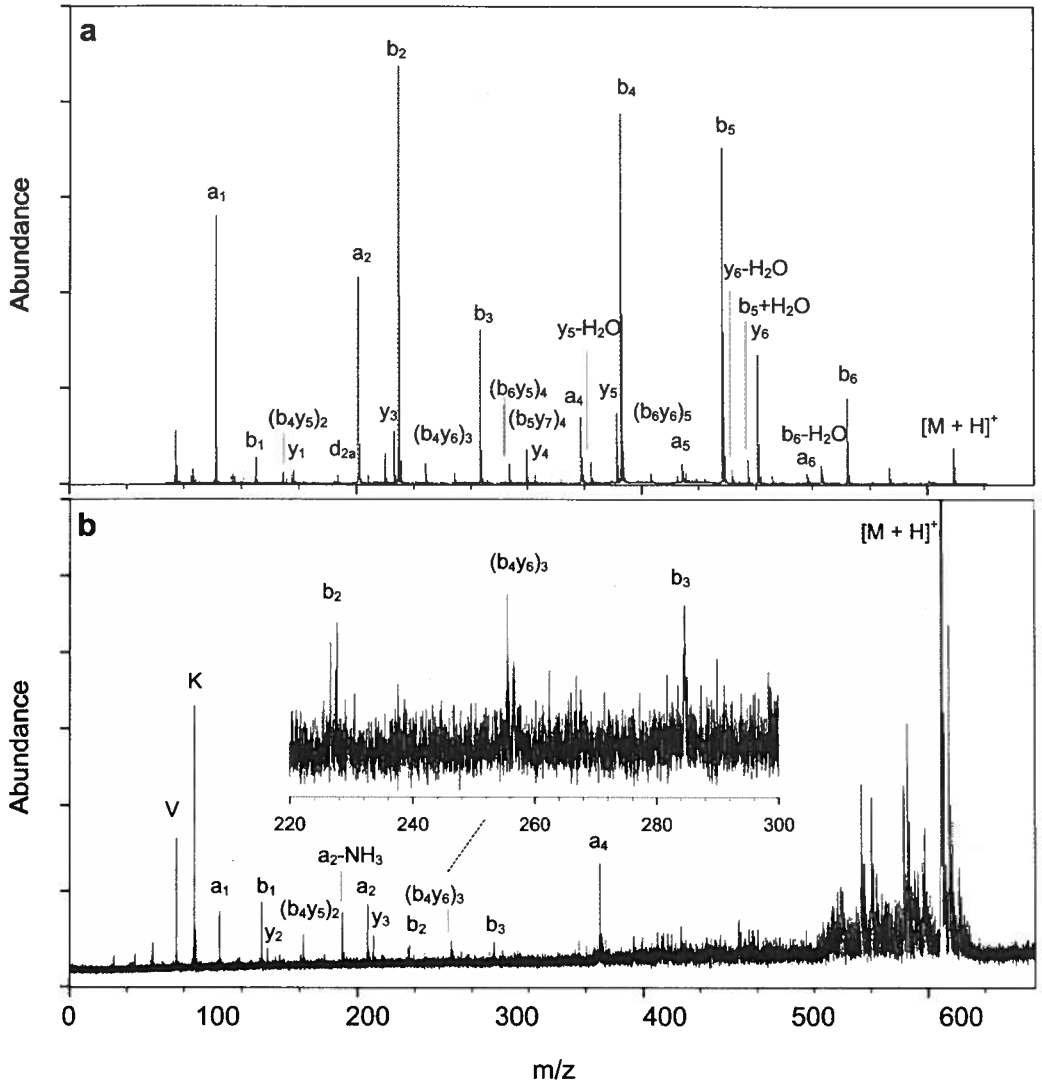


**Figure 19**. Tandem mass spectra for $[KVGVAGG+H]^+$.using (a) high-energy CID TOF-TOF and (b) photodissociation TOF-TOF.

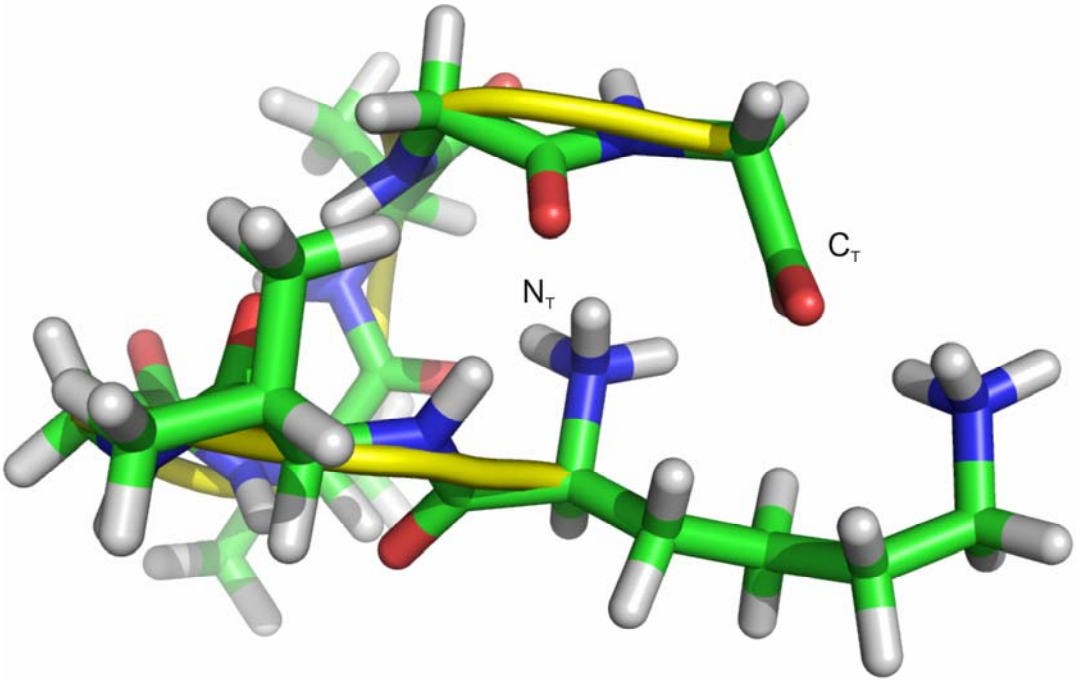


**Figure 20**. Candidate structure obtained for $[KVGVAGG+H]^+$.

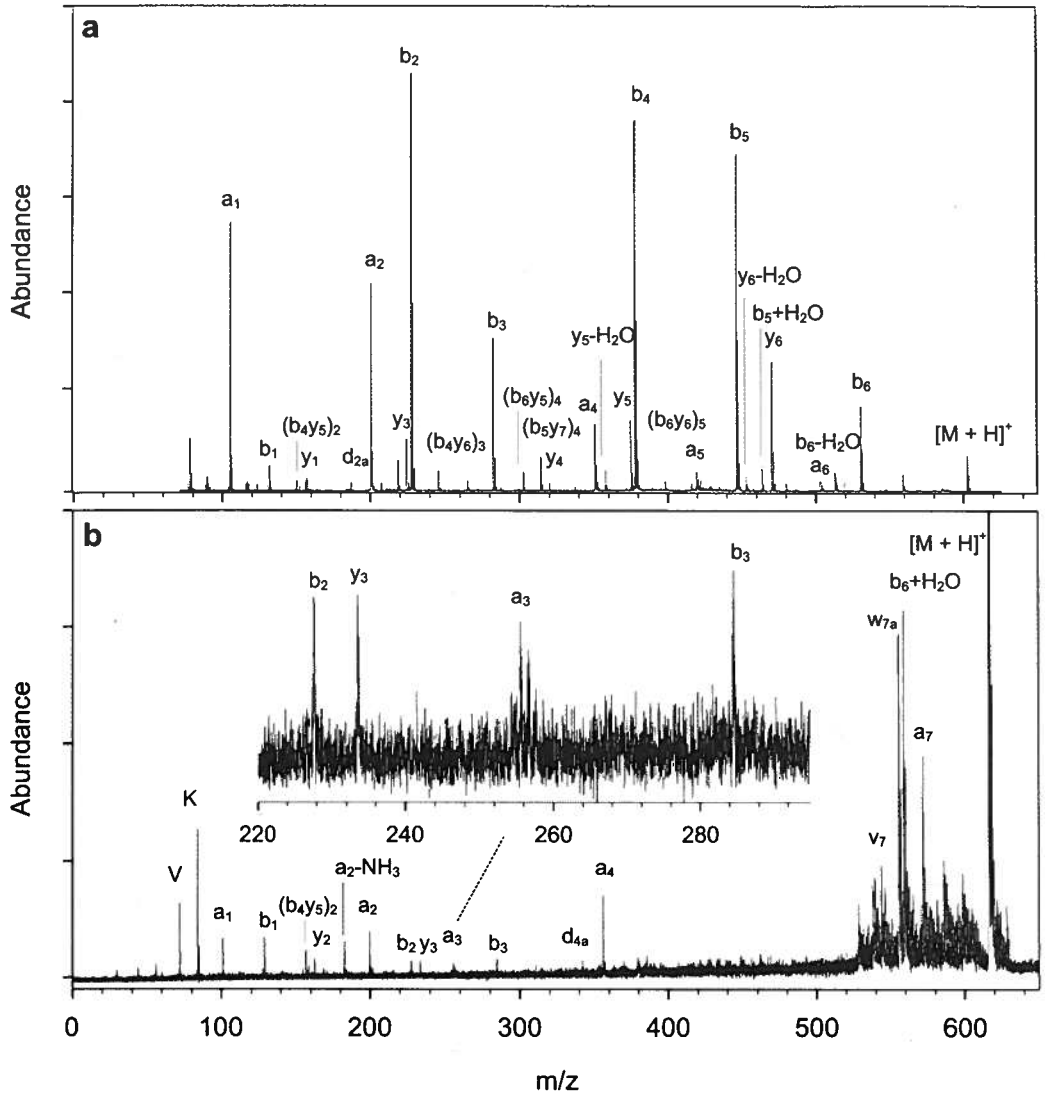


**Figure 21**. Tandem mass spectra for $[KVGVASG+H]^+$.using (a) high-energy CID TOF-TOF and (b) photodissociation TOF-TOF.

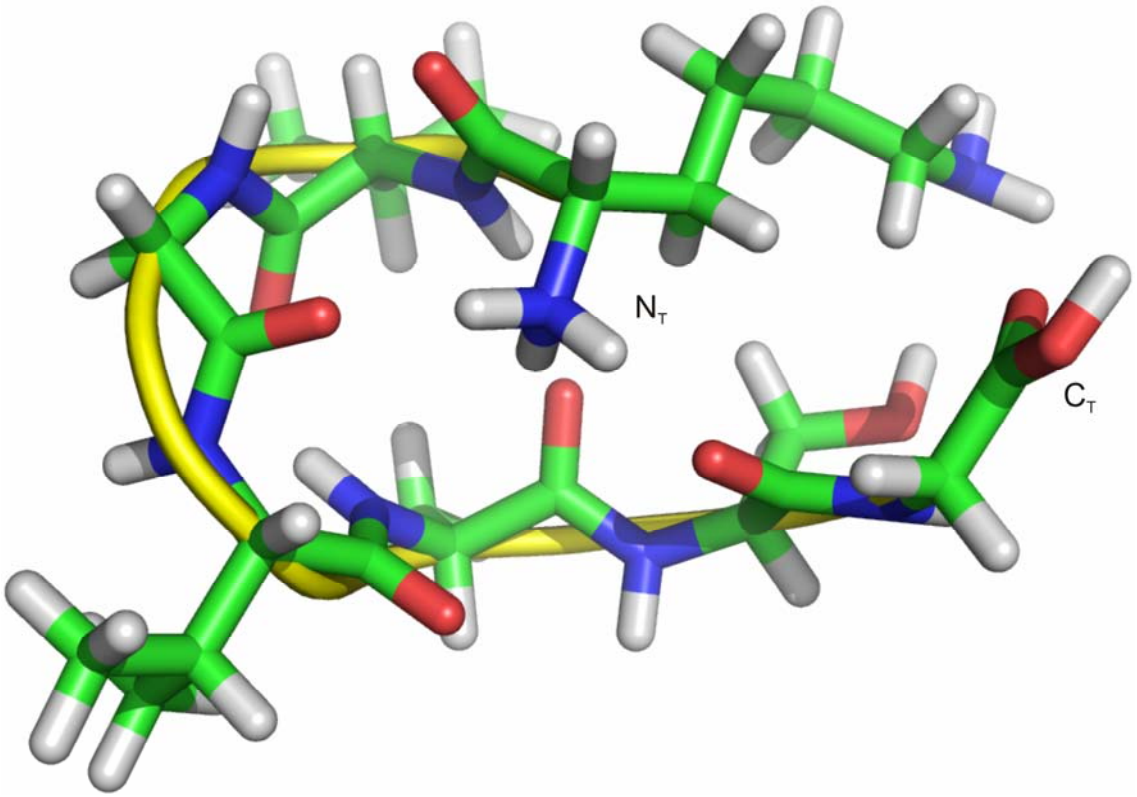


**Figure 22**. Candidate structure obtained for $[KVGVASG+H]^+$.

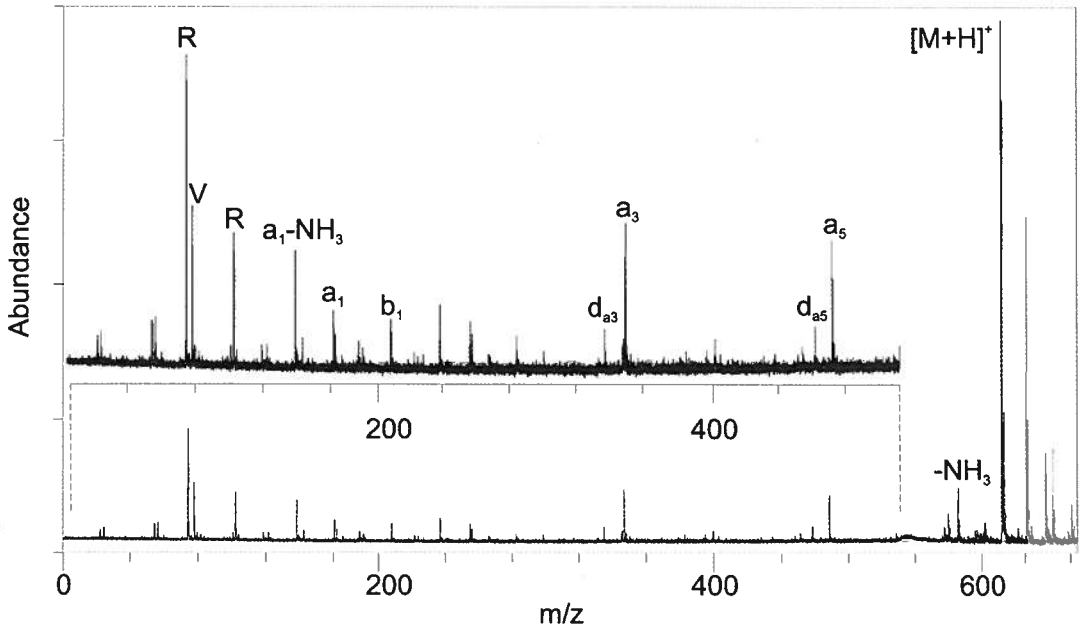


**Figure 23**. Photodissociation TOF-TOF spectrum for $[RAVGVGG+H]^+$.

In peptides that do not tend to form strongly charge-solvated structures, such as the phosphonium acetyl-derivatized ions of Allison or Wysocki, the observed differences between the products of both activation methods may be reduced.

# CHAPTER IV

# THE EFFECTS OF A SECOND HIGH PROTON/HIGH METAL ION AFFINITY RESIDUE ON PEPTIDE FRAGMENTATION

## Introduction

The preceding chapters have dealt with peptides that have one primary characteristic in common—a single basic residue at the N-terminus, or the lack thereof as a control. After the initial results with simple model peptides, we decided to move to more complex species, by replacing the sixth residue in the peptide backbone with histidine, introducing a second site of high proton and metal ion affinity. The peptides RVGVAHG (**11**), HVGVAHG, (**12**), KVGVAHG (**13**), and WVGVAHG (**14**), were prepared to examine the effects of a mid-chain competitor site and to probe whether the tryptophan residue would have any effect upon the fragmentation. An aspartic acid analogue was not prepared, as the residue's competition for the ionizing proton or the metal ion in the system was not thought to be sufficient to warrant study. In an effort to expand the study, additional metal ions, $Li^+$, $K^+$, and $Ag^+$ were used to further probe the fragmentation chemistry of the peptides.

## Experimental

The peptides were prepared as before, using the solid phase synthesis techniques outline in Chapter I. The metal doping to introduce the additional metal ions to the peptide sequences was performed in the same way as before, with the equal volumes of

dopant solution and peptide solution combined, where the final concentration of dopant is roughly 15 times that of the peptide.

**Results and Discussion**

Tandem mass spectra collected using high-energy CID TOF-TOF are shown in two clustersm the first showing spectra for the $[M+H]^+$, $[M+Cu]^+$ and $[M+Ag]^+$ ions and the second showing spectra for the $[M+Li]^+$, $[M+Na]^+$, and $[M+K]^+$ ions. The candidate structures obtained for the $[M+H]^+$, $[M+Na]^+$ and $[M+Cu]^+$ ions are shown between these two sets of spectra for an easier comparison of the spectra and precursor ion structures obtained. In the spectra shown, the ions which appear in red are those for which the charge site is different than the hypothesized location or, in the case of metalated precursor ions, it may also indicate that the fragment ion does not contain a metal ion, i. e., that the fragment ion is protonated. This seems to be most pronounced for the $[M+Li]^+$ species, which is thought to be a result of less-than-optimal ion selection prior to the activation process. That is to say, the $[M+Li]^+$ spectra include some fragments resulting from activation of $[M+H]^+$ ions. The non-metalated ions may also result from dissociation reactions in which the metal center is lost as part of the neutral fragment.

These spectra show that the $[M+Cu]^+$ and $[M+Ag]^+$ ions fragment similarly, with the main difference observed being the mass difference between $Cu^+$ and $Ag^+$ N-terminal fragment series. Both copper and silver have an isotopic signature, the most abundant of which are separated by 2 Da. The peptides that yield these fragment ion

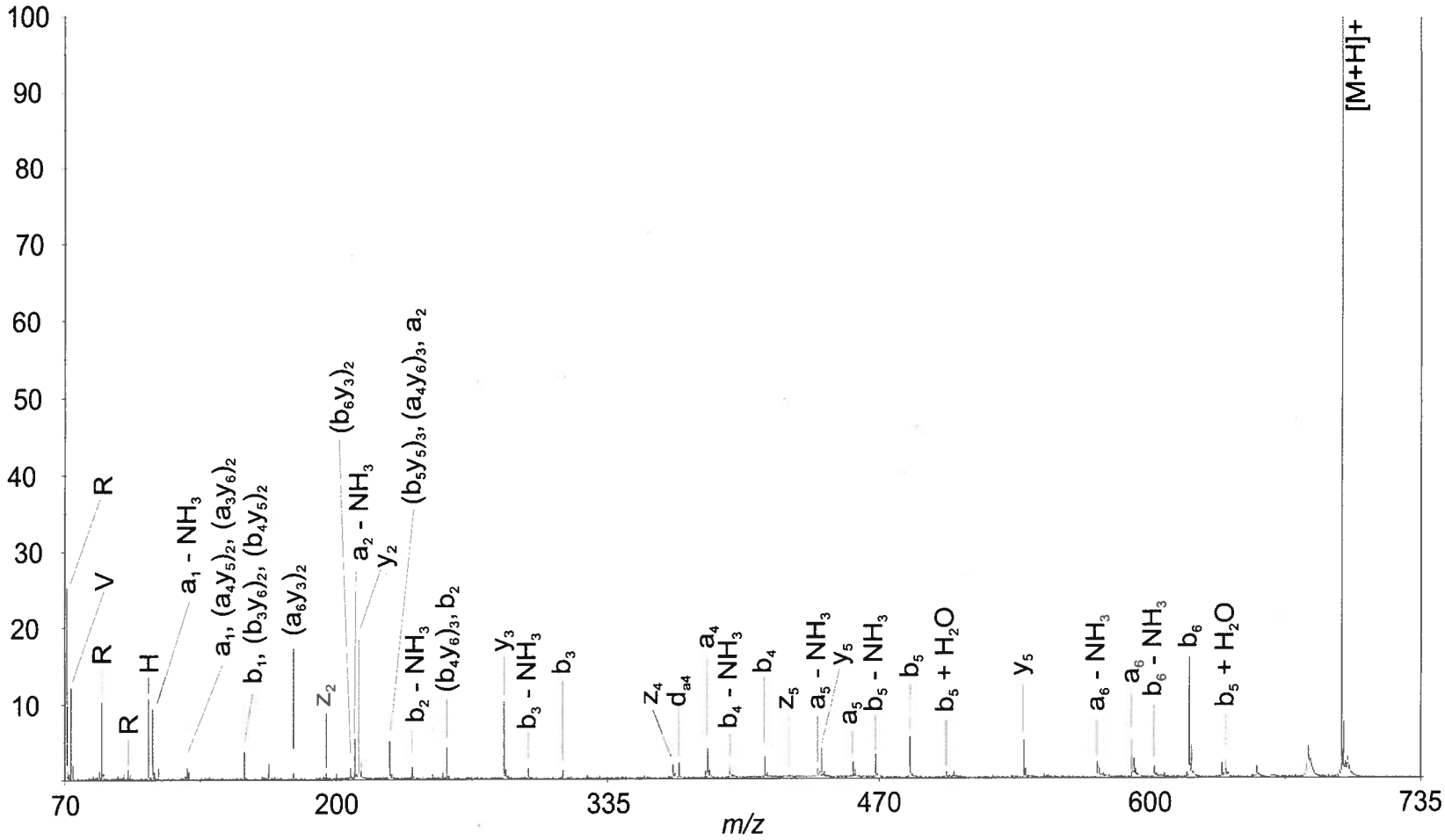


**Figure 24a**. High energy CID TOF-TOF spectrum for $[RVGVAHG+H]^+$.

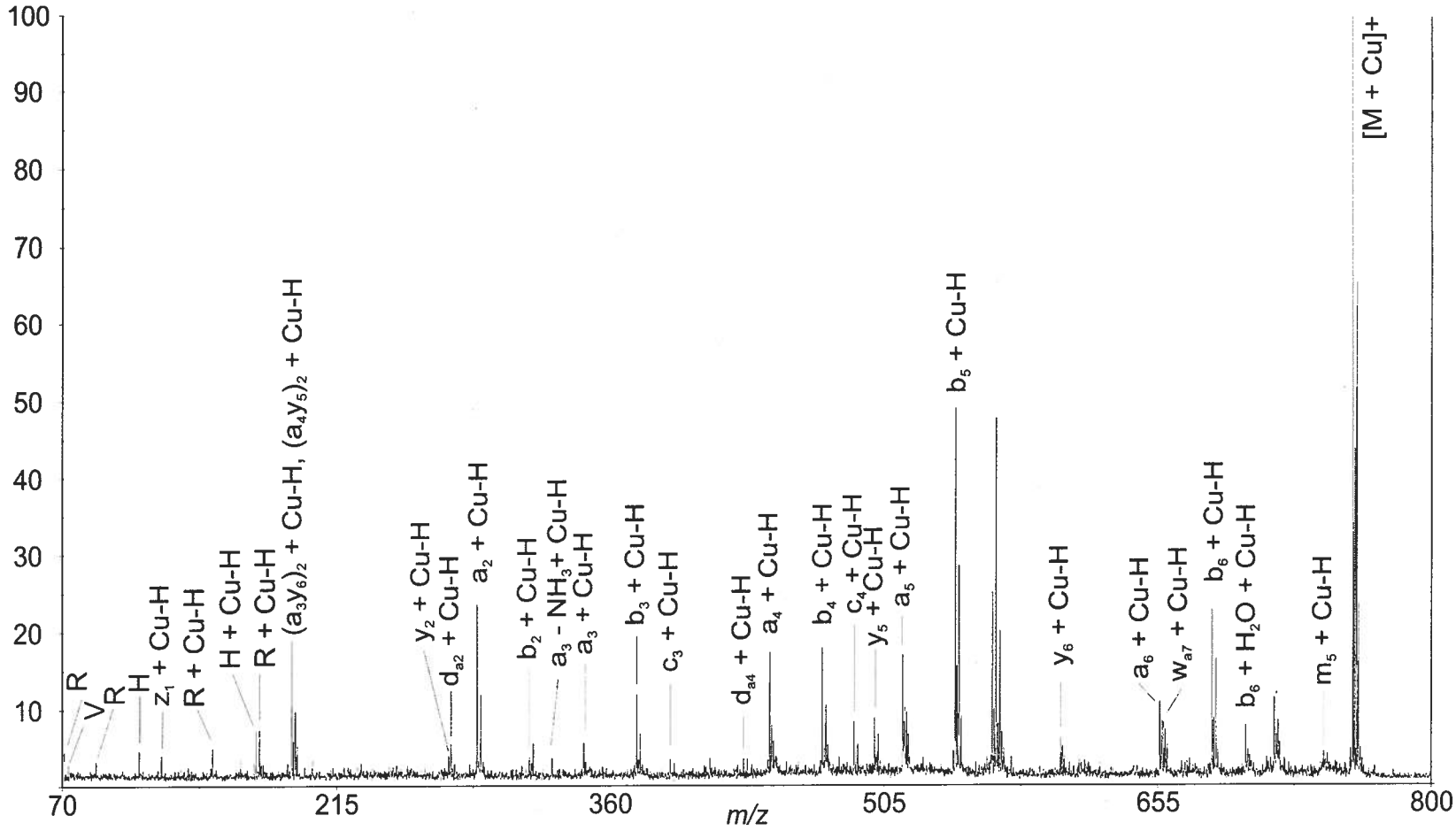


**Figure 24b**. High energy CID TOF-TOF spectrum for $[RVGVAHG+Cu]^{+}$.

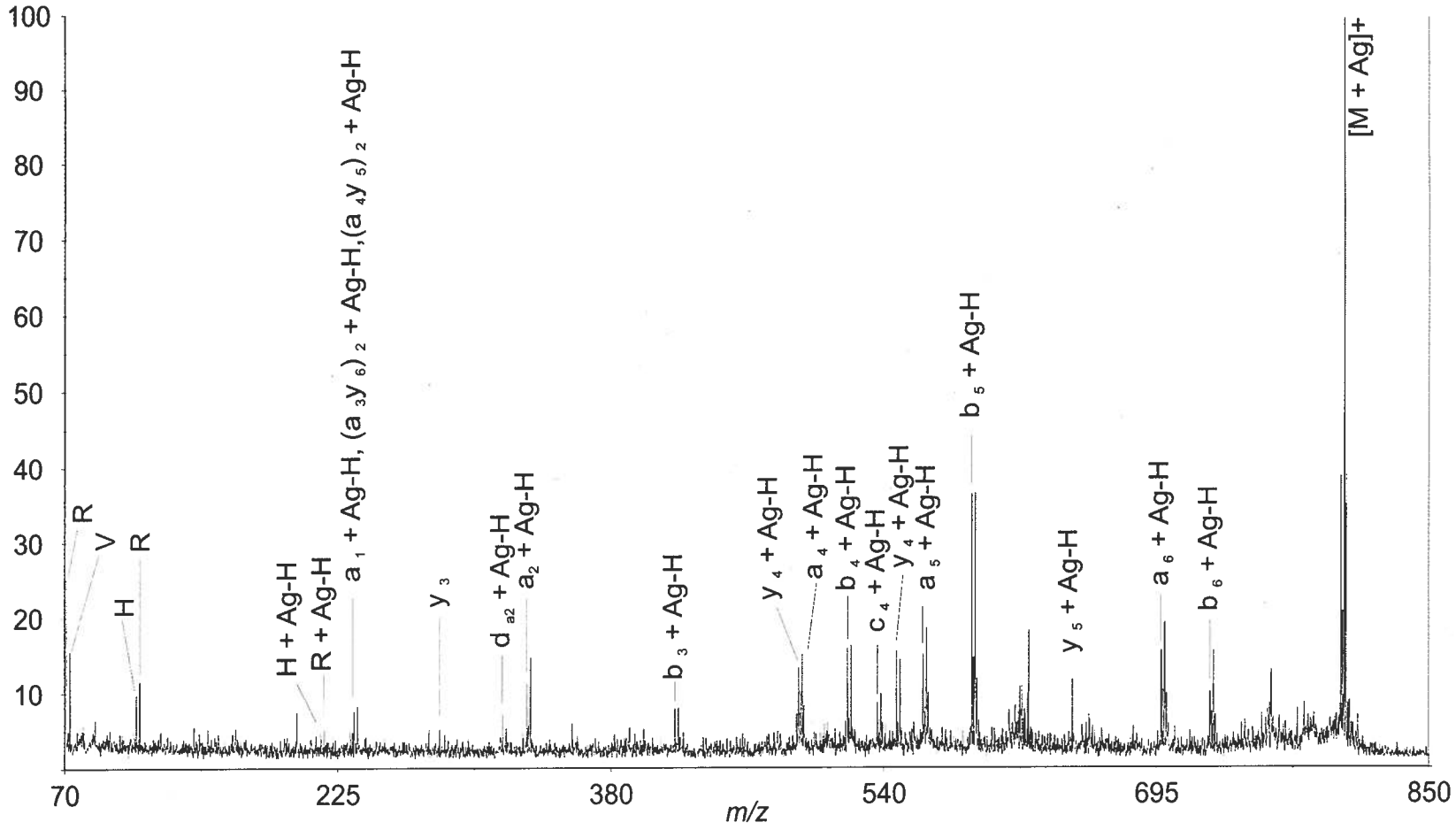


**Figure 24c**. High energy CID TOF-TOF spectrum for $[RVGVAHG+Ag]^{+}$.

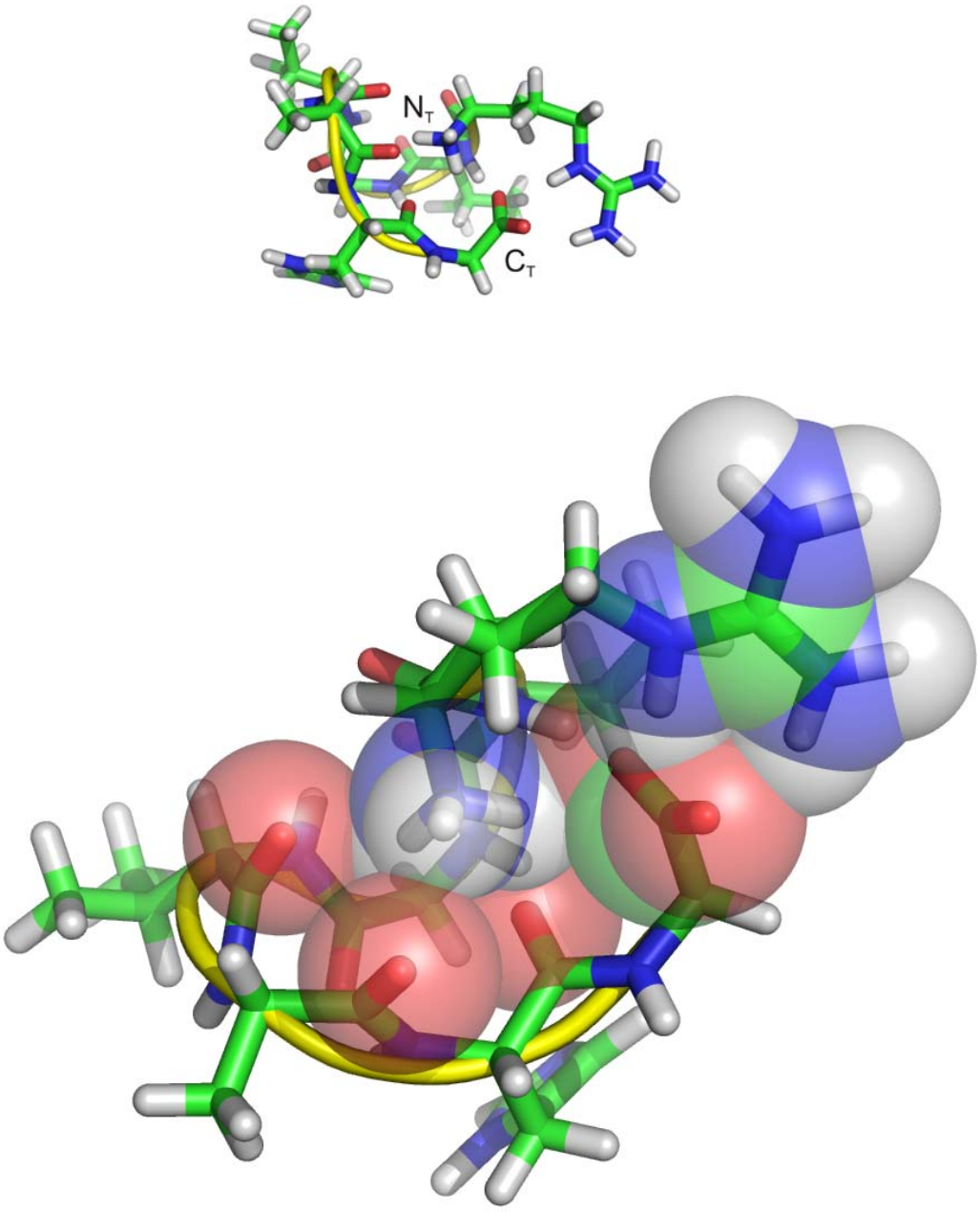


**Figure 25a**. Candidate structure for $[RVGVAHG+H]^+$.

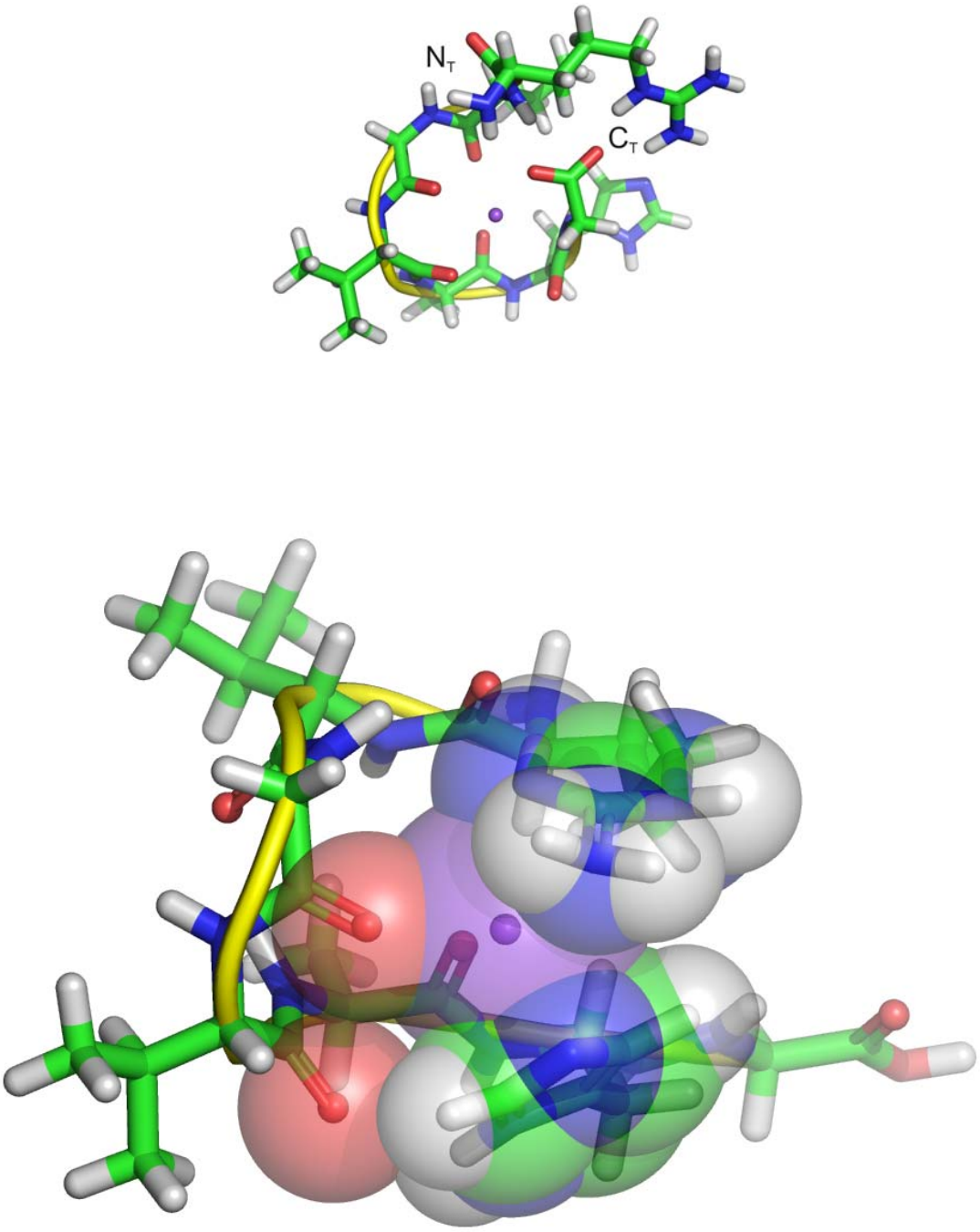


**Figure 25b**. Candidate structure for [RVGVAHG+Na]$^+$.

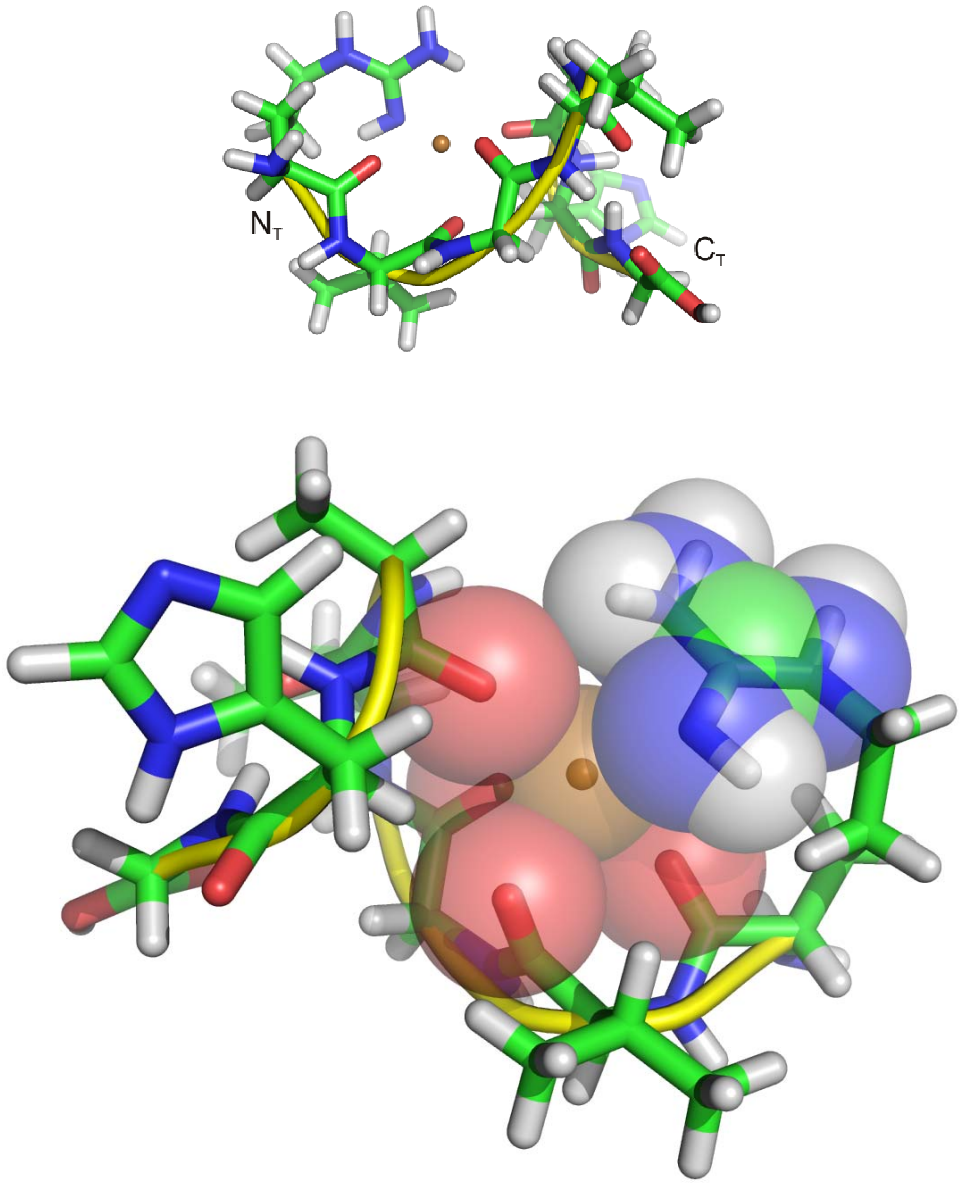


**Figure 25c**. Candidate structure for $[RVGVAHG+Cu]^+$.

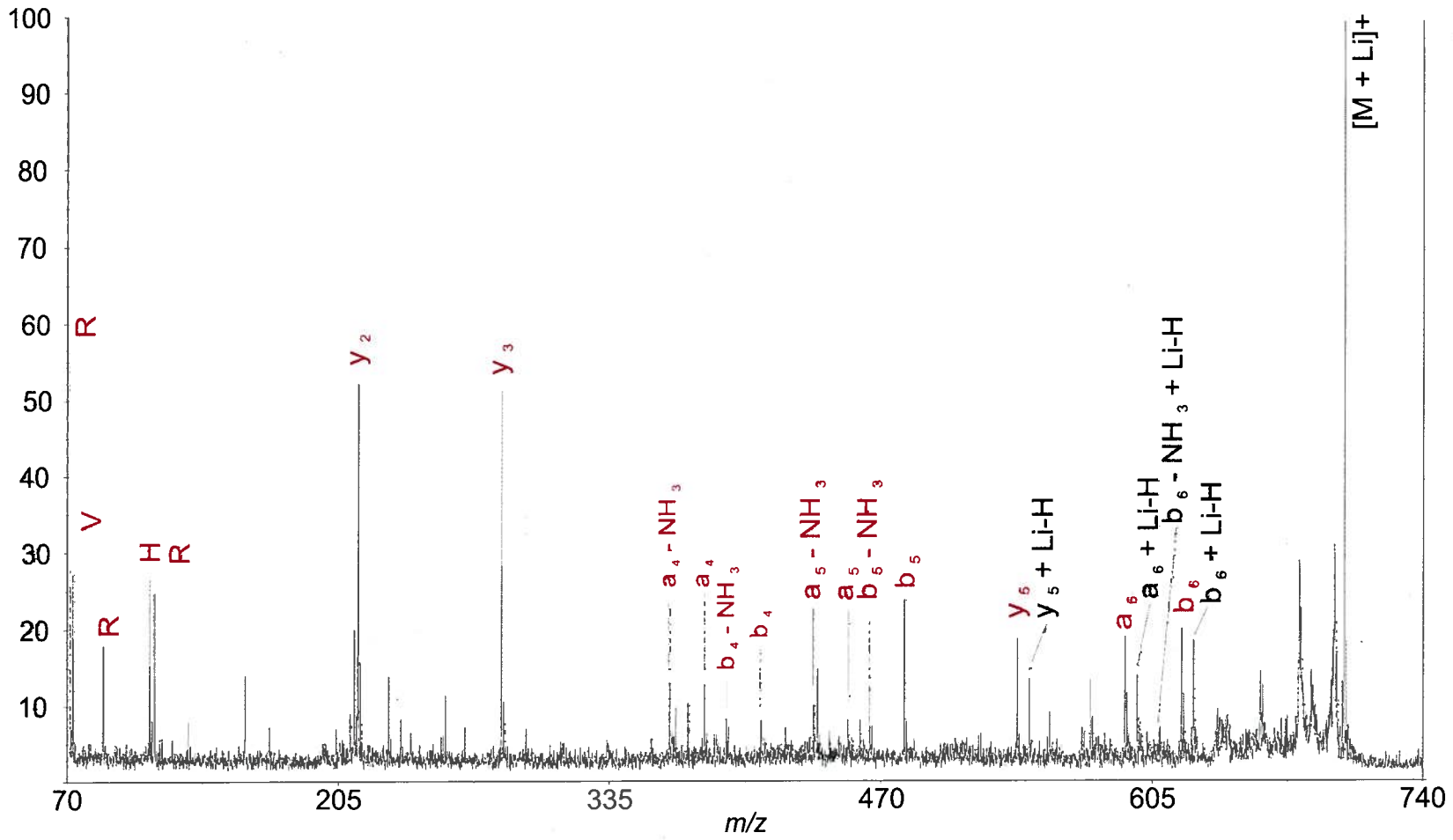


**Figure 26a**. High energy CID TOF-TOF spectrum for $[RVGVAHG+Li]^+$.

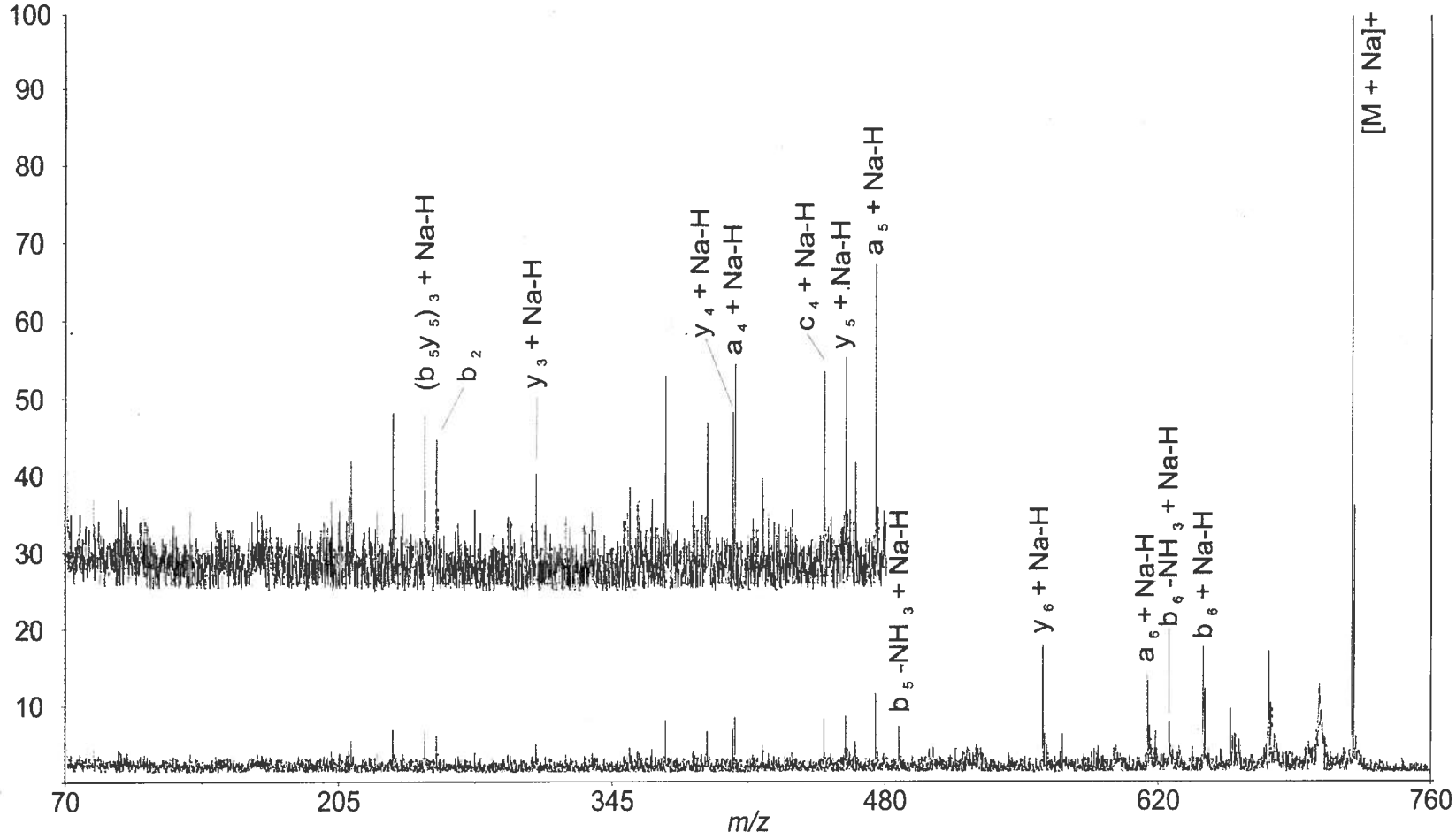


**Figure 26b**. High energy CID TOF-TOF spectrum for [RVGVAHG+Na]$^{+}$.

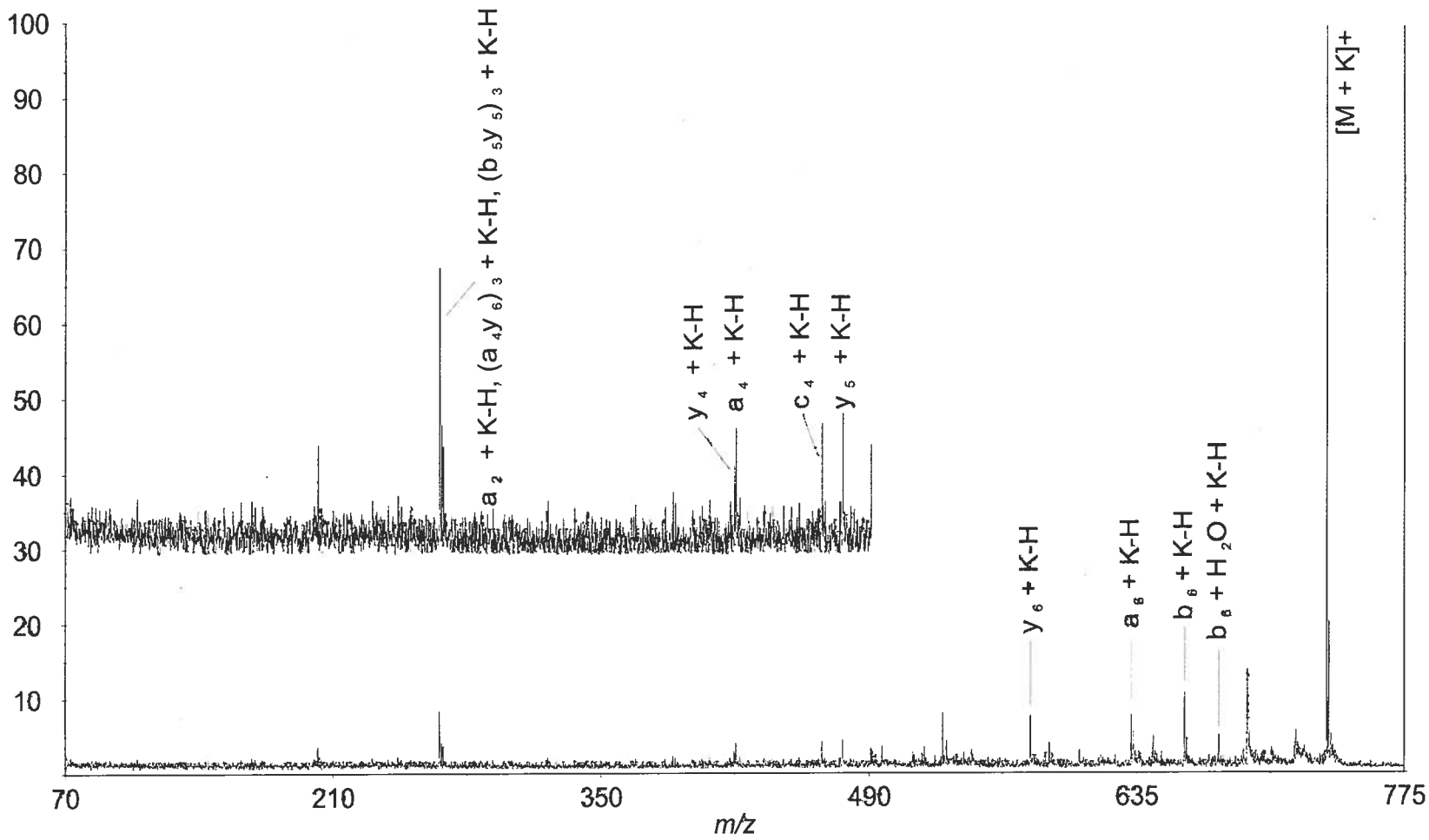


**Figure 26c**. High energy CID TOF-TOF spectrum for $[RVGVAHG+K]^+$.

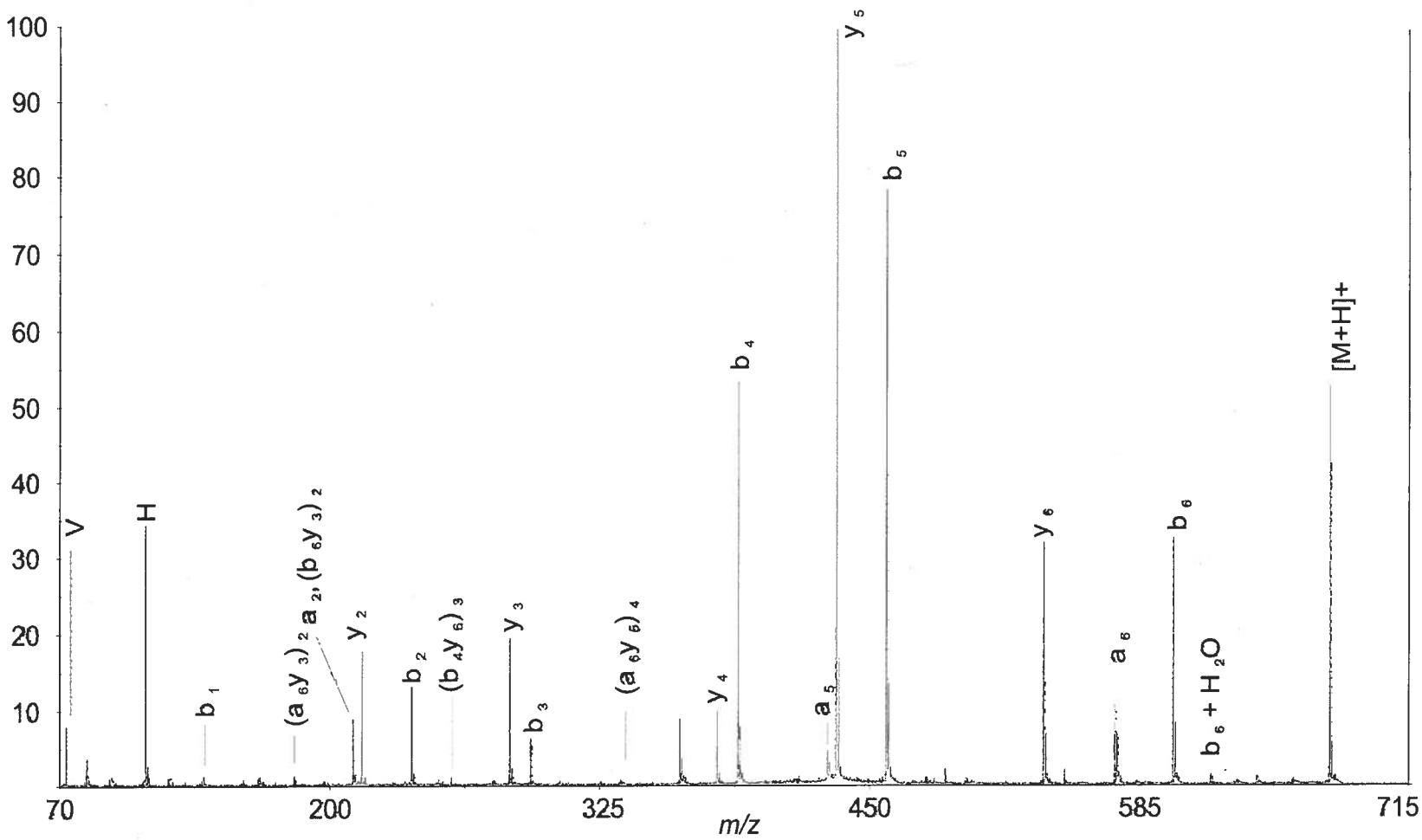


**Figure 27a**. High energy CID TOF-TOF spectrum for $[HVGVAHG+H]^+$.

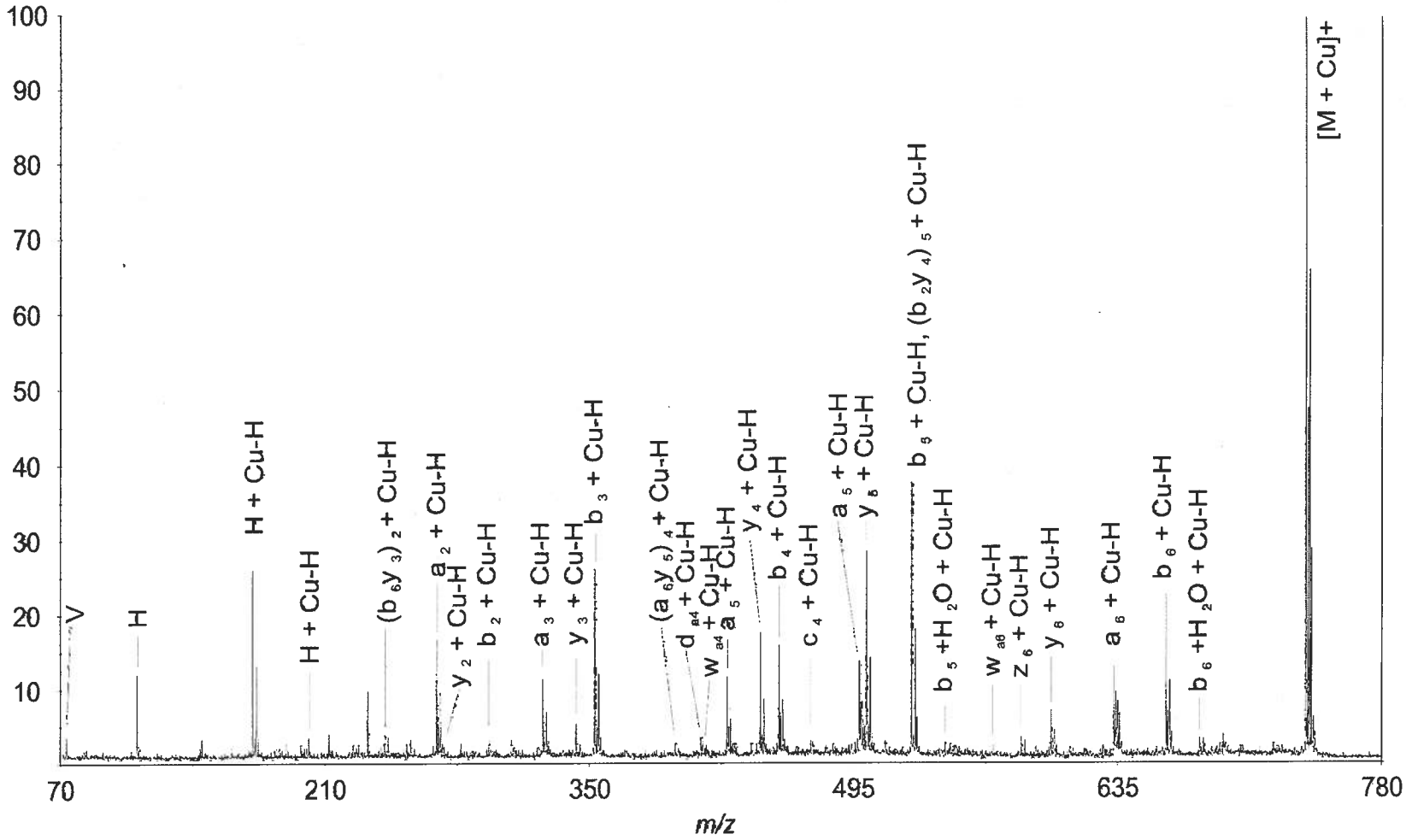


**Figure 27b**. High energy CID TOF-TOF spectrum for $[HVGVAHG+Cu]^{+}$.

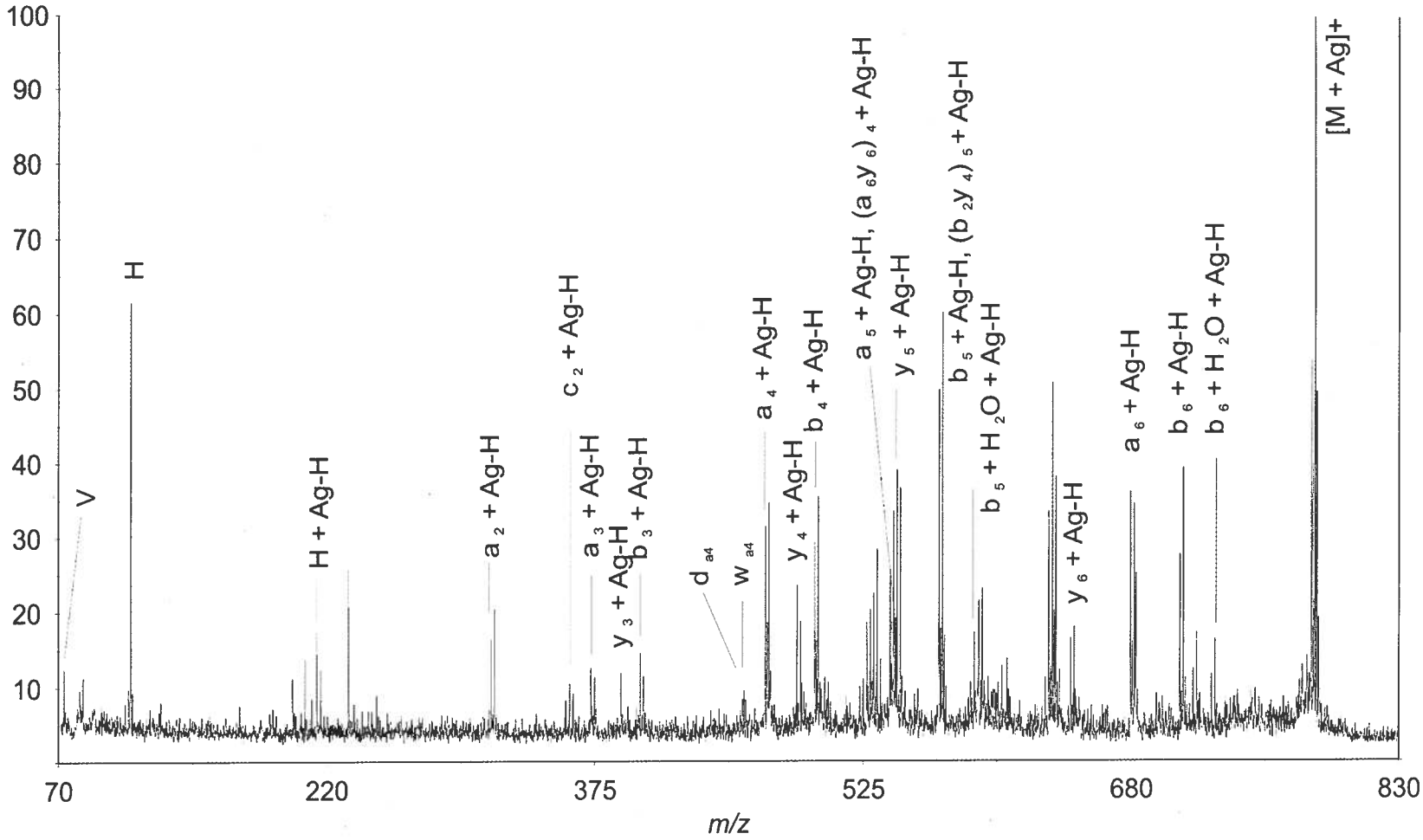


**Figure 27c**. High energy CID TOF-TOF spectrum for $[HVGVAHG+Ag]^+$.

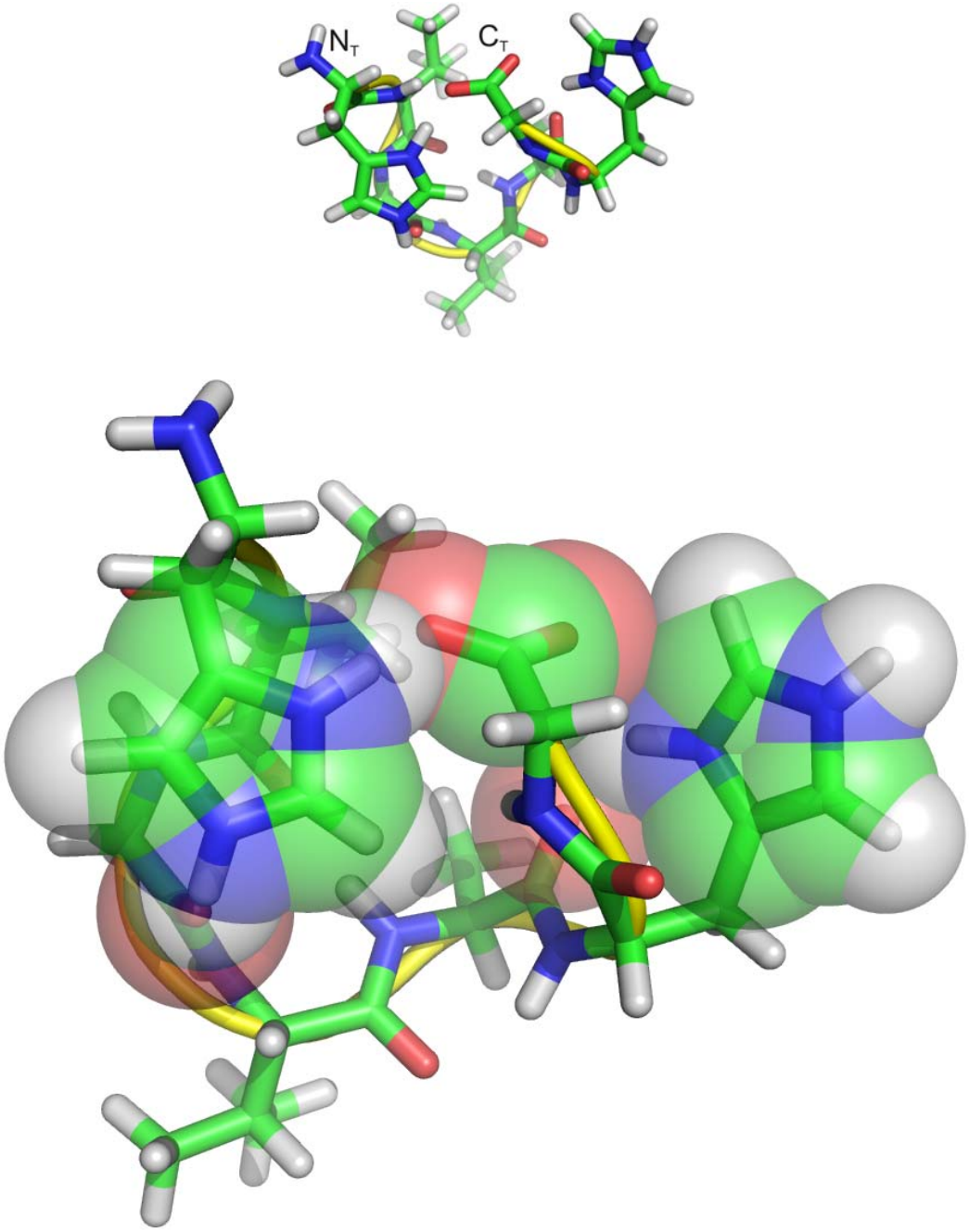


**Figure 28a**. Candidate structure for $[HVGVAHG+H]^+$

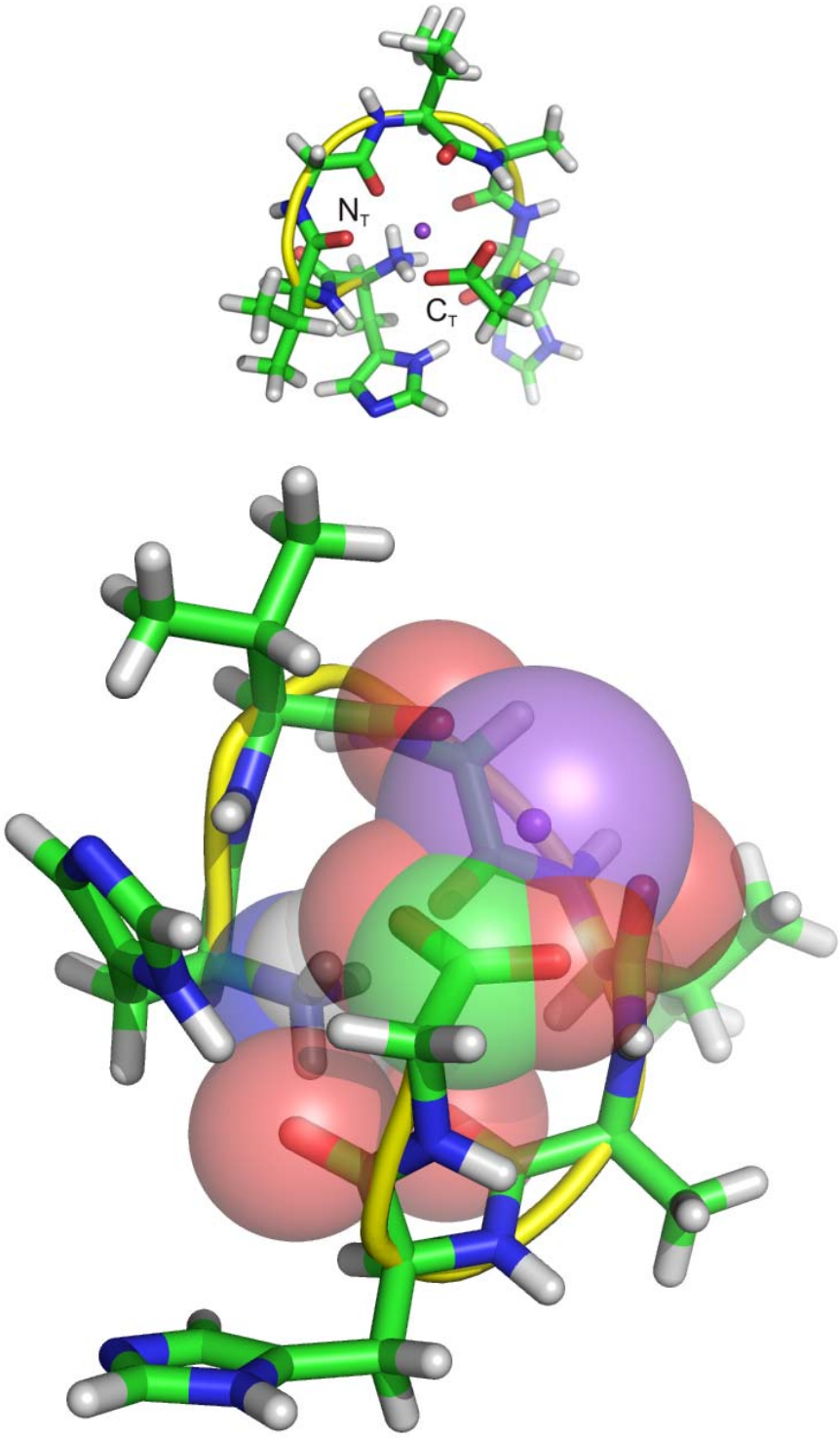


**Figure 28b**. Candidate structure for $[HVGVAHG+Na]^+$

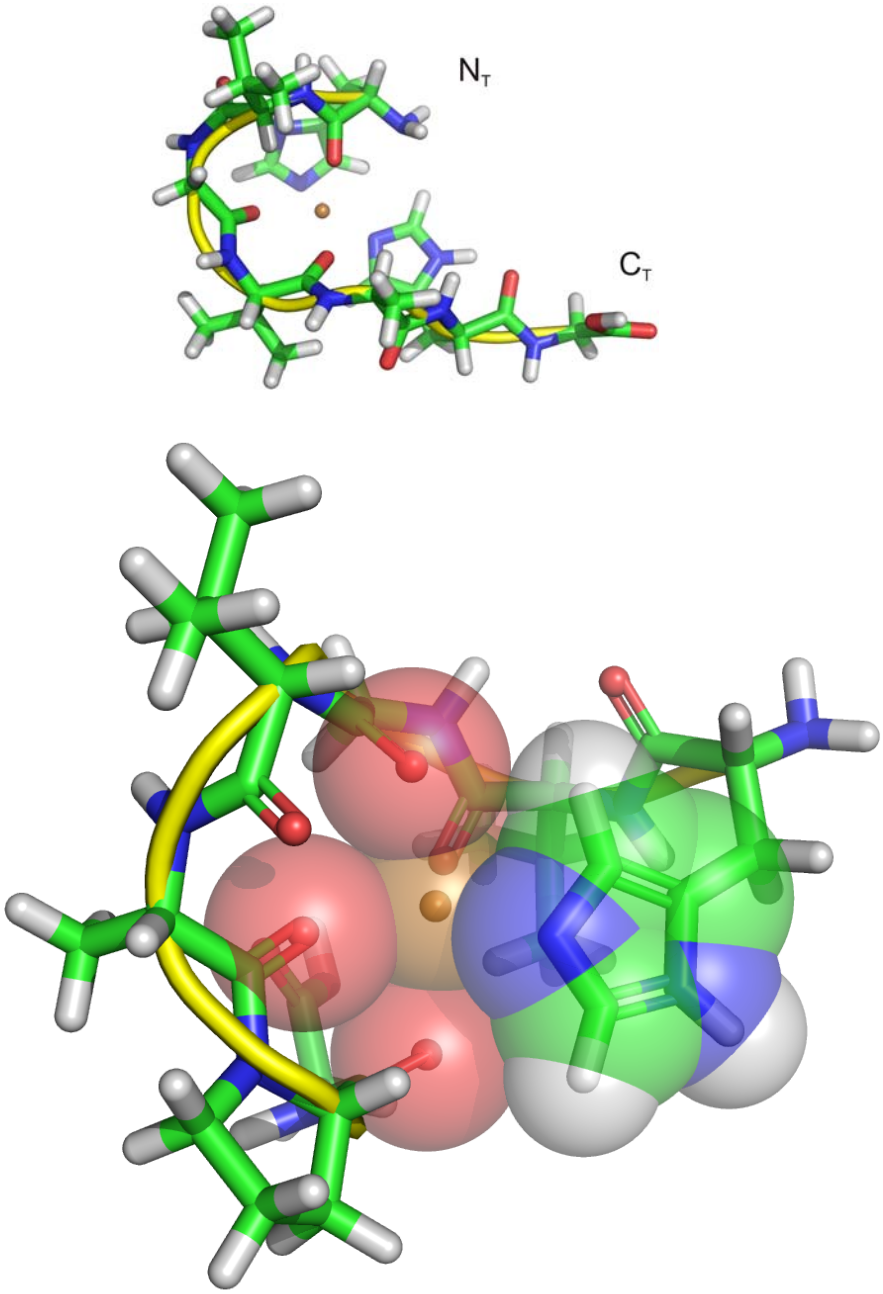


**Figure 28c**. Candidate structure for $[HVGVAHG+Cu]^+$

.

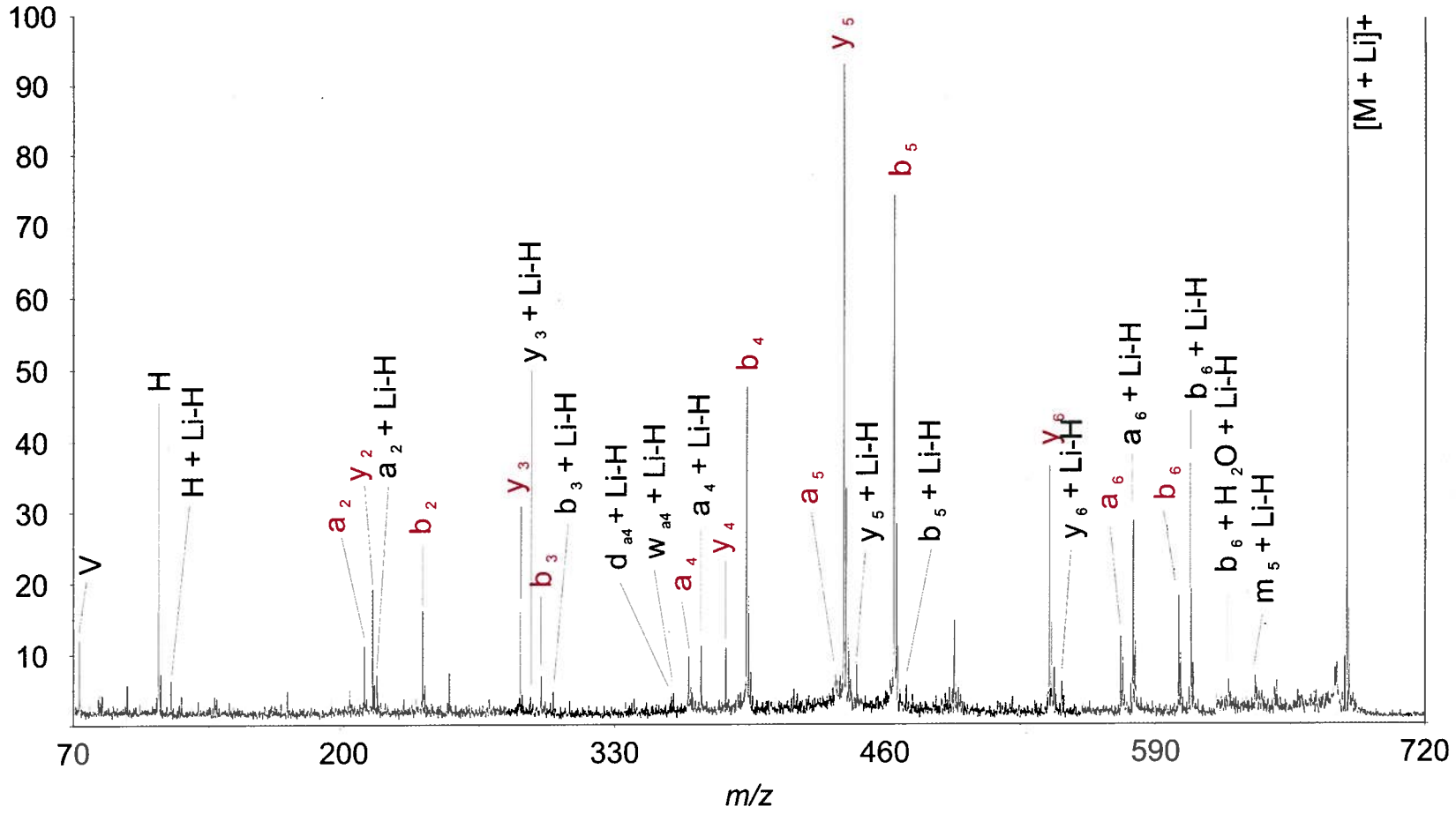


**Figure 29a**. High energy CID TOF-TOF spectrum for $[HVGVAHG+Li]^+$.

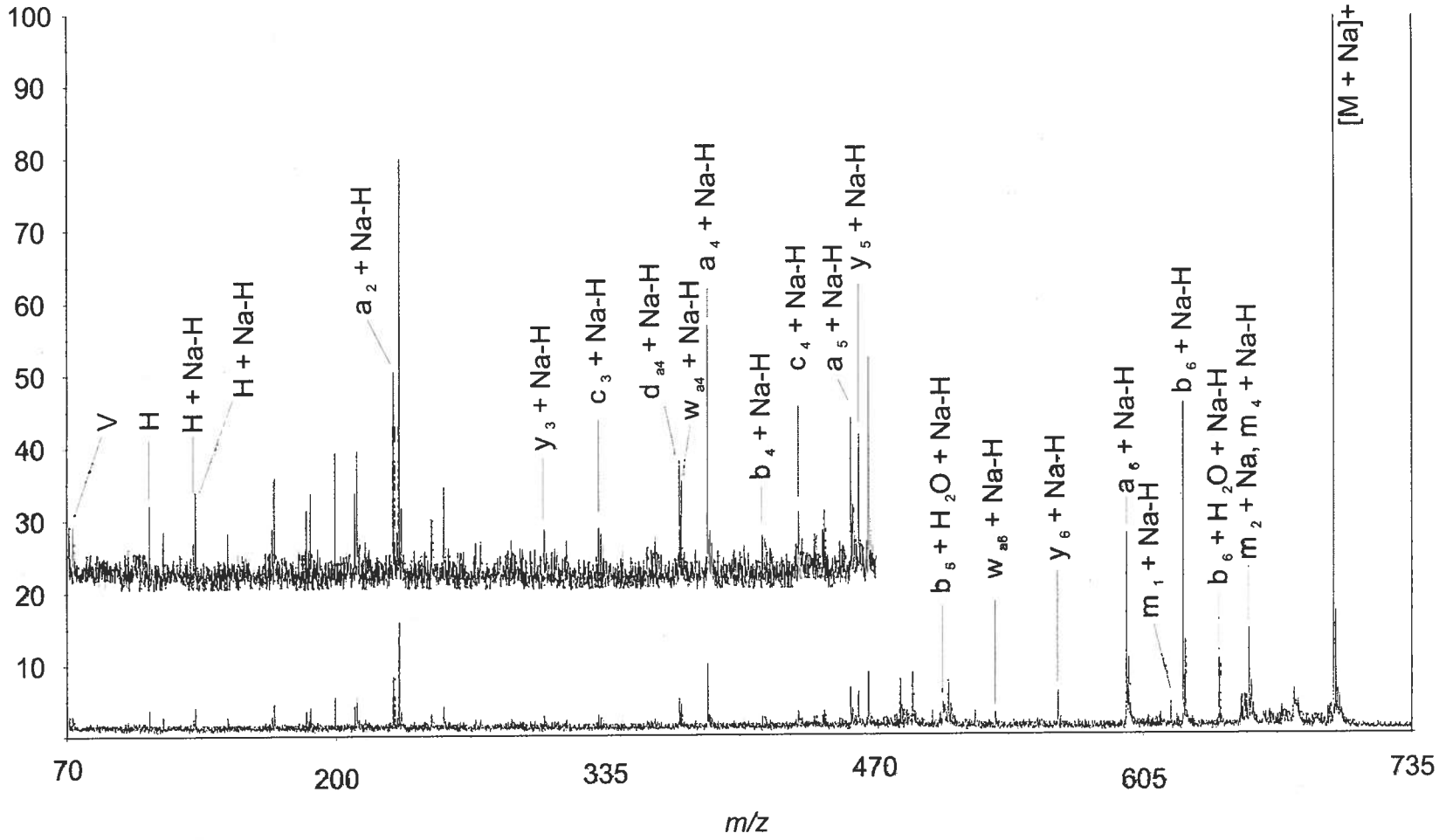


**Figure 29b**. High energy CID TOF-TOF spectrum for $[HVGVAHG+Na]^+$.

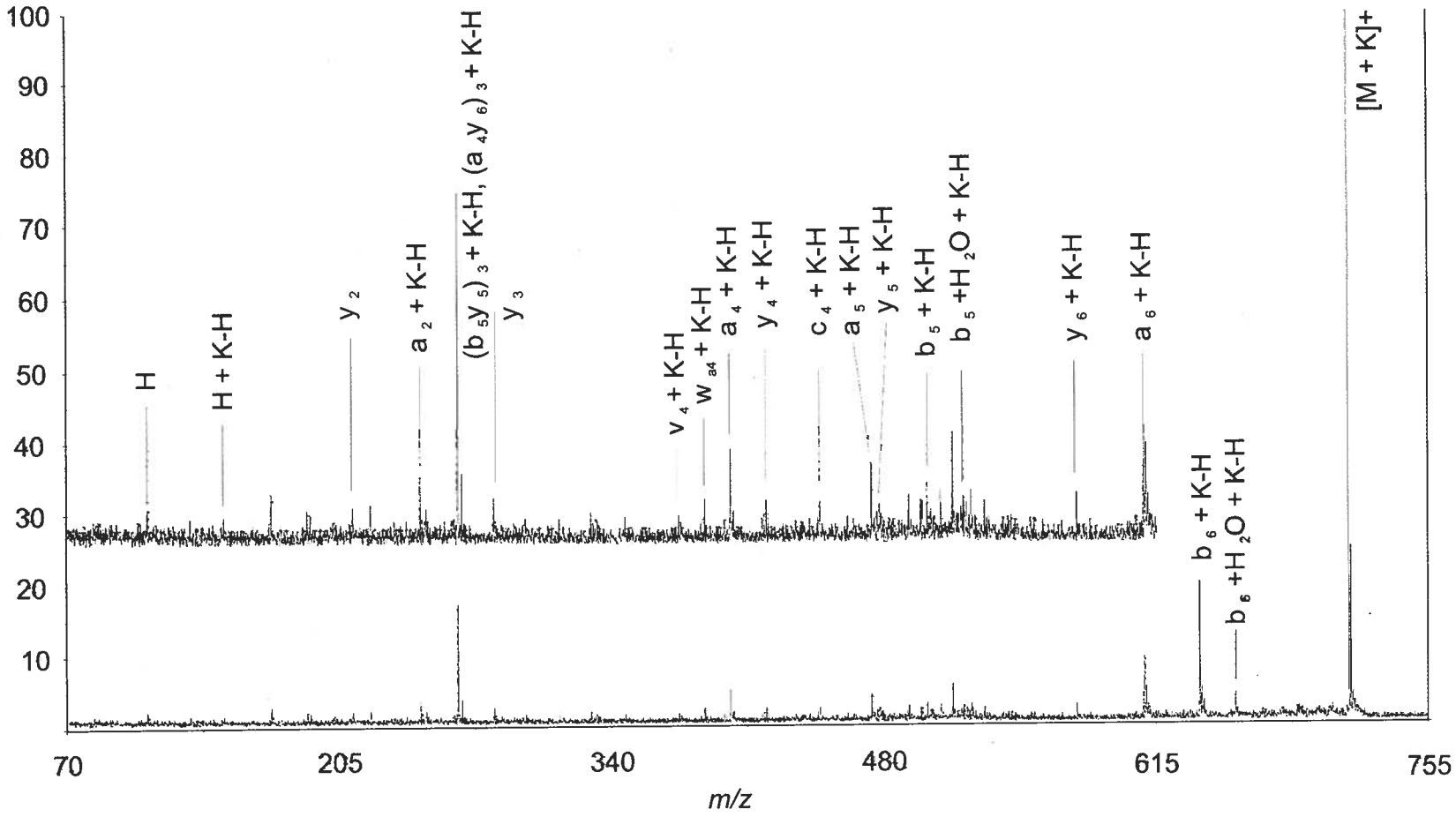


**Figure 29c**. High energy CID TOF-TOF spectrum for $[HVGVAHG+K]^+$.

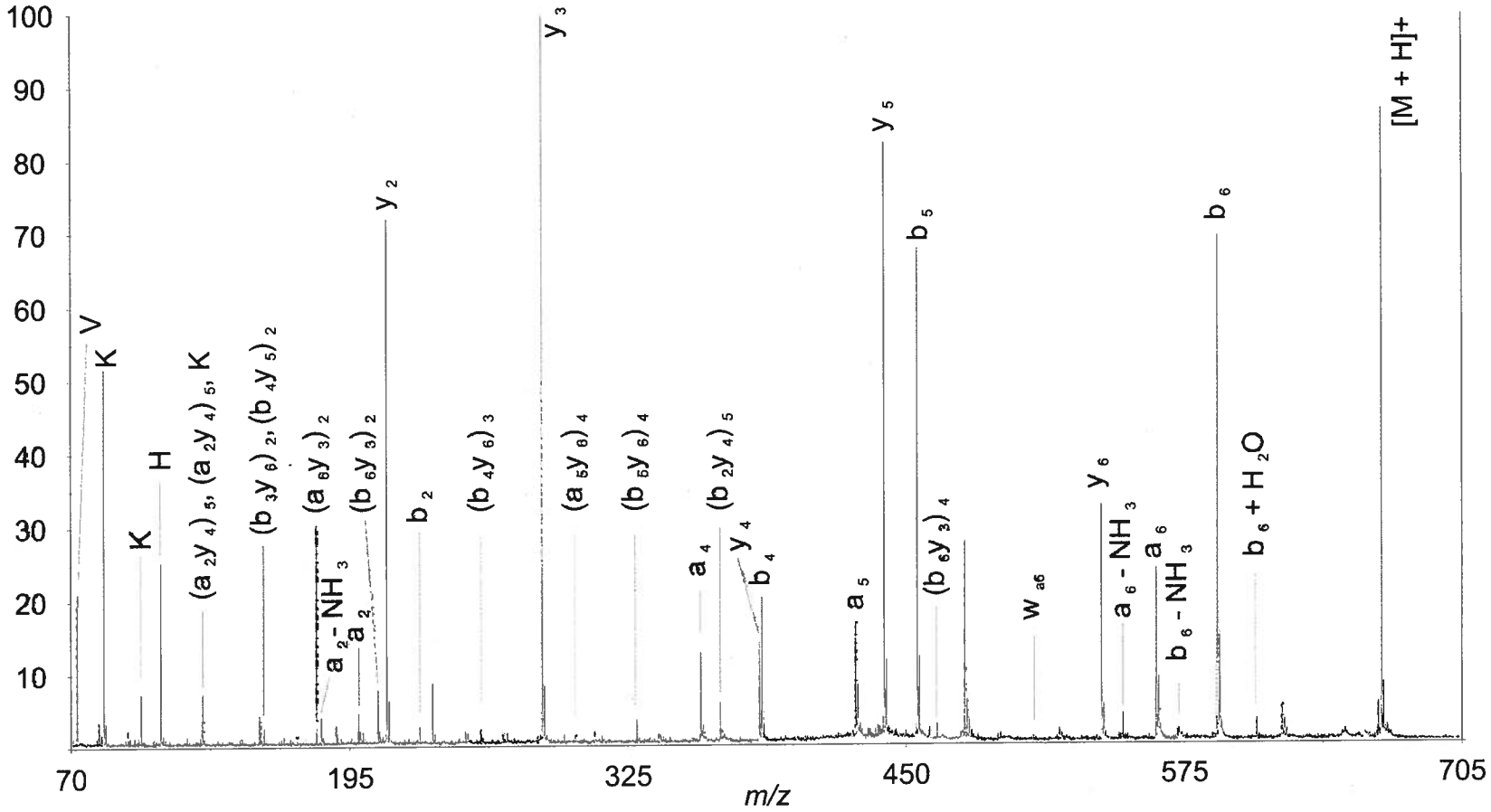


**Figure 30a**. High energy CID TOF-TOF spectrum for $[KVGVAHG+H]^+$.

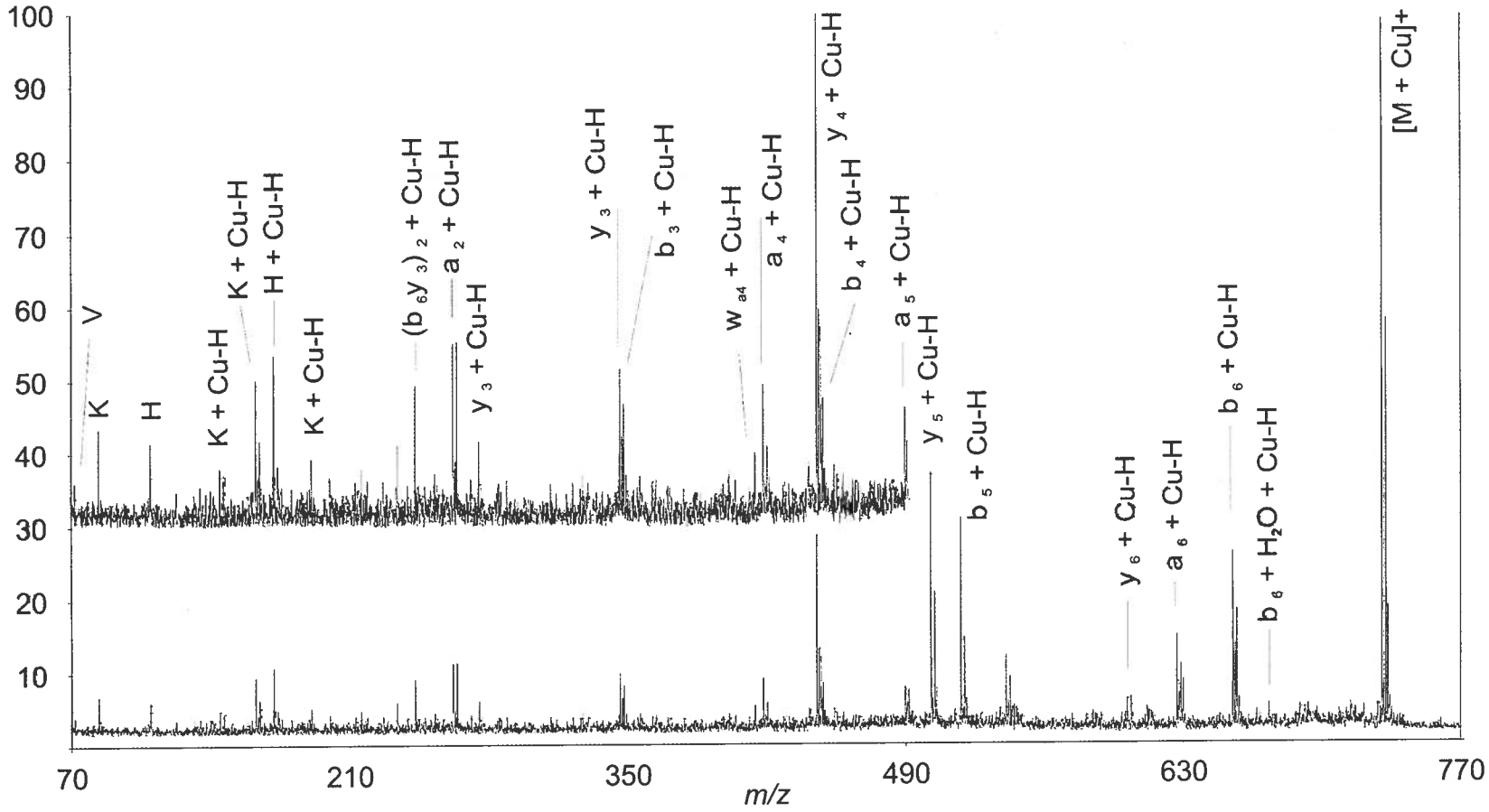


**Figure 30b**. High energy CID TOF-TOF spectrum for $[KVGVAHG+Cu]^+$.

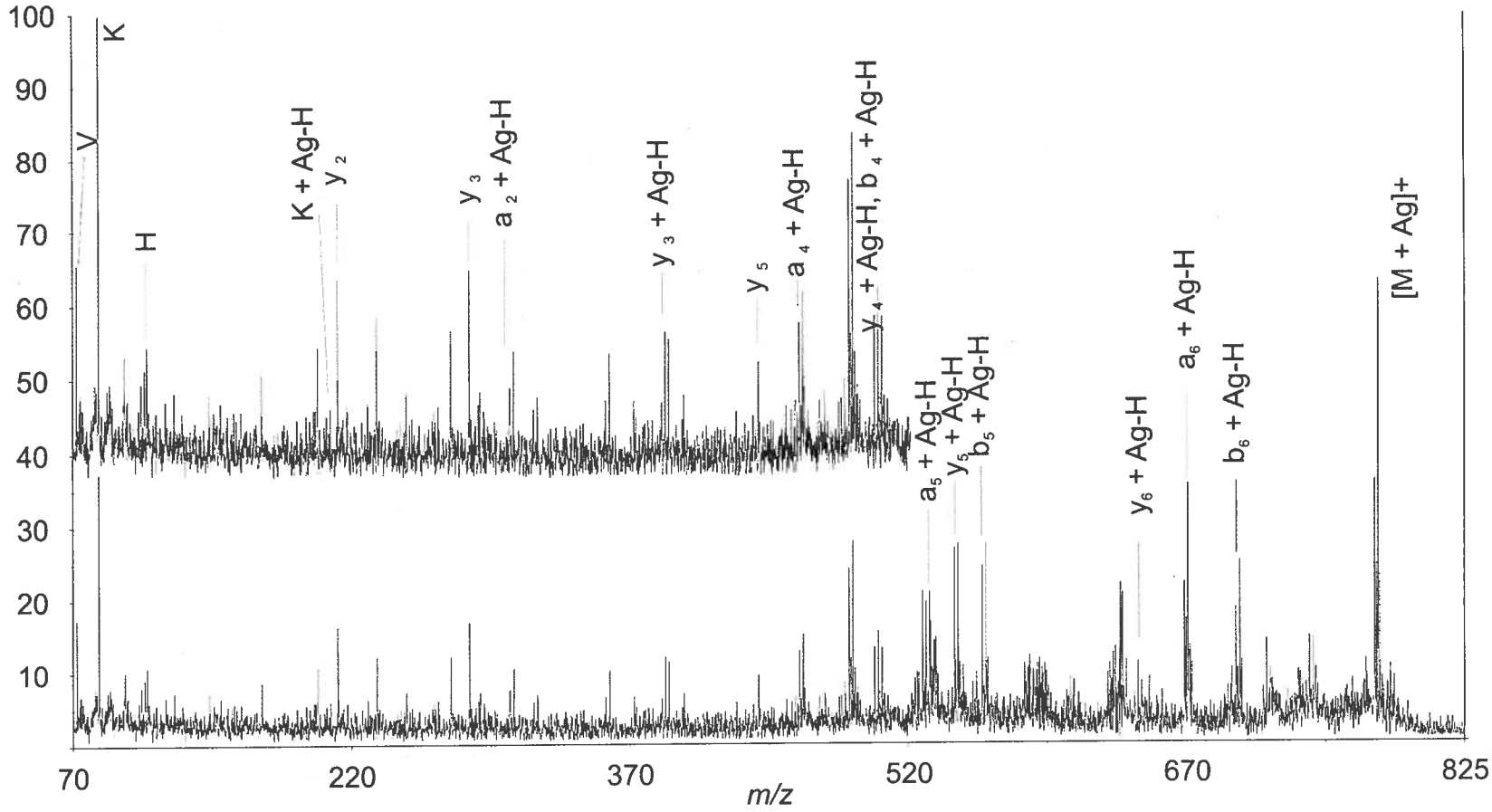


**Figure 30c**. High energy CID TOF-TOF spectrum for $[KVGVAHG+Ag]^+$.

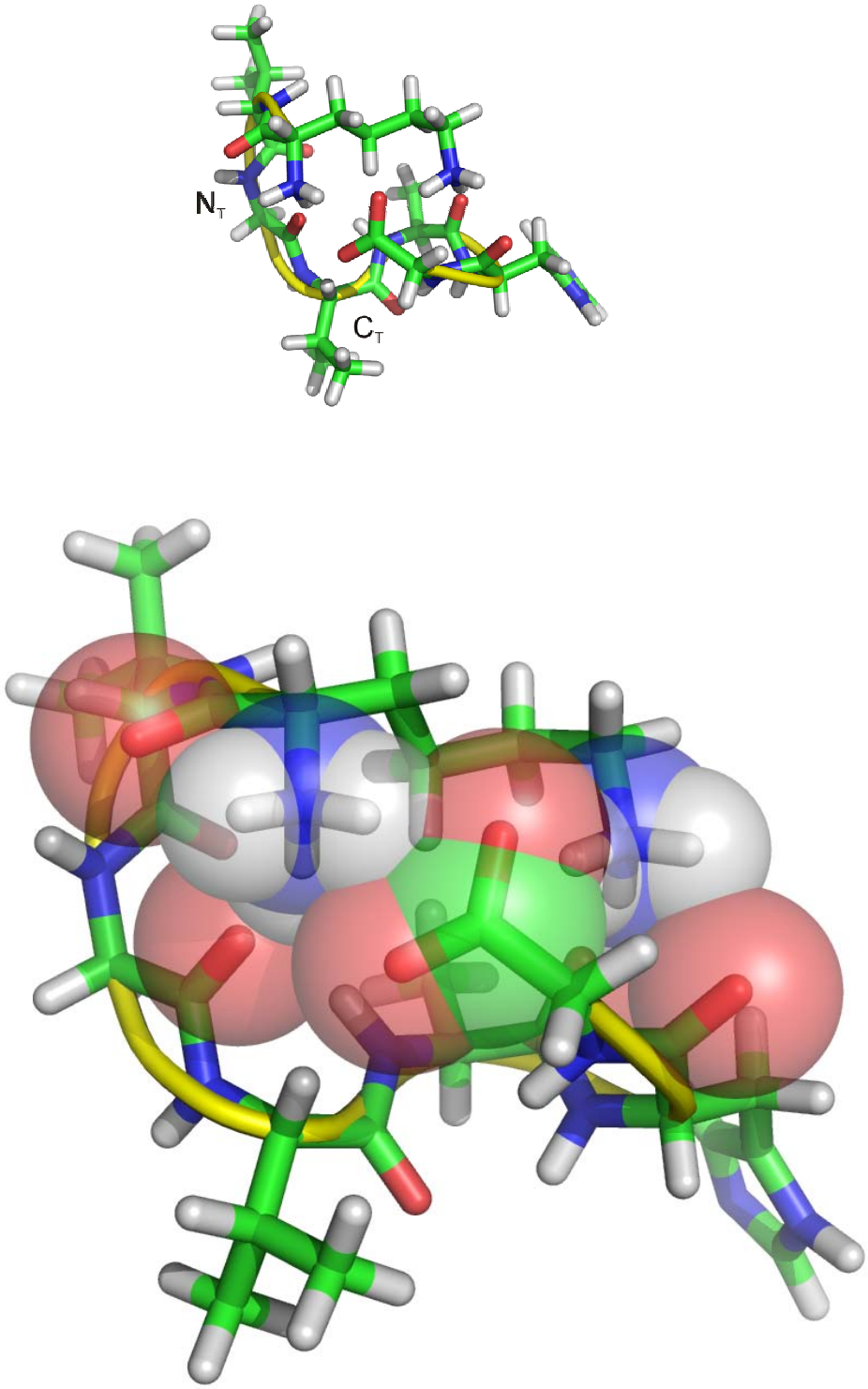


**Figure 31a**. Candidate structure for $[KVGVAHG+H]^+$.

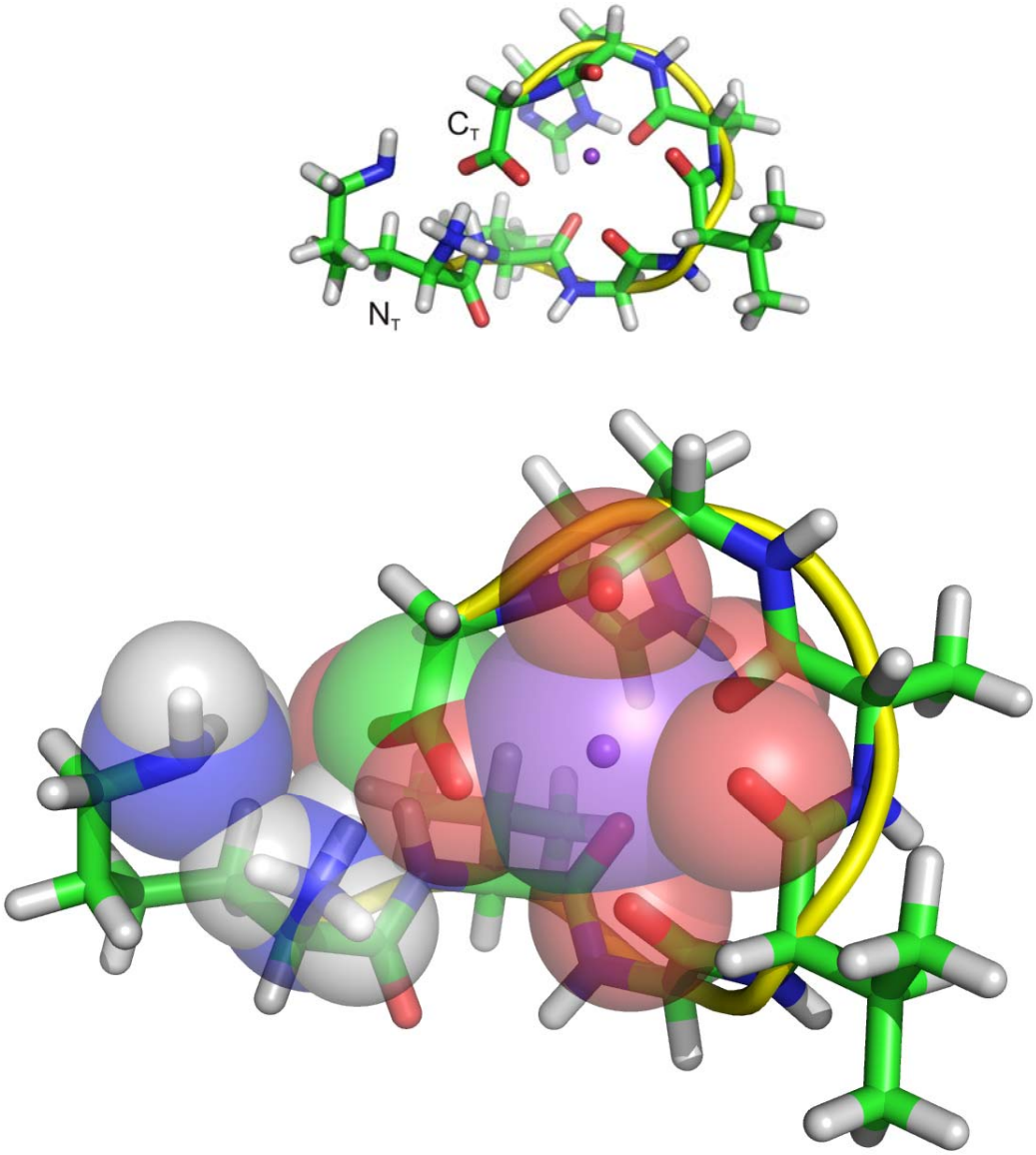


**Figure 31b**. Candidate structure for [KVGVAHG+Na]$^+$.

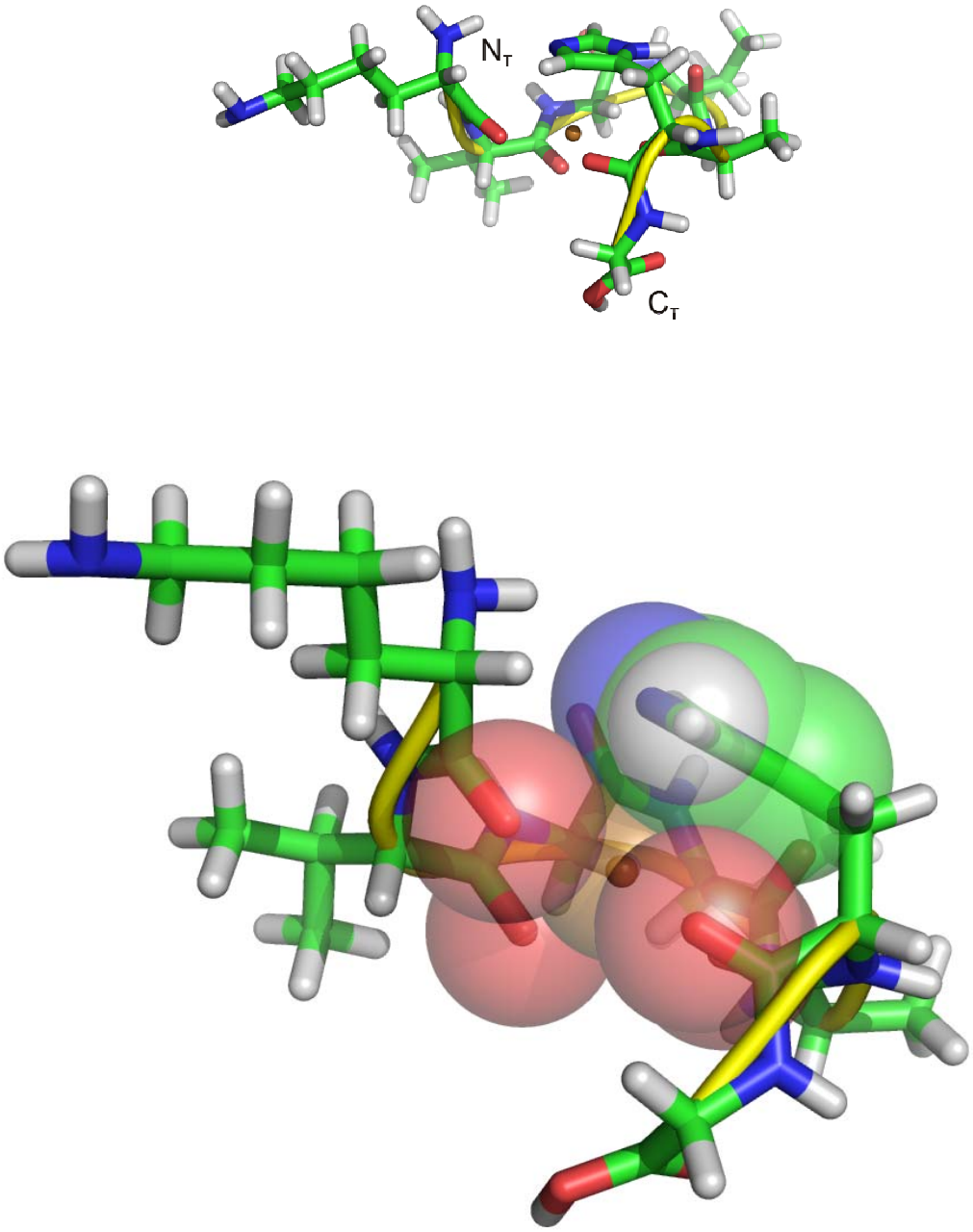


**Figure 31c**. Candidate structure for [KVGVAHG+Cu]$^+$.

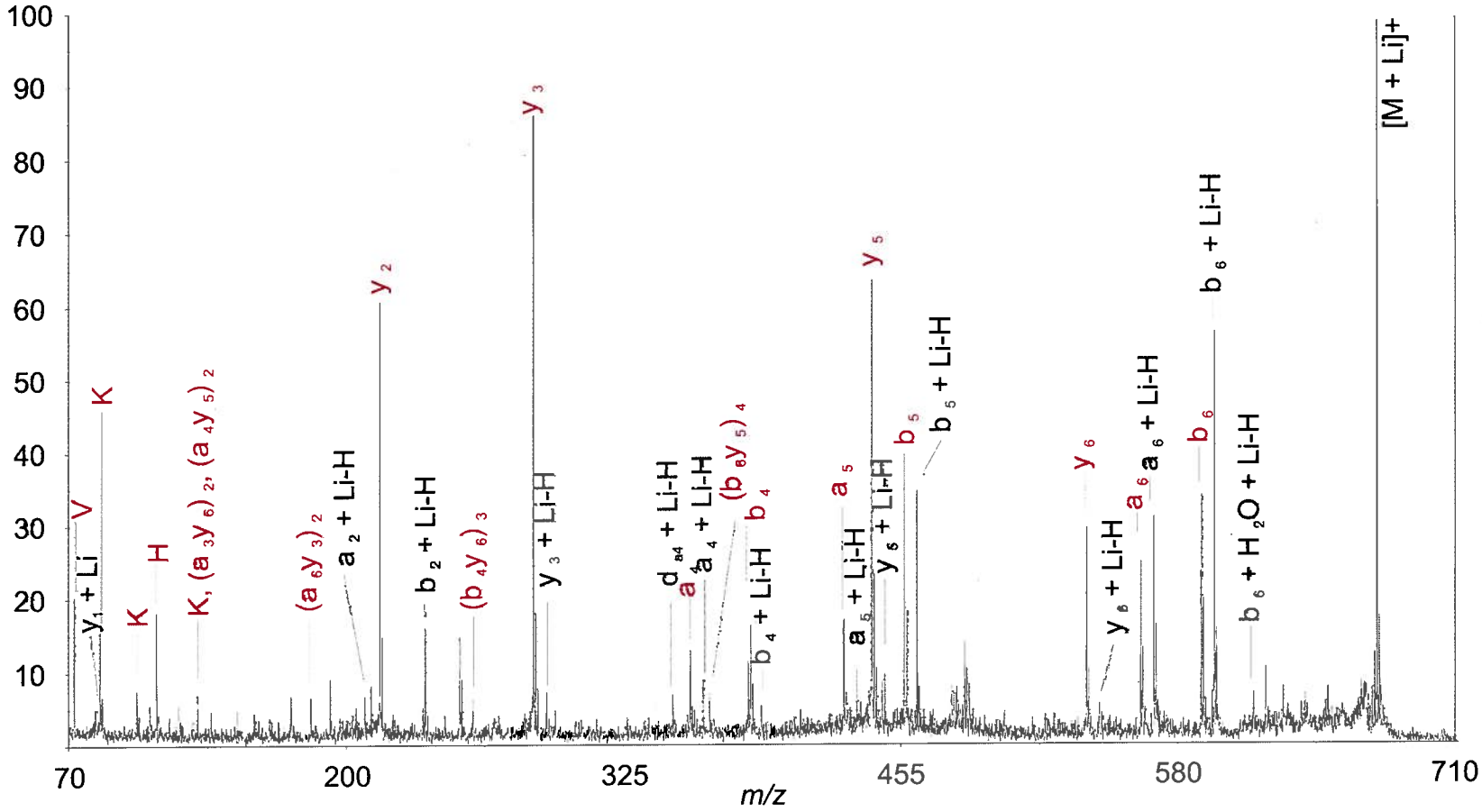


**Figure 32a**. High energy CID TOF-TOF spectrum for $[KVGVAHG+Li]^+$.

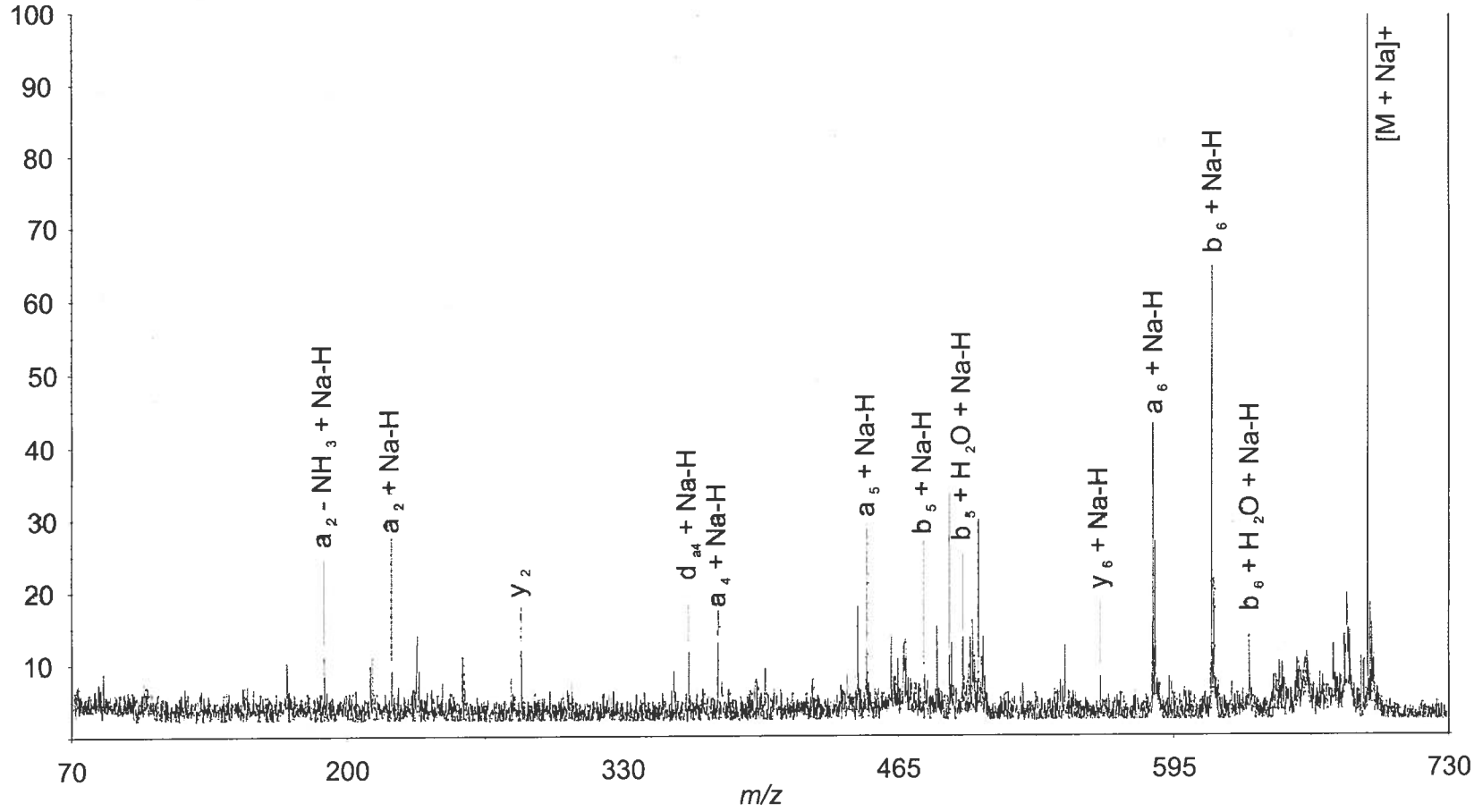


**Figure 32b**. High energy CID TOF-TOF spectrum for $[KVGVAHG+Na]^+$.

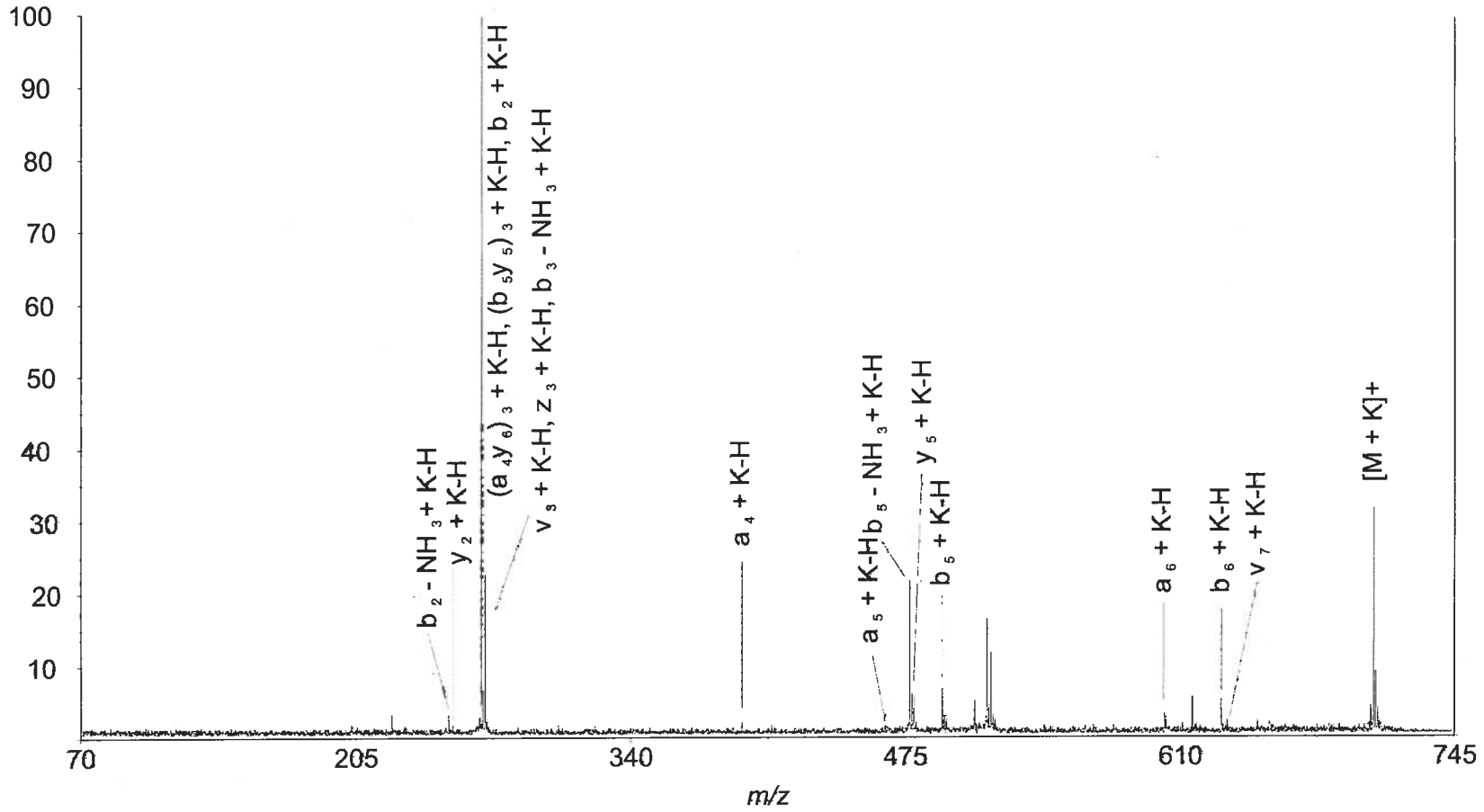


**Figure 32c**. High energy CID TOF-TOF spectrum for $[KVGVAHG+K]^+$.

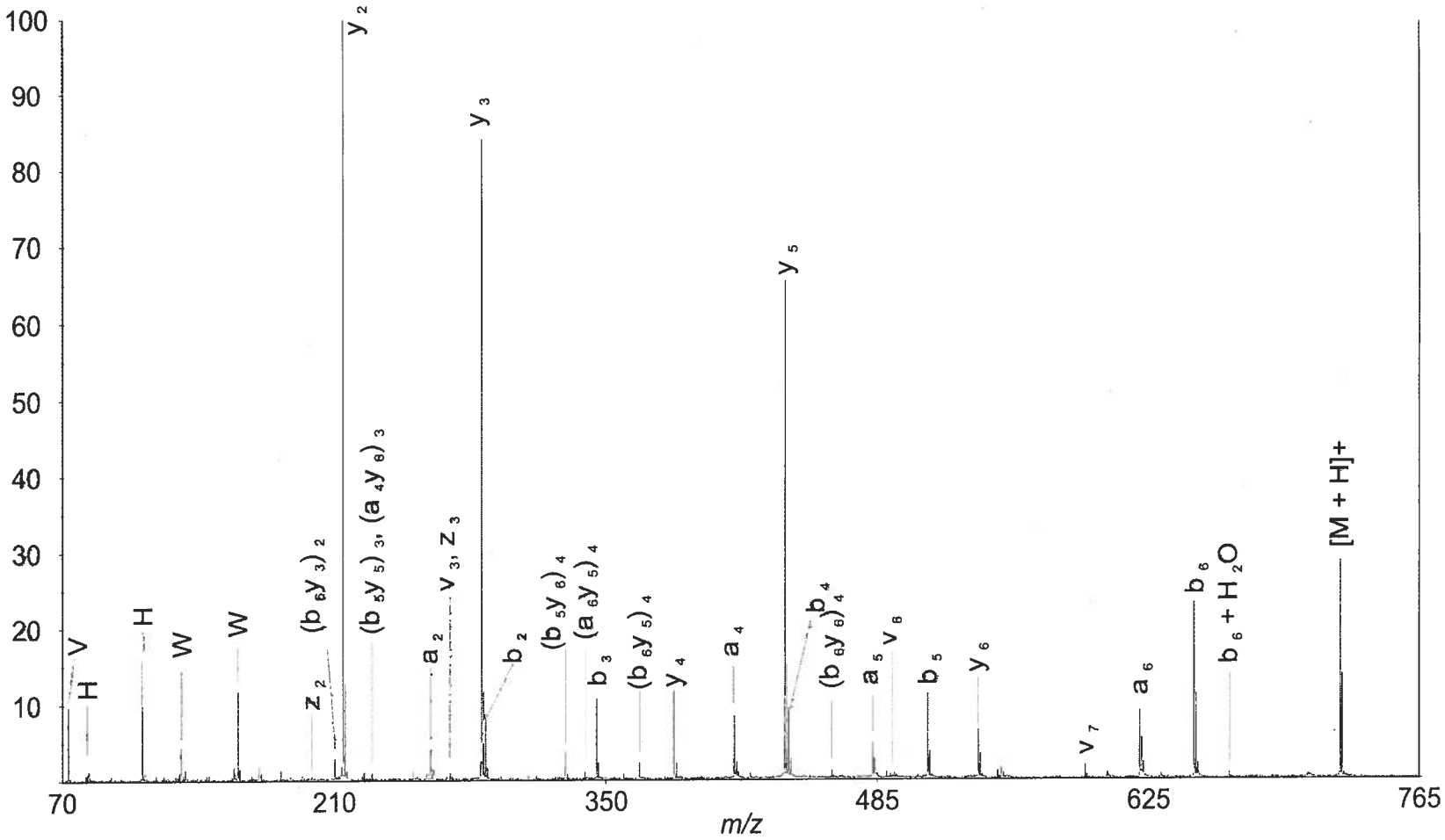


**Figure 33a**. High energy CID TOF-TOF spectrum for $[WVGVAHG+H]^{+}$.

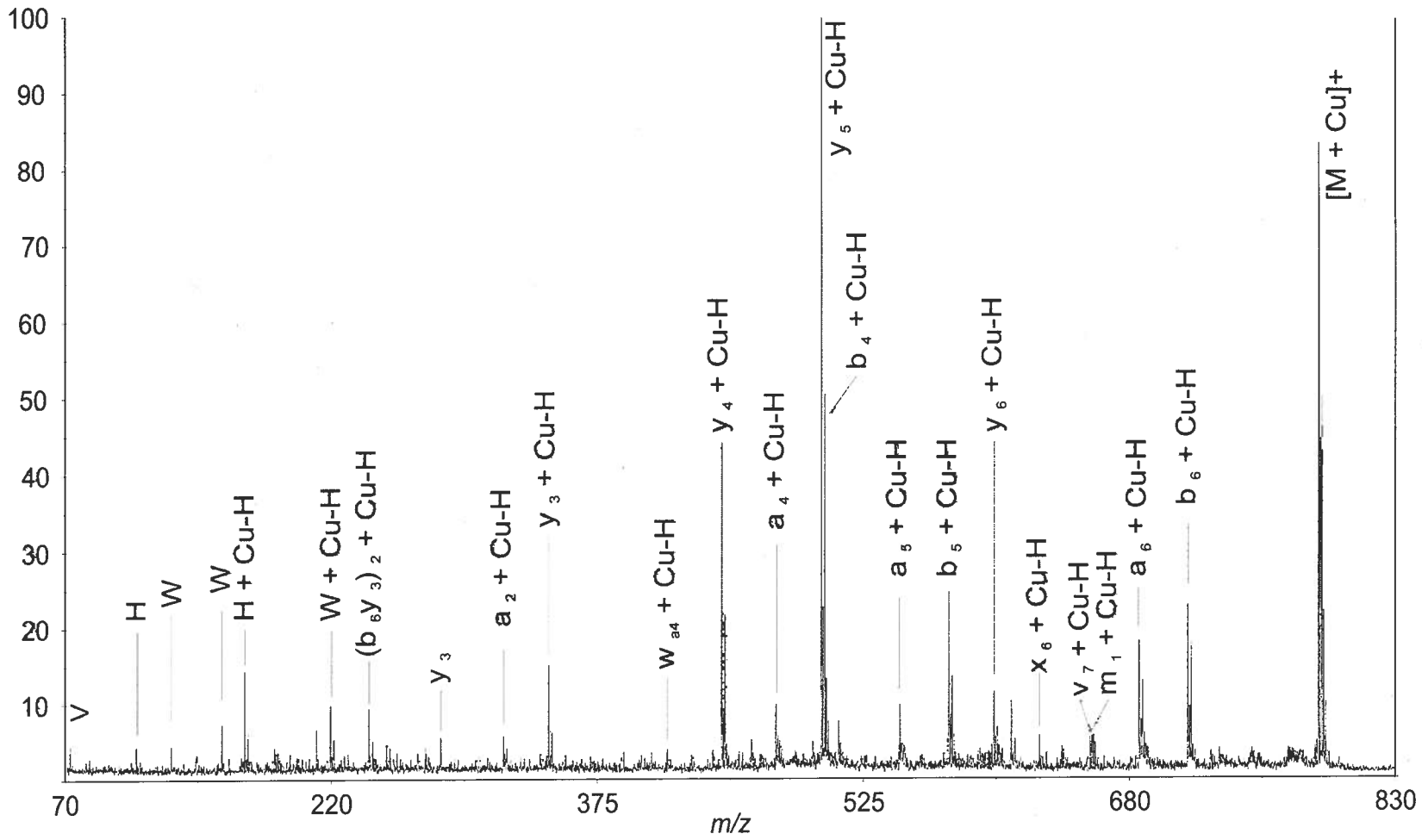


**Figure 33b**. High energy CID TOF-TOF spectrum for $[WVGVAHG+Cu]^+$.

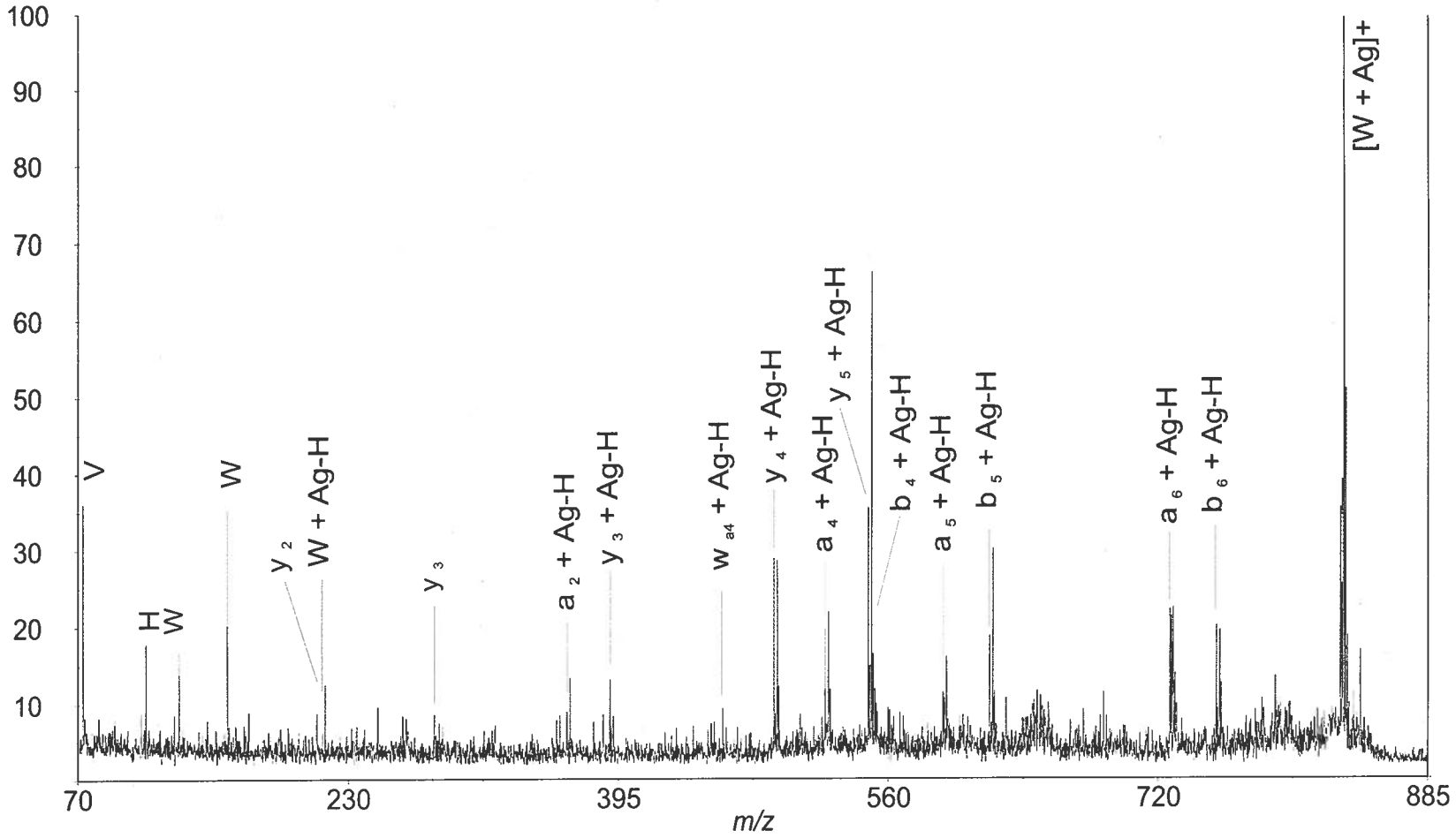


**Figure 33c**. High energy CID TOF-TOF spectrum for $[WVGVAHG+Ag]^+$.

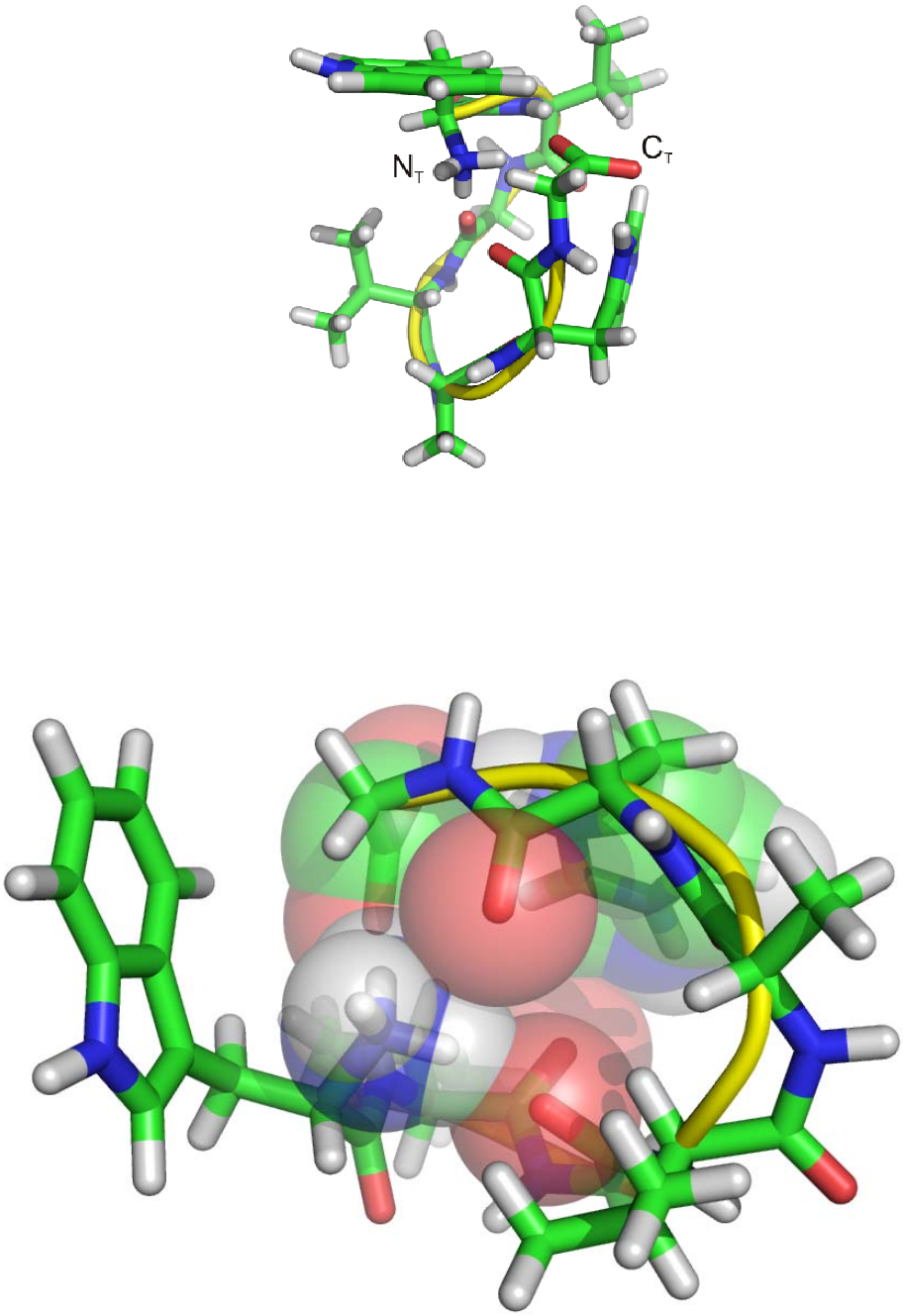


**Figure 34a**. Candidate structure for [WVGVAHG+H]$^+$.

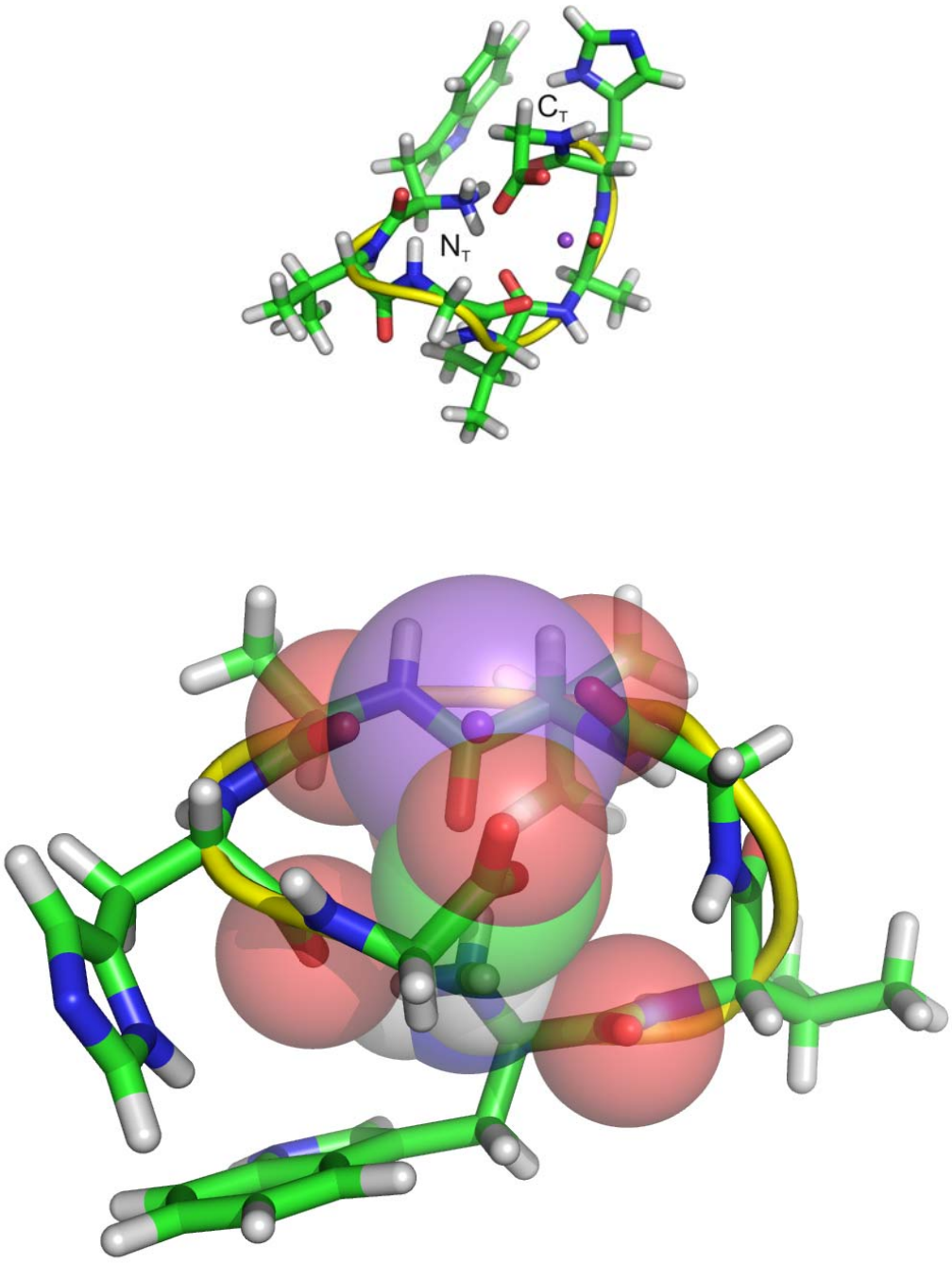


**Figure 34b**. Candidate structure for [WVGVAHG+Na]$^+$.

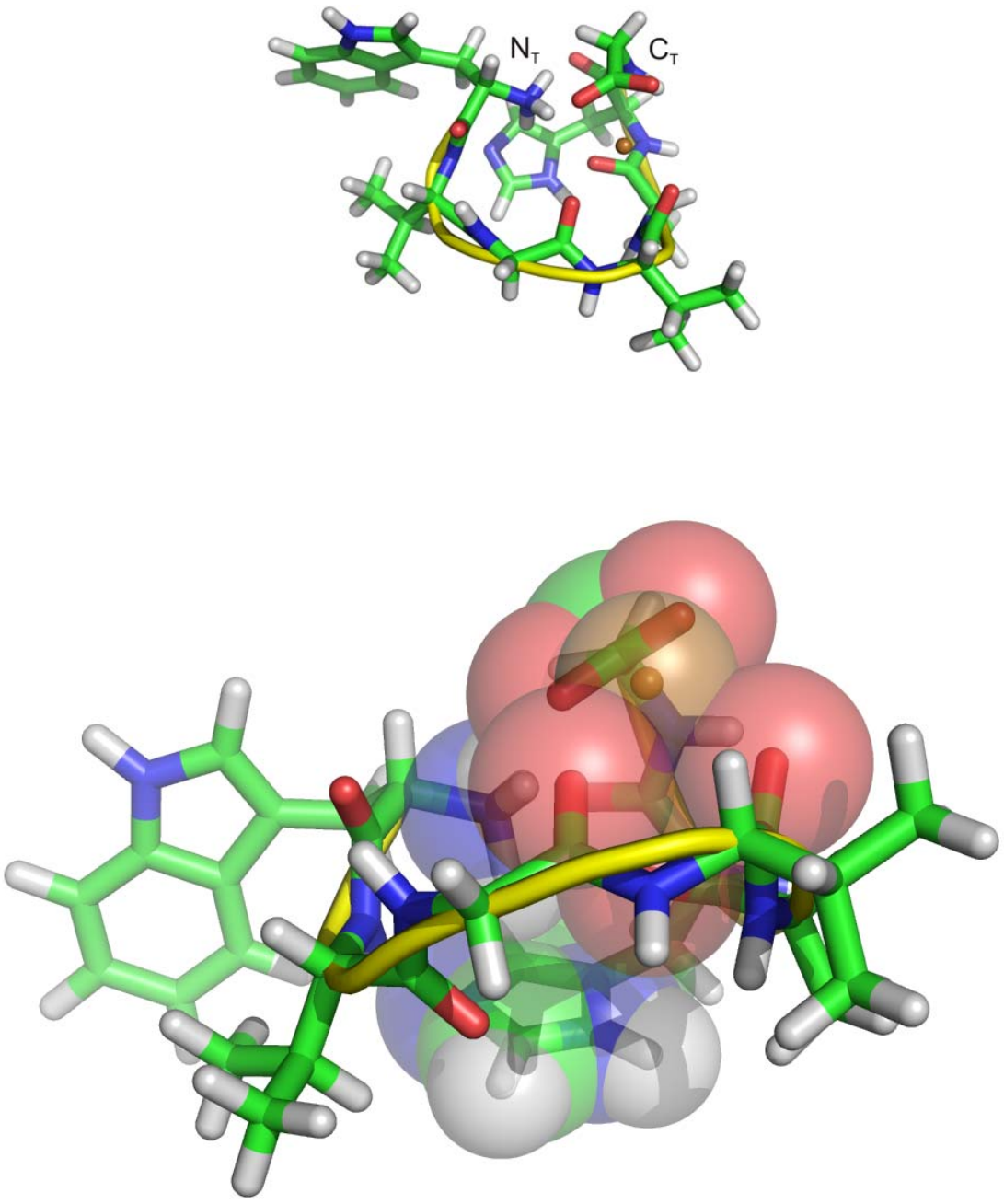


**Figure 34c**. Candidate structure for [WVGVAHG+Cu]$^+$.

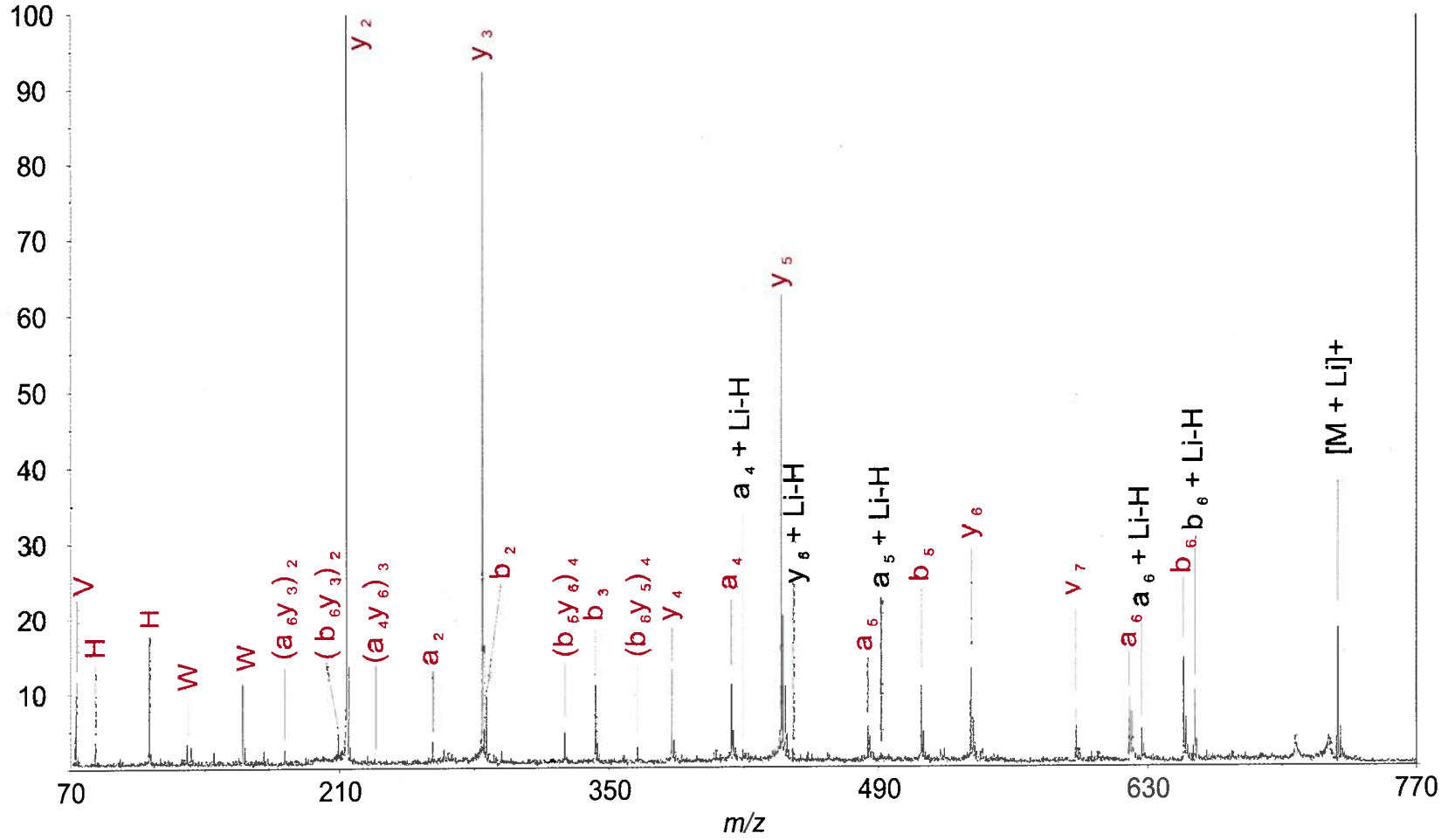


**Figure 35a**. High energy CID TOF-TOF spectrum for [WVGVAHG+Li]$^+$.

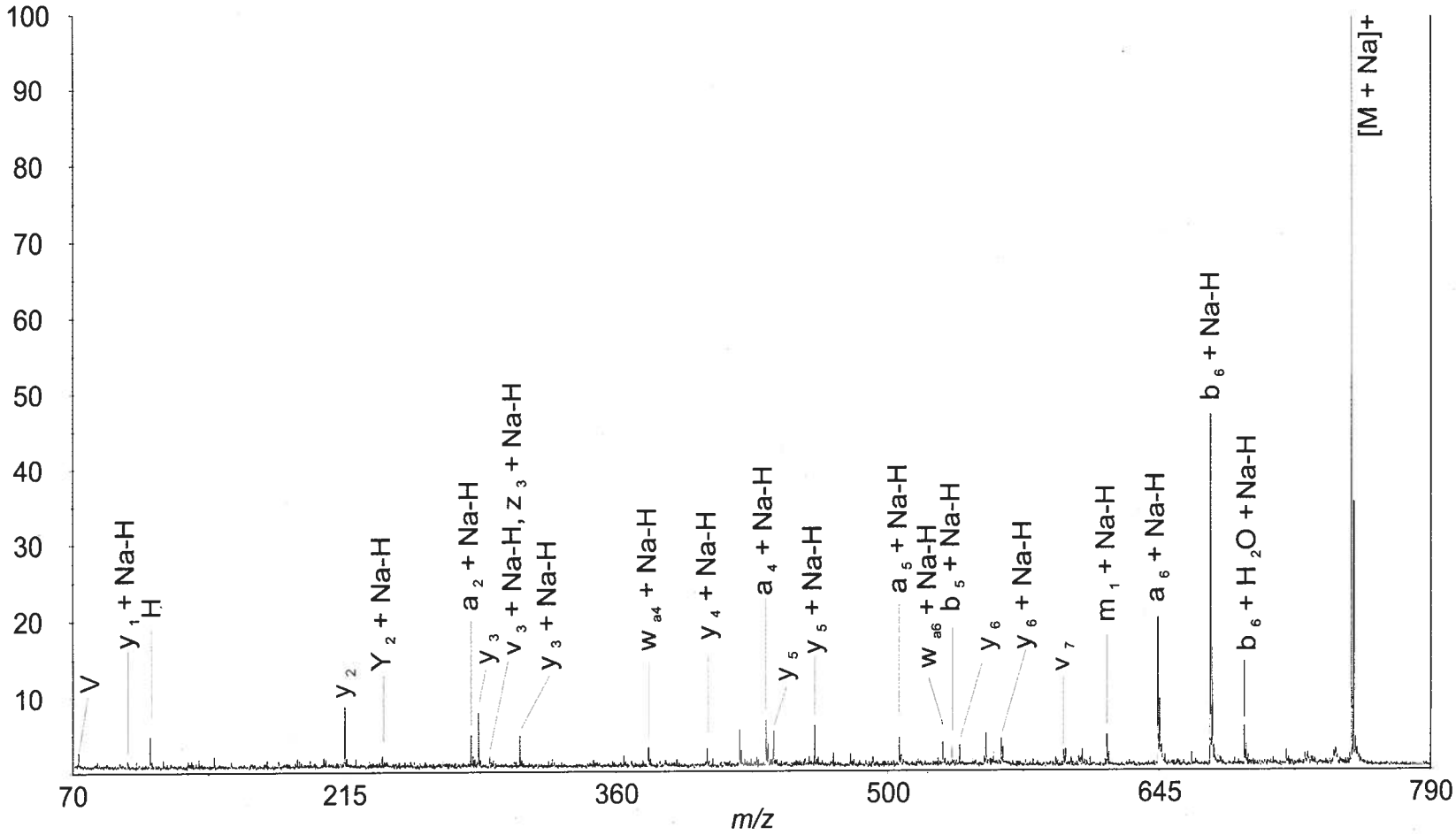


**Figure 35b**. High energy CID TOF-TOF spectrum for $[WVGVAHG+Na]^+$.

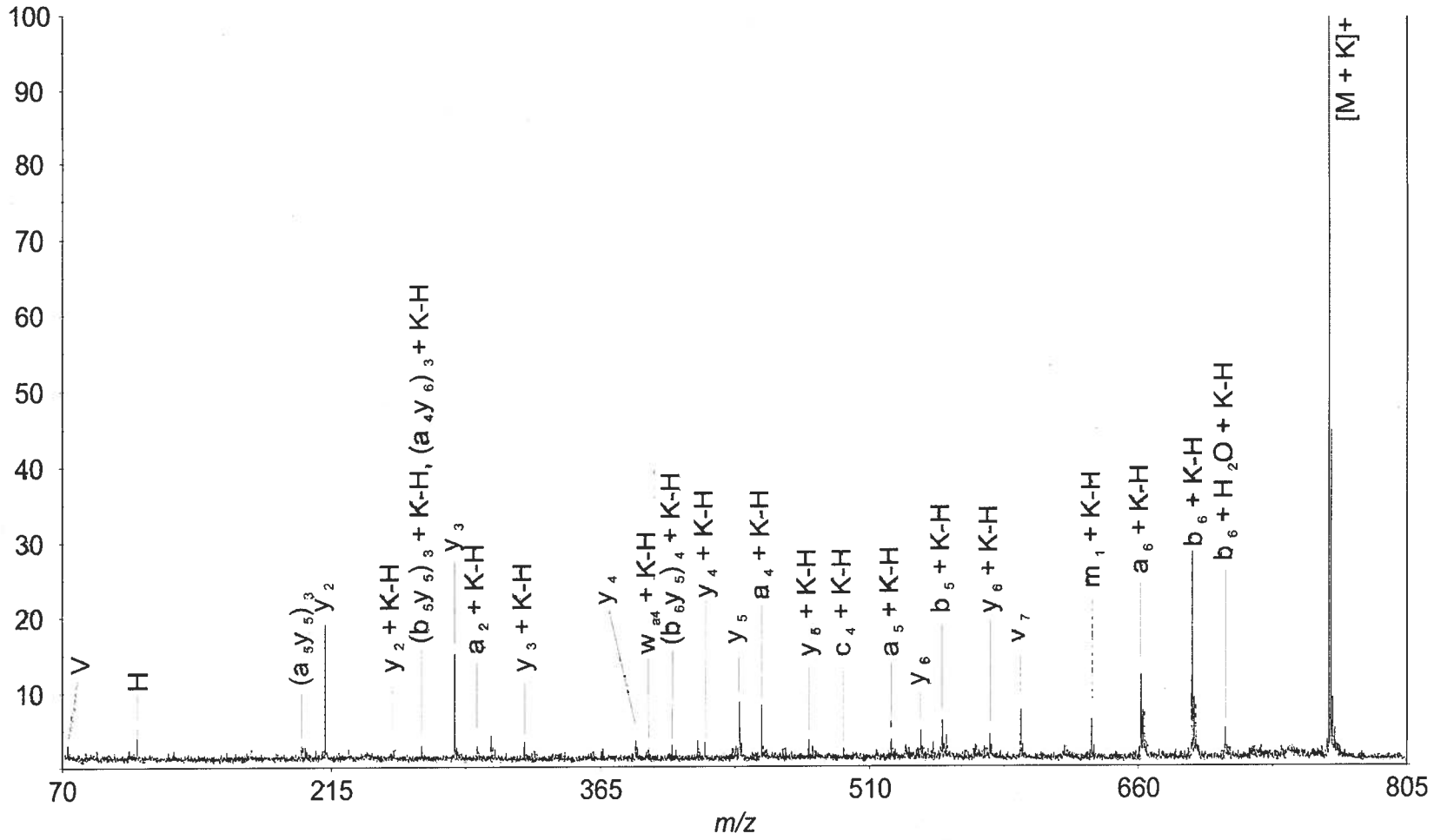


**Figure 35c**. High energy CID TOF-TOF spectrum for $[WVGVAHG+K]^{+}$.

spectra are more complex than those described in previous chapters. The fragmentation is therefore more complex as well. Though many examples are shown here, the main observation is that the inclusion of a second coordination site makes the data more complex, and the preference for one class of ion over another difficult to establish.

Collision cross sections for all relevant ions are contained in Table 5.

**Table 5**. Collision cross sections of XVGVAHG ions.

| Collision cross sections of ions, Å$^2$ | | | |
|---|---|---|---|
| Peptide | $H^+$ | $Na^+$ | $Cu^+$ |
| RVGVAHG, **12** | 190.1 | 196.7 | 201.6 |
| HVGVAHG, **13** | 183.5 | 187.2 | 192.4 |
| KVGVAHG, **14** | 185.8 | 192.6 | 200.5 |
| WVGVAHG, **15** | 196.7 | 198.7 | 195.5 |

Non-sequence ions are abundant in the tandem mass spectra of these metalated ions, likely due to the additional strongly-coordinating imidazole ring (see **Figures 25**, **28**, **31**, and **34**). $[M+H]^+$, $[M+Cu]^+$, and $[M+Ag]^+$ ions yield numerous fragment ions distributed over both N- and C-terminal containing, with $a_i$, $b_i$, and $y_i$ being the most abundant(see **Figures 24**, **27**, **30**, and **33**. The alkali metalated ions have previously shown a preference for C-terminal fragment ions (earlier chapters), but even that trend is less pronounced here, as alkali metalated $a_i$ and $b_i$ ions are commonplace, and in significant abundance, (see **Figures 26**, **29**, **32**, and **35**).

**Conclusions**

The introduction of the second site leads to structures with greater contribution to the metal center complexation and charge solvation with the histidine side chain than with the serine residue hydroxyl group, as shown by the fragment ion patterns and the candidate structures obtained. Rather than the fragment spectra being dominated by N-terminal fragment ion series, a mixture of fragment ion series including both the N- and C-terminus are observed, indicating that the charge site of the ion is distributed more evenly along the backbone. The structures show that the charge sites in both protonated and metalated ions are heavily solvated by the peptide backbone carbonyl oxygen atoms and the histidine side chain. These ions are far more complex in terms of fragment ion spectra than those observed for the single basic residue series, for example **1-3**.

# CHAPTER V

# CONCLUSIONS

The results presented here support our earlier charge-directed mechanism for fragmentation of $[M+Cu]^+$ ions [18]. The complexation of the metal displaces a proton, which behaves similar to the ionizing proton in a protonated peptide. Even though the metal itself is not mobile, as evidenced by the candidate structures obtained and the observed immonium ions complexed to metal ions, the net charge is not necessarily sequestered at one site. Our mechanism is not applicable to that proposed by Allison, in that the charge derivative that was employed in that work was both inert and very large, likely eliminating any contribution from charge-directed fragmentation.

In order to probe further the chemistry of these model peptides, photodissociation experiments were performed on peptides from the series. From comparing a pair of isomers, it was shown that the position of valine within the peptide backbone influences the formation of $a_i$ ions, owing to the stability of the intermediate, which includes a tertiary carbon. This is the first documentation of what might be termed, "the valine effect." The differences in fragmentation in the CID and photodissociation experiments suggests different fragmentation mechanisms at work in the two experiments. A remote charge site mechanism is the prompt fragmentation, where simple bond cleavage and radical migration yields $a_i$ and $d_{ai}$ ions, and a mobile proton mechanism in the CID experiments, which yield numerous fragments.

After expanding the study to include peptides with additional strongly coordinating functional groups (the side chain of histidine), our experiments to apply the same

mechanism of fragmentation was inconclusive based upon the rich fragmentation chemistry observed. Since the histidine peptides are more complex, this does not seem to present a counterargument to our original mechanism, it is simply not applicable to the other systems. These systems proved interesting in that the fragment ion spectra had good figures of merit and metal ions $Cu^+$ and $Ag^+$ yielded similar spectral results, but as mechanistic probes, they are not very useful, as most of the spectra yielded similar spectral results as well, owing to the presence of a second high proton affinity and high metal ion affinity functional group near the C-terminal end of the peptide.

Site replacement studies of homologs are a great way to establish factors that influence peptide fragmentation. The theme of careful modifications to peptide sequences in order to study peptide ion fragmentation coupled with structural analysis via ion mobility has great potential to further the understanding of peptide fragmentation. Most studies of peptide fragmentation seem to use sequences that are too dissimilar to draw meaningful comparisons between the fragmentation patterns. It is paramount to remove as many variables as possible in the study of such complex systems. There are many possible avenues that this research project could take, and I am interested in seeing a better understanding of intrinsic factors that influence peptide fragmentation develop from more work in this area.

# REFERENCES


1. Cheng, C. and Gross, M. L. Applications and Mechanisms of Charge-Remote Fragmentation. *Mass Spectrom. Rev.* **2000**, *19*, 398-420.

2. Wysocki, V. H.; Tsaprailis, G.; Smith, L. L. and Breci, L. A. Mobile and Localized Protons: A Framework for Understanding Peptide Dissociation. *J. Mass Spectrom.* **2000**, *35*, 1399-1406.

3. Roepstorff, P. and Fohlman, J. Proposal for a Common Nomenclature for Sequence Ions in Mass Spectra of Peptides. *Biomed. Mass Spectrom.* **1984**, *11*, 601.

4. Mendez, I. I.; She, Y.-M.; Ens, W. and Coombs, K. M. Digestion Pattern of Reovirus Outer Capsid Protein S3 Determined by Mass Spectrometry. *Virology* **2003**, *311*, 289-304.

5. Williams, K. E.; Carver, T. A.; Miranda, J. J. L.; Kautiainen, A.; Vogel, J. S.; Dingley, K.; Baldwin, M. A.; Turteltaub, K. W. and Burlingame, A. L. Attomole Detection of In Vivo Protein Targets of Benzene in Mice. Evidence for a Highly Reactive Metabolite. *Mol. Cell. Proteomics* **2002**, *1*, 885-895.

6. Stanley, S. M. R. and Poljak, A. Matrix-Assisted Laser-Desorption Time-of Flight Ionisation and High-Performance Liquid Chromatography-Electrospray Ionisation Mass Spectral Analyses of Two Glycosylated Recombinant Epoetins. *J. Chromatogr., B: Anal. Technol. Biomed. Life Sci.* **2003**, *785*, 205-218.

7. Choudhary, G.; Wu, S.-L.; Shieh, P. and Hancock, W. S. Multiple Enzymatic Digestion for Enhanced Sequence Coverage of Proteins in Complex Proteomic Mixtures Using Capillary LC with Ion Trap MS/MS. *J. Proteome Res.* **2003**, *2*, 59-67.

8. Ramstroem, M.; Hagman, C.; Tsybin, Y. O.; Markides, K. E.; Hakansson, P.; Salehi, A.; Lundquist, I.; Hakanson, R. and Bergquist, J. A Novel Mass Spectrometric Approach to the Analysis of Hormonal Peptides in Extracts of Mouse Pancreatic Islets. *Eur. J. Biochem.* **2003**, *270*, 3146-3152.

9. Chen, Z.-W.; Eriste, E.; Jonsson, A. P.; Norberg, A.; Nepomuceno, D.; Lovenberg, T. W.; Bergman, T.; Efendic, S.; Jornvall, H. and Sillard, R. $Ser^{13}$-Phosphorylated PYY from Porcine Intestine with a Potent Biological Activity. *FEBS Lett.* **2001**, *492*, 119-122.

10. Chen, H.; O'Connor, S.; Cane, D. E. and Walsh, C. T. Epothilone Biosynthesis: Assembly of the Methylthiazolylcarboxy Starter Unit on the EpoB Subunit. *Chem. Biol.* **2001**, *8*, 899-912.

11. Keller, U. and Schauwecker, F. Combinatorial Biosynthesis of Non-Ribosomal Peptides. *Comb. Chem. High Throughput Screening* **2003**, *6*, 527-540.

12. Liepke, C.; Zucht, H. D.; Forssmann, W. G. and Standker, L. Purification of Novel Peptide Antibiotics from Human Milk. *J. Chromatogr., B: Anal. Technol. Biomed. Life Sci.* **2001**, *752*, 369-377.

13. Jaworski, A. and Bruckner, H. Sequences of Polypeptide Antibiotics Stilboflavins, Natural Peptaibol Libraries of the Mold *Stilbella Flavipes*. *J. Pept. Sci.* **2001**, *7*, 433-447.

14. Keough, T.; Youngquist, R. S. and Lacey, M. P. A Method for High Sensitivity Peptide Sequencing Using Postsource Decay Matrix-Assisted Laser Desorption Ionization Mass Spectrometry. *Proc. Natl. Acad. Sci. U. S. A.* **1999**, *96*, 7131-7136.

15. Dikler, S.; Kelly, J. W. and Russell, D. H. Improving Mass Spectrometric Sequencing of Arginine-Containing Peptides by Derivatization with Acetylacetone. *J. Mass Spectrom.* **1997**, *32*, 1337-1349.

16. Liao, P.-C.; Huang, Z.-H. and Allison, J. Charge Remote Fragmentation of Peptides Following Attachment of a Fixed Positive Charge: A Matrix-Assisted Laser Desorption/Ionization Postsource Decay Study. *J. Am. Soc. Mass Spectrom.* **1997**, *8*, 501-509.

17. Shields, S. J.; Bluhm, B. K. and Russell, D. H. Novel Method for $[M + Cu]^+$ Ion Formation by Matrix-Assisted Laser Desorption Ionization. *Int. J. Mass Spectrom.* **1999**, 182/183, 185-195.

18. Shields, S. J.; Bluhm, B. K. and Russell, D. H. Fragmentation Chemistry of $[M + Cu]^+$ Peptide Ions Containing an *N*-terminal Arginine. *J. Am. Soc. Mass Spectrom.* **2000**, *11*, 626-638.

19. Liao, P.-C. and Allison, J. Enhanced Detection of Peptides in Matrix-Assisted Laser Desorption/Ionization Mass Spectrometry Through the Use of Charge-Localized Derivatives. *J. Mass Spectrom.* **1995**, *30*, 511-512.

20. Herrmann, K. A.; Wysocki, V. H. and Vorpagel, E. R. Computational Investigation and Hydrogen/Deuterium Exchange of the Fixed Charge Derivative Tris(2,4,6-trimethoxyphenyl)Phosphonium: Implications for the Aspartic Acid Cleavage Mechanism. *J. Am. Soc. Mass Spectrom.* **2005**, *16*, 1067-1080.

21. Harrison, A. G.; Young, A. B.; Bleiholder, C.; Suhai, S. and Paizs, B. Scrambling of Sequence Information in Collision-Induced Dissociation of Peptides. *J. Am. Chem. Soc.* **2006**, *128*, 10364-10365.

22. Clemmer, D. E.; Hudgins, R. R. and Jarrold, M. F. Naked Protein Conformations: Cytochrome C in the Gas Phase. *J. Am. Chem. Soc.* **1995**, *117*, 10141-10142.

23. Wyttenbach, T.; von Helden, G. and Bowers, M. T. Gas-phase Conformation of Biological Molecules: Bradykinin. *J. Am. Chem. Soc.* **1996**, *118*, 8355-8364.

24. Ruotolo, B. T.; Verbeck, G. F.; Thomson, L. M.; Gillig, K. J. and Russell, D. H. Observation of Conserved Solution-phase Secondary Structure in Gas-phase Tryptic Peptides. *J. Am. Chem. Soc.* **2002**, *124*, 4214-4215.

25. Shelimov, K. B.; Clemmer, D. E.; Hudgins, R. R. and Jarrold, M. F. Protein Structure in Vacuo: Gas-phase Conformations of BPTI and Cytochrome C. *J. Am. Chem. Soc.* **1997**, *119*, 2240-2248.

26. Wyttenbach, T.; Witt, M. and Bowers, M. T. On the Stability of Amino Acid Zwitterions in the Gas Phase: the Influence of Derivatization, Proton Affinity, and Alkali Ion Addition. *J. Am. Chem. Soc.* **2000**, *122*, 3458-3464.

27. Dougherty, D. A. Cation-π Interactions in Chemistry and Biology: A New View of Benzene, Phe, Tyr, and Trp. *Science (Washington, D.C., U. S.)* **1996**, *271*, 163-168.

28. Raju, K. and Anwar, R. A. Primary Structure of Bovine Elastin A, B, and C Deduced from the Sequences of cDNA Clones. *J. Biol. Chem.* **1987**, *262*, 5755-5762.

29. Indik, Z.; Yeh, H.; Ornstein-Goldstein, N.; Sheppard, P.; Anderson, N.; Rosenbloom, J. C.; Peltonen, L. and Rosenbloom, J. Alternative Splicing of Human Elastin mRNA Indicated by Sequence Analysis of Cloned Genomic and Complementary DNA. *Proc. Natl. Acad. Sci. U. S. A.* **1987**, *84*, 5680-5684.

30. Sandberg, L. B.; Soskel, N. T. and Leslie, J. G. Elastin Structure, Biosynthesis, and Relation to Disease States. *N. Engl. J. Med.* **1981**, *304*, 566-579.

31. Lim, J. and Vachet, R. W. Using Mass Spectrometry to Study Copper-Protein Binding under Native and Non-Native Conditions: $\beta_2$-Microglobulin. *Anal. Chem.* **2004**, *76*, 3498-3504.

32. Gejyo, F.; Yamada, T.; Odani, S.; Nakagawa, Y.; Arakawa, M.; Kunitomo, T.; Kataoka, H.; Suzuki, M.; Hirasawa, Y.; Shirahama, T.; Cohen, A. S. and Schmid, K. A New Form of Amyloid Protein Associated with Chronic Hemodialysis Was Identified as $\beta_2$-Microglobulin. *Biochem. Biophys. Res. Commun.* **1985**, *129*, 701-706.

33. Chiti, F.; De Lorenzi, E.; Grossi, S.; Mangione, P.; Giorgetti, S.; Caccialanza, G.; Dobson, C. M.; Merlini, G.; Ramponi, G. and Bellotti, V. A Partially Structured

Species of $\beta_2$-Microglobulin is Significantly Populated under Physiological Conditions and Involved in Fibrillogenesis. *J. Biol. Chem.* **2001**, *276*, 46714-46721.

34. Mallis, L. M. and Russell, D. H. Fast-Atom-Bombardment-Tandem Mass Spectrometry Studies of Alkali-Metal Ions of Small Peptides. *Anal. Chem.* **1986**, *58*, 1076-1080.

35. Biemann, K. and Martin, S. A. Mass Spectrometric Determination of the Amino Acid Sequence of Peptides and Proteins. *Mass Spectrom. Rev.* **1987**, *6*, 1-76.

36. McDaniel, E. W. and Mason, E. A. *The Mobility and Diffusion of Ions in Gases*, 1st ed., Wiley-Interscience: New York, 1973, p 372.

37. Mason, E. A. and McDaniel, E. W. *Transport Properties of Ions in Gases*, 1st ed., Wiley-Interscience: New York, 1988, p 560.

38. Mesleh, M. F.; Hunter, J. M.; Shvartsburg, A. A.; Schatz, G. C. and Jarrold, M. F. Structural Information from Ion Mobility Measurements: Effects of the Long-Range Potential. *J. Phys. Chem.* **1996**, *100*, 16082-16086.

39. Shvartsburg, A. A.; Siu, K. W. M. and Clemmer, D. E. Prediction of Peptide Ion Mobilities Via A Priori Calculations from Intrinsic Size Parameters of Amino Acid Residues. *J. Am. Soc. Mass Spectrom.* **2001**, *12*, 885-888.

40. Vachet, R. W.; Asam, M. R. and Glish, G. L. Secondary Interactions Affecting the Dissociation Patterns of Arginine-Containing Peptide Ions. *J. Am. Chem. Soc.* **1996**, *118*, 6252-6256.

41. Lee, S.-W.; Kim, H. S. and Beauchamp, J. L. Salt Bridge Chemistry Applied to Gas-Phase Peptide Sequencing: Selective Fragmentation of Sodiated Gas-Phase Peptide Ions Adjacent to Aspartic Acid Residues. *J. Am. Chem. Soc.* **1998**, *120*, 3188-3195.

42. Tsaprailis, G.; Nair, H.; Somogyi, A.; Wysocki, V. H.; Zhong, W.; Futrell, J. H.; Summerfield, S. G. and Gaskell, S. J. Influence of Secondary Structure on the Fragmentation of Protonated Peptides. *J. Am. Chem. Soc.* **1999**, *121*, 5142-5154.

43. Griffiths, W. J. and Jonsson, A. P. Gas Phase Conformation Can Have an Influence on Peptide Fragmentation. *Proteomics* **2001**, *1*, 934-945.

44. Demmers, J. A. A.; Rijkers, D. T. S.; Haverkamp, J.; Killian, J. A. and Heck, A. J. R. Factors Affecting Gas-Phase Deuterium Scrambling in Peptide Ions and Their Implications for Protein Structure Determination. *J. Am. Chem. Soc.* **2002**, *124*, 11191-11198.

45. Feng, W. Y.; Gronert, S.; Fletcher, K. A.; Warres, A. and Lebrilla, C. B. The Mechanism of *C*-terminal Fragmentations in Alkali Metal Ion Complexes of Peptides. *Int. J. Mass Spectrom.* **2003**, *222*, 117-134.

46. Breci, L. A.; Tabb, D. L.; Yates, J. R. and Wysocki, V. H. Cleavage *N*-terminal to Proline: Analysis of a Database of Peptide Tandem Mass Spectra. *Anal. Chem.* **2003**, *75*, 1963-1971.

47. Bluhm, B. K.; Shields, S. J.; Bayse, C. A.; Hall, M. B. and Russell, D. H. Determination of Copper Binding Sites in Peptides Containing Basic Residues: A Combined Experimental and Theoretical Study. *Int. J. Mass Spectrom.* **2001**, *204*, 31-46.

48. Ruotolo, B. T. and Russell, D. H. Gas-phase Conformations of Proteolytically Derived Protein Fragments: Influence of Solvent on Peptide Conformation. *J. Phys. Chem. B* **2004**, *108*, 15321-15331.

49. Sawyer, H. A.; Marini, J. T.; Stone, E. G.; Ruotolo, B. T.; Gillig, K. J. and Russell, D. H. The Structure of Gas-Phase Bradykinin Fragment 1-5 (RPPGF) Ions: An Ion Mobility Spectrometry and H/D Exchange Ion-Molecule Reaction Chemistry Study. *J. Am. Soc. Mass Spectrom.* **2005**, *16*, 893-905.

50. Dongre, A. R.; Jones, J. L.; Somogyi, A. and Wysocki, V. H. Influence of Peptide Composition, Gas-Phase Basicity, and Chemical Modification on Fragmentation Efficiency: Evidence for the Mobile Proton Model. *J. Am. Chem. Soc.* **1996**, *118*, 8365-8374.

51. Nachman, R. J.; Coast, G. M.; Tichy, S. E.; Russell, D. H.; Miller, J. A. and Predel, R. Occurrence of Insect Kinins in the Flesh Fly, Stable Fly and Horn Fly-Mass Spectrometric Identification from Single Nerves and Diuretic Activity. *Peptides* **2002**, *23*, 1885-1894.

52. Nachman, R. J.; Russell, W. K.; Coast, G. M.; Russell, D. H. and Predel, R. Mass Spectrometric Assignments of Leu/Ile in Neuropeptides from Signal Neurohemal Organ Preparations of Insects. *Peptides* **2005**, *26*, 2151-2156.

53. Tecklenburg, R. E., Jr.; Miller, M. N. and Russell, D. H. Laser Ion Beam Photodissociation Studies of Model Amino Acids and Peptides. *J. Am. Chem. Soc.* **1989**, *111*, 1161-1171.

54. Wang, D. and Cotter, R. J. Approach for Determining Protein Ubiquitination Sites by MALDI-TOF Mass Spectrometry. *Anal. Chem.* **2005**, *77*, 1458-1466.

55. Bunk, D. M. and Macfarlane, R. D. Study of the Charge-Remote Fragmentation of Bradykinin Using Californium-252 Plasma Desorption Mass Spectrometry. *Int. J. Mass Spectrom. Ion Processes* **1991**, *111*, 55-75.

56. Gillig, K. J. and Russell, D. H., A Periodic Field Focusing Ion Mobility Spectrometer. U.S. Patent 6,639213, October 28, 2003.

57. *Cerius*$^{2}$, 4.9; Accelrys: San Diego, CA, USA, 2004.

58. *Insight*$^{II}$, 2000.2; Accelrys: San Diego, CA, USA, 2000.

59. Pappalardo, M.; Milardi, D.; Grasso, D. M. and La Rosa, C. Free Energy Perturbation and Molecular Dynamics of Copper Binding to Azurin. *J. Comput. Chem.* **2003**, *24*, 779-785.

60. Hunter, E. P. and Lias, S. G. Evaluated Gas Phase Basicities and Proton Affinities of Molecules: an Update. *J. Phys. Chem. Ref. Data* **1998**, *27*, 413-656.

61. Kish, M. M.; Ohanessian, G. and Wesdemiotis, C. The $Na^+$ Affinities of α-Amino Acids: Side-Chain Substituent Effects. *Int. J. Mass Spectrom.* **2003**, *227*, 509-524.

62. Lau, J. K. C.; Wong, C. H. S.; Ng, P. S.; Siu, F. M.; Ma, N. L. and Tsang, C. W. Absolute Potassium Cation Affinities (PCAs) in the Gas Phase. *Chem.--Eur. J.* **2003**, *9*, 3383-3396.

63. Russell, D. H.; McGlohon, E. S. and Mallis, L. M. Fast-Atom Bombardment-Tandem Mass Spectrometry Studies of Organo-Alkali-Metal Ions of Small Peptides. Competitive Interaction of Sodium with Basic Amino Acid Substituents. *Anal. Chem.* **1988**, *60*, 1818-1824.

64. Harrison, A. G. The Gas-Phase Basicities and Proton Affinities of Amino Acids and Peptides. *Mass Spectrom. Rev.* **1997**, *16*, 201-217.

65. Martell, A. E. and Hancock, R. D. *Metal Complexes in Aqueous Solutions*, 2nd ed., Springer: New York, 2005, p 268.

66. Yalcin, T.; Csizmadia, I. G.; Peterson, M. R. and Harrison, A. G. Why Are B Ions Stable Species in Peptide Spectra? *J. Am. Soc. Mass Spectrom.* **1995**, *6*, 1165-1174.

67. Huang, Y.; Tichy, S. E. and Russell, D. H., manuscript in preparation, Dept. of Chemistry, Texas A&M University, 2007.

68. Sanderson, R. T. *Chemical Bonds and Bond Energy*, 2nd Ed., Academic Press: New York, 1976, p. 218.

69. Slaton, J. G.; Russell, W. K. and Russell, D. H., manuscript in preparation, Dept. of Chemistry, Texas A&M University, 2007.

70. Morgan, J. W. and Russell, D. H. Comparative Studies of 193-nm Photodissociation and TOF-TOFMS Analysis of Bradykinin Analogs: The Effects of Charge Site(s) and Fragmentation Timescales. *J. Am. Soc. Mass Spectrom.* **2006**, *17*, 721-729.

71. Johnson, R. S.; Martin, S. A. and Biemann, K. Collision-Induced Fragmentation of $(M + H)^+$ Ions of Peptides. Side Chain Specific Sequence Ions. *Int. J. Mass Spectrom. Ion Processes* **1988**, *86*, 137-154.

72. Cooks, R. G.; Ast, T. and Mabud, M. A. Collisions of Polyatomic Ions with Surfaces. *Int. J. Mass Spectrom. Ion Processes* **1990**, *100*, 209-265.

73. Jackson, A. T.; Despeyroux, D. and Jennings, K. R. The Observation of Broad Metastable Ion Peaks in the Surface-Induced Dissociation Mass Spectra of Protonated and Cationated Peptides. *Int. J. Mass Spectrom. Ion Processes* **1995**, *141*, 91-99.

74. Barbacci, D. C. and Russell, D. H. Sequence and Side-Chain Specific Photofragment (193 nm) Ions from Protonated Substance P by Matrix-Assisted Laser Desorption Ionization Time-of-Flight Mass Spectrometry. *J. Am. Soc. Mass Spectrom.* **1999**, *10*, 1038-1040.

75. Thompson, M. S.; Cui, W. and Reilly, J. P. Mass Spectrometry: Fragmentation of Singly Charged Peptide Ions by Photodissociation at $\lambda = 157$ nm. *Angew. Chem., Int. Ed.* **2004**, *43*, 4791-4794.

76. Farrugia, J. M. and O'Hair, R. A. J. Involvement of Salt Bridges in a Novel Gas Phase Rearrangement of Protonated Arginine-Containing Dipeptides Which Precedes Fragmentation. *Int. J. Mass Spectrom.* **2003**, *222*, 229-242.

77. Paisz, B. and Suhai, S. Towards Understanding the Tandem Mass Spectra of Protonated Oligopeptides. 1: Mechanism of Amide Bond Cleavage. *J. Am. Soc. Mass Spectrom.* **2004**, *15*, 103-113.

78. Komaromi, I.; Somogyi, A. and Wysocki, V. H. Proton Migration and its Effect on the MS Fragmentation of N-acetyl OMe Proline: MS/MS Experiments and *ab initio* and Density Functional Calculations. *Int. J. Mass Spectrom.* **2005**, *241*, 315-323.

79. Cui, W.; Thompson, M. S. and Reilly, J. P. Pathways of Peptide Ion Fragmentation Induced by Vacuum Ultraviolet Light. *J. Am. Soc. Mass Spectrom.* **2005**, *16*, 1384-1398.

80. Anbalagan, V. and Van Stipdonk, M. J. Gas-Phase Investigation of Pd(II)-Alanine Complexes with Small Native and Derivatized Peptides Containing Histidine. *J. Mass Spectrom.* **2003**, *38*, 982-989.

81. Kapp, E. A.; Schuetz, F.; Reid, G. E.; Eddes, J. S.; Moritz, R. L.; O'Hair, R. A. J.; Speed, T. P. and Simpson, R. J. Mining a Tandem Mass Spectrometry Database to Determine the Trends and Global Factors Influencing Peptide Fragmentation. *Anal. Chem.* **2003**, *75*, 6251-6264.

82. Tsaprailis, G.; Nair, H.; Zhong, W.; Kuppannan, K.; Futrell, J. H. and Wysocki, V. H. A Mechanistic Investigation of the Enhanced Cleavage at Histidine in the Gas-Phase Dissociation of Protonated Peptides. *Anal. Chem.* **2004**, *76*, 2083-2094.

83. Slaton, J. G.; Russell, W. K. and Russell, D. H., manuscript in preparation, Dept. of Chemistry, Texas A&M University, 2007.

84. Gillig, K. J.; Ruotolo, B.; Stone, E. G.; Russell, D. H.; Fuhrer, K.; Gonin, M. and Schultz, A. J. Coupling High-Pressure MALDI with Ion Mobility/Orthogonal Time-of-Flight Mass Spectrometry. *Anal. Chem.* **2000**, *72*, 3965-3971.

85. Bienvenut, W. V.; Deon, C.; Pasquarello, C.; Campbell, J. M.; Sanchez, J.-C.; Vestal, M. L. and Hochstrasser, D. F. Matrix-Assisted Laser Desorption/Ionization-Tandem Mass Spectrometry with High Resolution and Sensitivity for Identification and Characterization of Proteins. *Proteomics* **2002**, *2*, 868-876.

86. Yergey, A. L.; Coorssen, J. R.; Backlund, P. S.; Blank, P. S.; Humphrey, G. A.; Zimmerberg, J.; Campbell, J. M. and Vestal, M. L. De Novo Sequencing of Peptides Using MALDI/TOF-TOF. *J. Am. Soc. Mass Spectrom.* **2002**, *13*, 784-791.

87. Morgan, J. W. and Russell, D. H., manuscript in preparation, Dept. of Chemistry, Texas A&M University, 2007.

88. Huang, Y.; Marini, J. T.; Tichy, S. E. and Russell, D. H., manuscript in preparation, Dept. of Chemistry, Texas A&M University, 2007.

89. Wyttenbach, T.; Paizs, B.; Barran, P.; Breci, L.; Liu, D.; Suhai, S.; Wysocki, V. H. and Bowers, M. T. The Effect of the Initial Water of Hydration on the Energetics, Structures, and H/D Exchange Mechanism of a Family of Pentapeptides: An Experimental and Theoretical Study. *J. Am. Chem. Soc.* **2003**, *125*, 13768-13775.

90. Atkins, P. W. *Physical Chemistry*, 5th ed., W. H. Freeman and Company: New York, 1994, p. 1031.

91. Paizs, B. and Suhai, S. Combined Quantum Mechanical and RRKM Modeling of the Main Fragmentation Pathways of Protonated GGG. I. *Cis-trans* Isomerization Around Protonated Amide Bonds. *Rapid Commun. Mass Spectrom.* **2001**, *15*, 2307-2323.

92. Hettick, J. M.; McCurdy, D. L.; Barbacci, D. C. and Russell, D. H. Optimization of Sample Preparation for Peptide Sequencing by MALDI-TOF Photofragment Mass Spectrometry. *Anal. Chem.* **2001**, *73*, 5378-5386.

93. Paizs, B. and Suhai, S. Fragmentation Pathways of Protonated Peptides. *Mass Spectrom. Rev.* **2005**, *24*, 508-548.

# APPENDIX A

## EXAMPLE SIMULATED ANNEALING COMPARISONS

PLOT Page

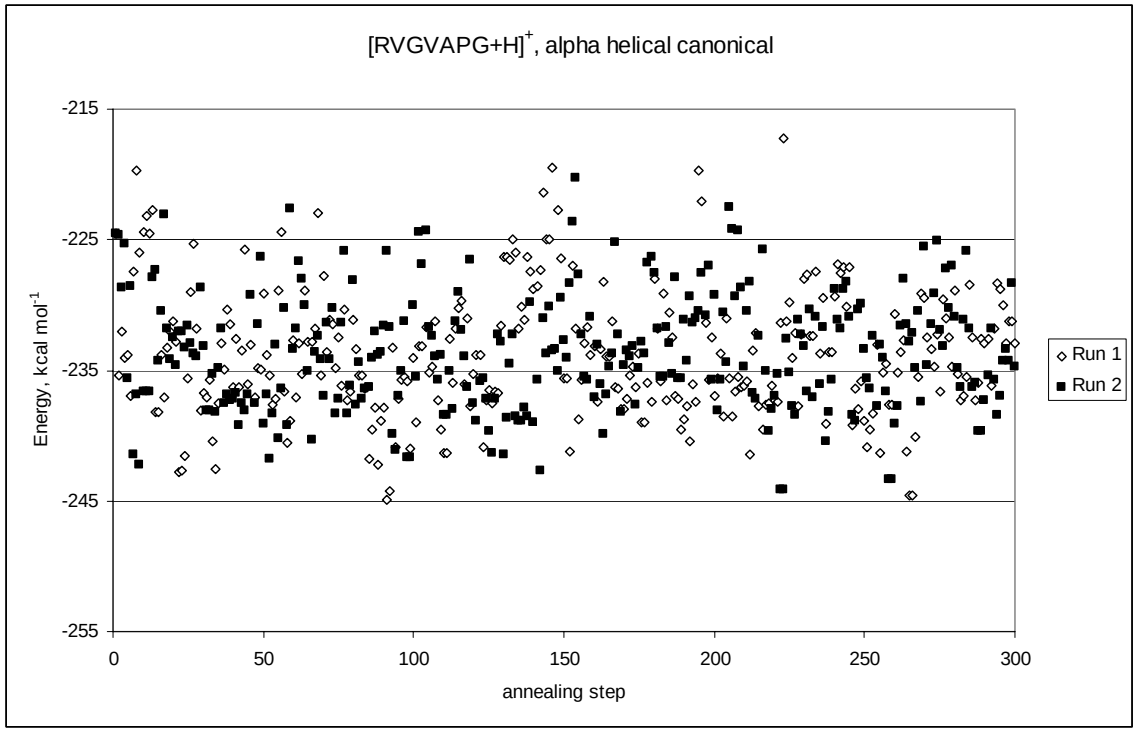
[RVGVAPG+H]+, alpha helical canonical
-215
-225
-235
-245
-255
Energy, kcal mol-1
0
50
100
150
200
250
300
annealing step
Run 1
Run 2

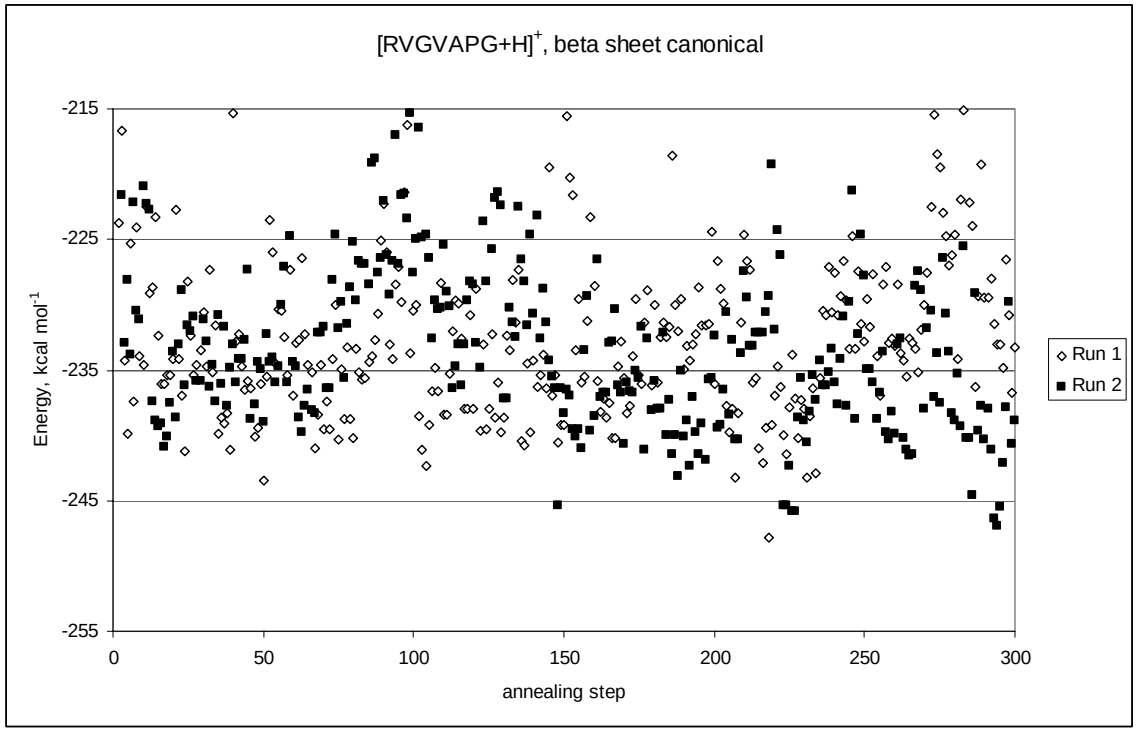
[RVGVAPG+H]+, beta sheet canonical
-215
-225
-235
-245
-255
Energy, kcal mol-1
0
50
100
150
200
250
300
annealing step
Run 1
Run 2

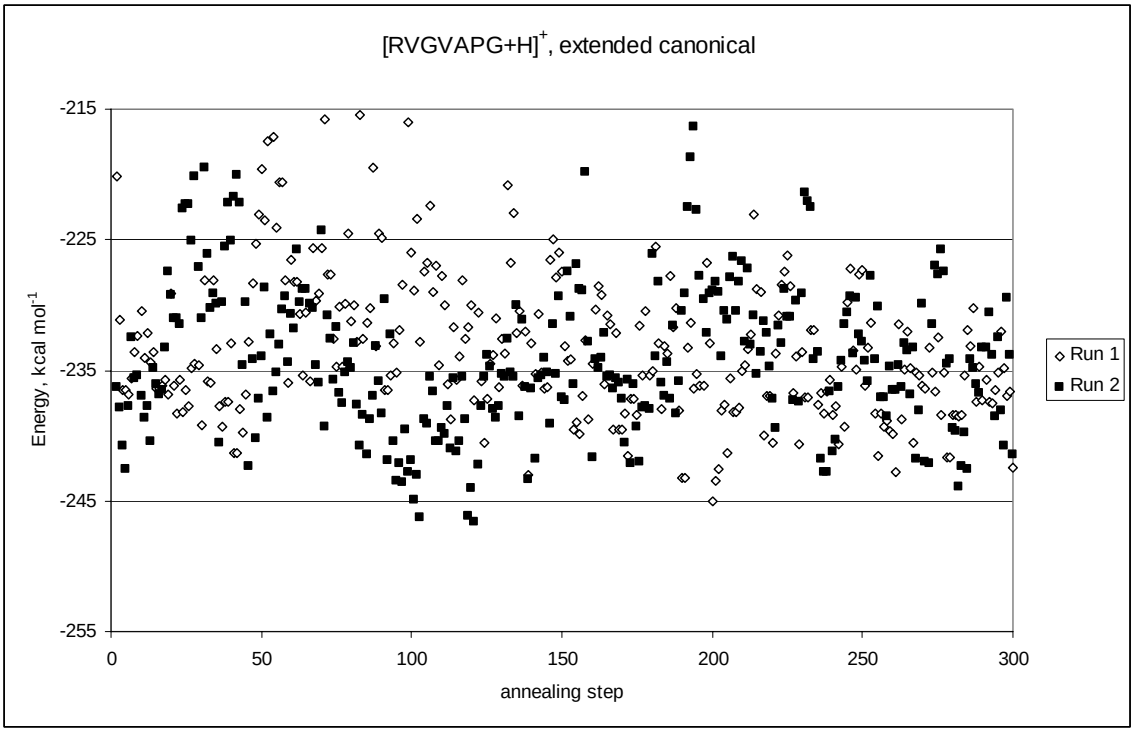
[RVGVAPG+H]+, extended canonical
-215
-225
-235
-245
-255
Energy, kcal mol-1
0
50
100
150
200
250
300
annealing step
Run 1
Run 2

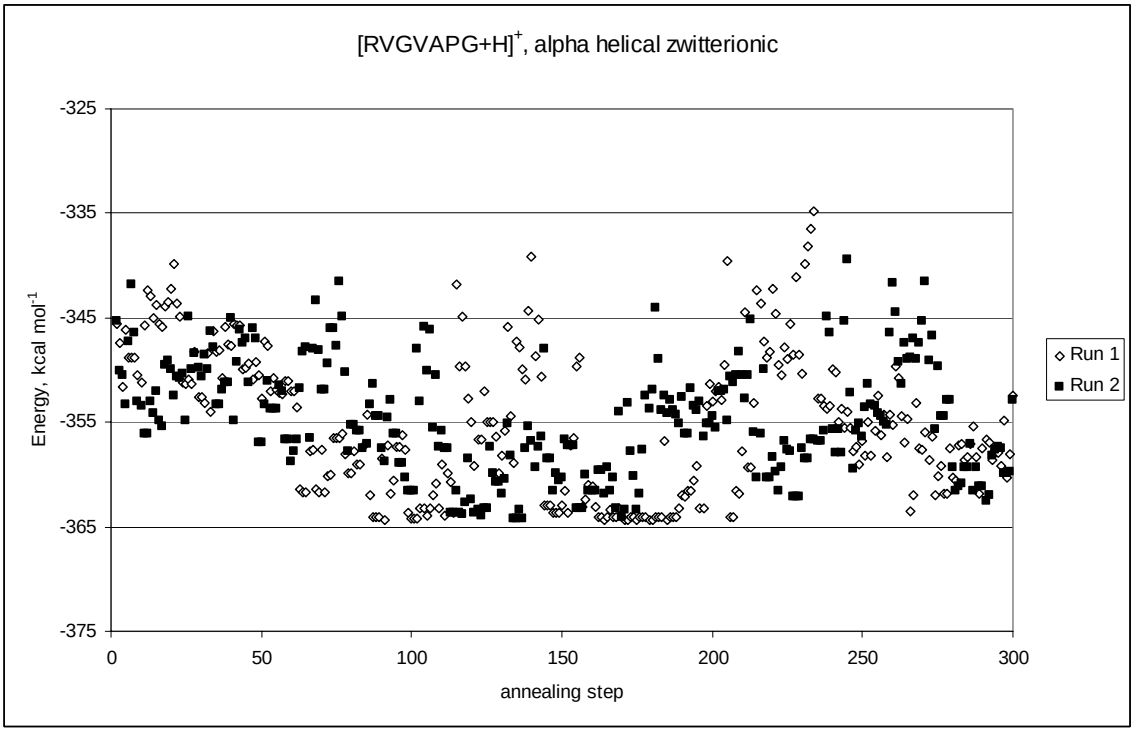
[RVGVAPG+H]+, alpha helical zwitterionic
-325
-335
-345
-355
-365
-375
Energy, kcal mol-1
0
50
100
150
200
250
300
annealing step
Run 1
Run 2

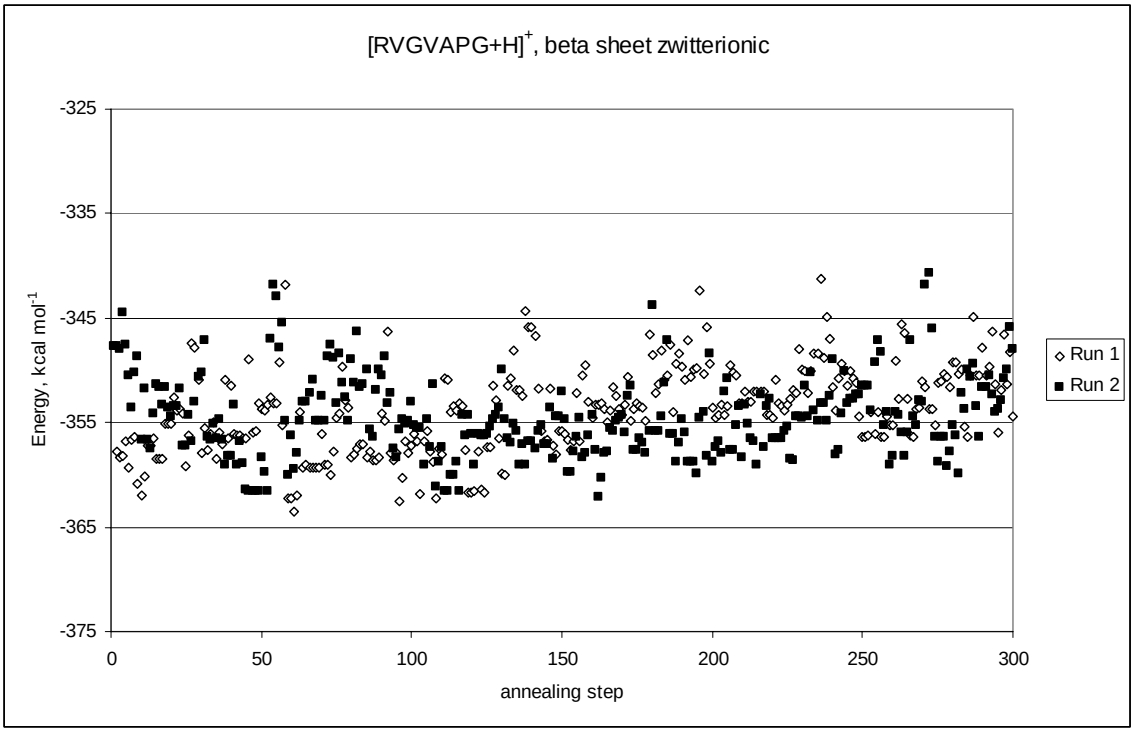
[RVGVAPG+H]+, beta sheet zwitterionic
-325
-335
-345
-355
-365
-375
Energy, kcal mol-1
0
50
100
150
200
250
300
annealing step
Run 1
Run 2

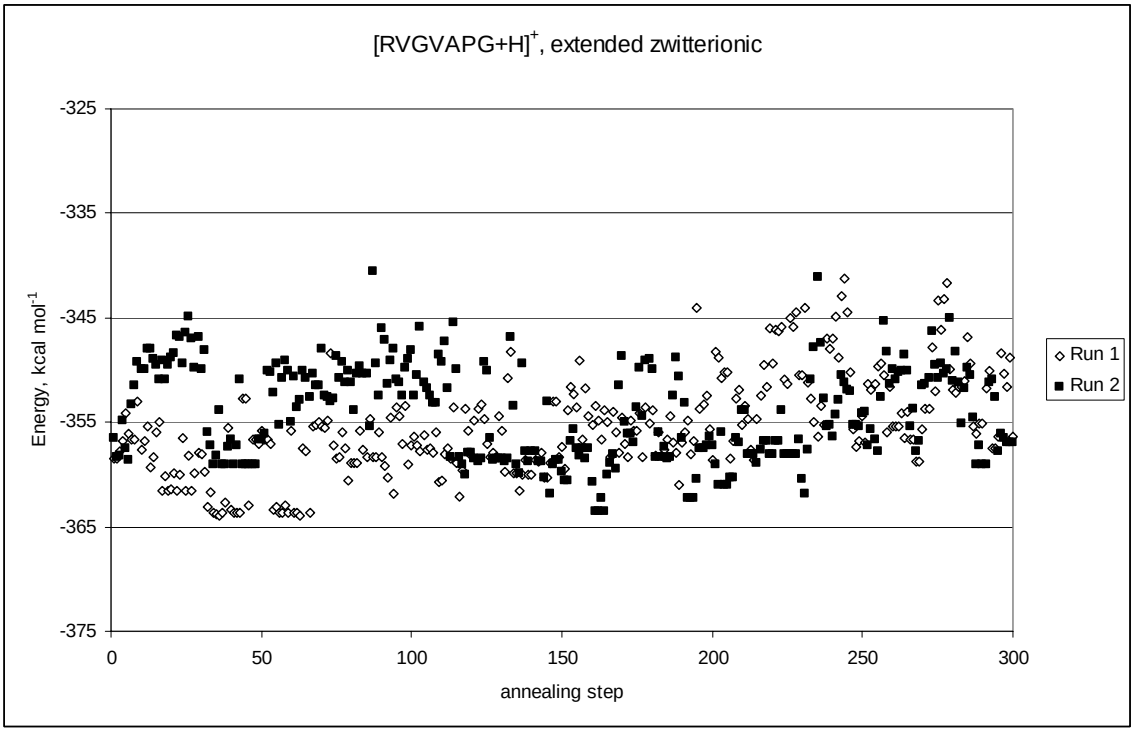
[RVGVAPG+H]+, extended zwitterionic
-325
-335
-345
-355
-365
-375
Energy, kcal mol-1
0
50
100
150
200
250
300
annealing step
Run 1
Run 2

# APPENDIX B

## CLUSTER PLOTS FOR STRUCTURE SELECTION

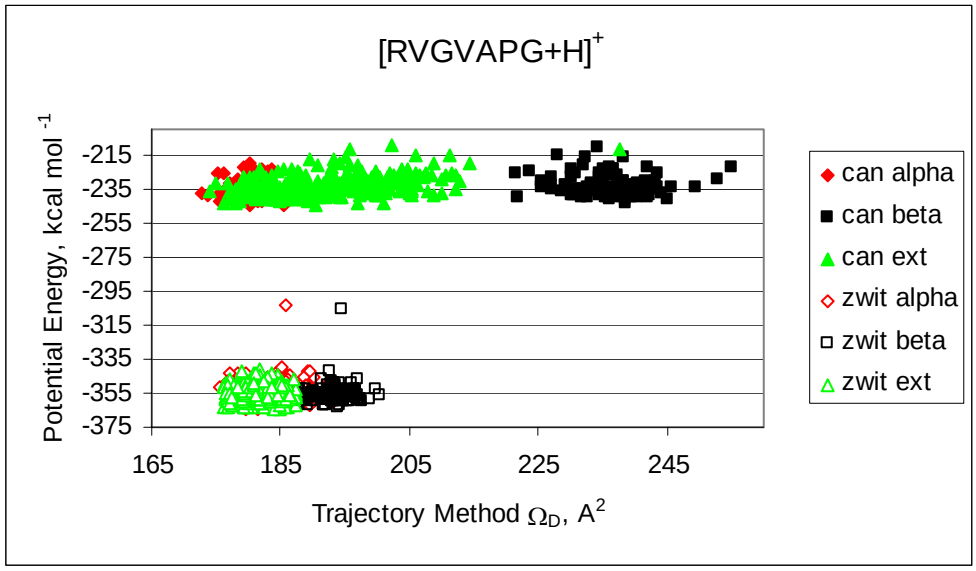
[RVGVAPG+H]+
Potential Energy, kcal mol -1
-215
-235
-255
-275
-295
-315
-335
-355
-375
165
185
205
225
245
Trajectory Method ΩD, A2
can alpha
can beta
can ext
zwit alpha
zwit beta
zwit ext

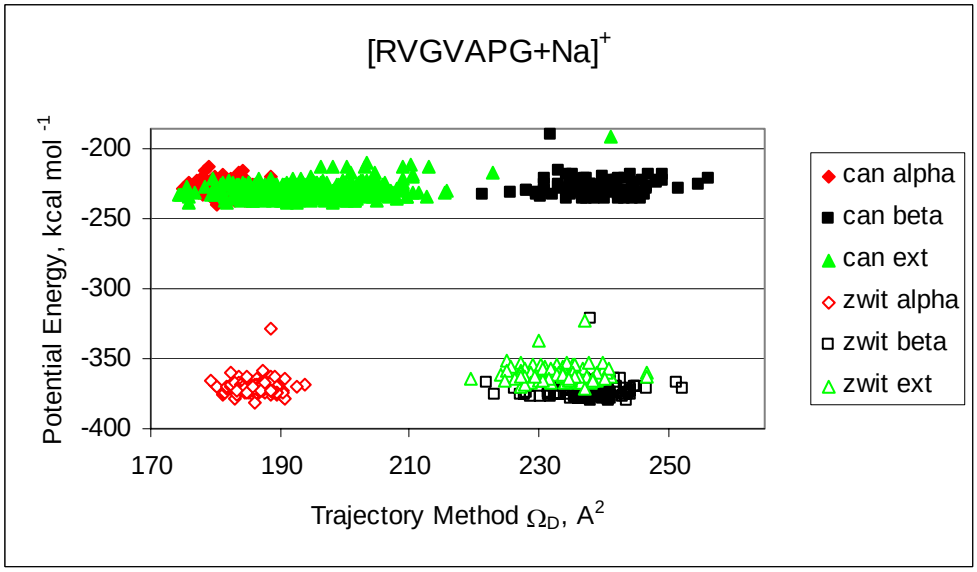
[RVGVAPG+Na]+
Potential Energy, kcal mol -1
-200
-250
-300
-350
-400
170
190
210
230
250
Trajectory Method ΩD, A2
can alpha
can beta
can ext
zwit alpha
zwit beta
zwit ext

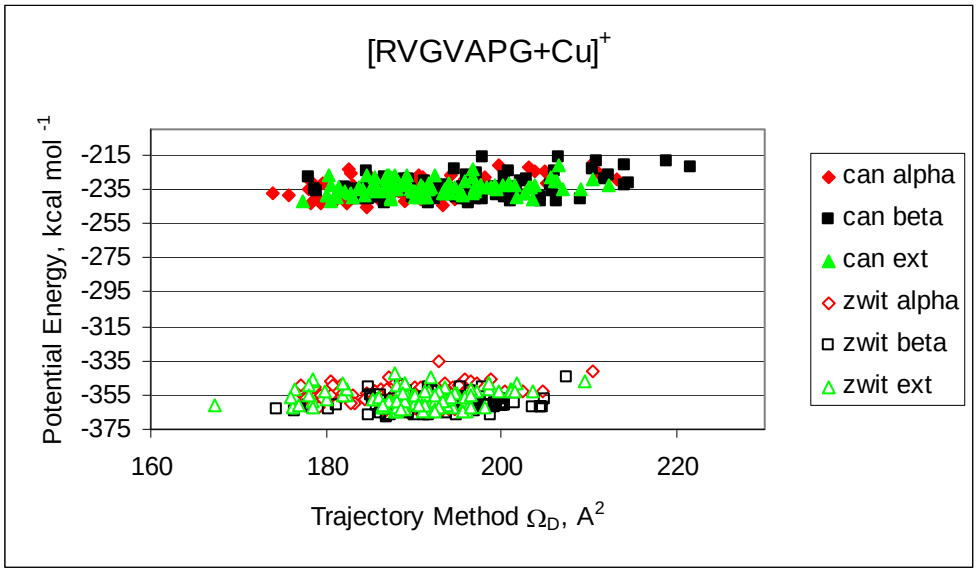
[RVGVAPG+Cu]+
Potential Energy, kcal mol -1
-215
-235
-255
-275
-295
-315
-335
-355
-375
160
180
200
220
Trajectory Method ΩD, A2
can alpha
can beta
can ext
zwit alpha
zwit beta
zwit ext

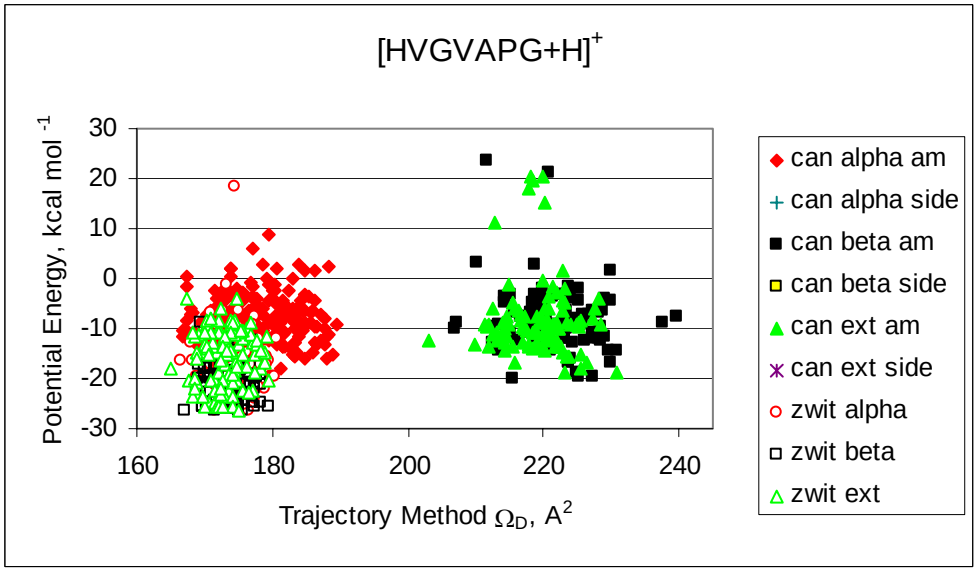
[HVGVAPG+H]+
Potential Energy, kcal mol -1
30
20
10
0
-10
-20
-30
160
180
200
220
240
Trajectory Method ΩD, A2
can alpha am
can alpha side
can beta am
can beta side
can ext am
can ext side
zwit alpha
zwit beta
zwit ext

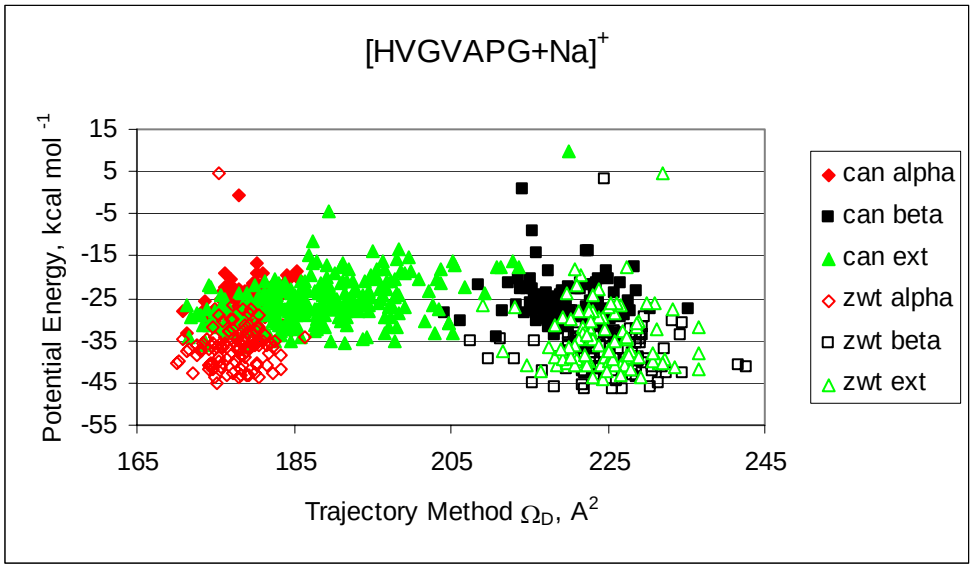
[HVGVAPG+Na]+
Potential Energy, kcal mol -1
15
5
-5
-15
-25
-35
-45
-55
165
185
205
225
245
Trajectory Method ΩD, A2
can alpha
can beta
can ext
zwt alpha
zwt beta
zwt ext

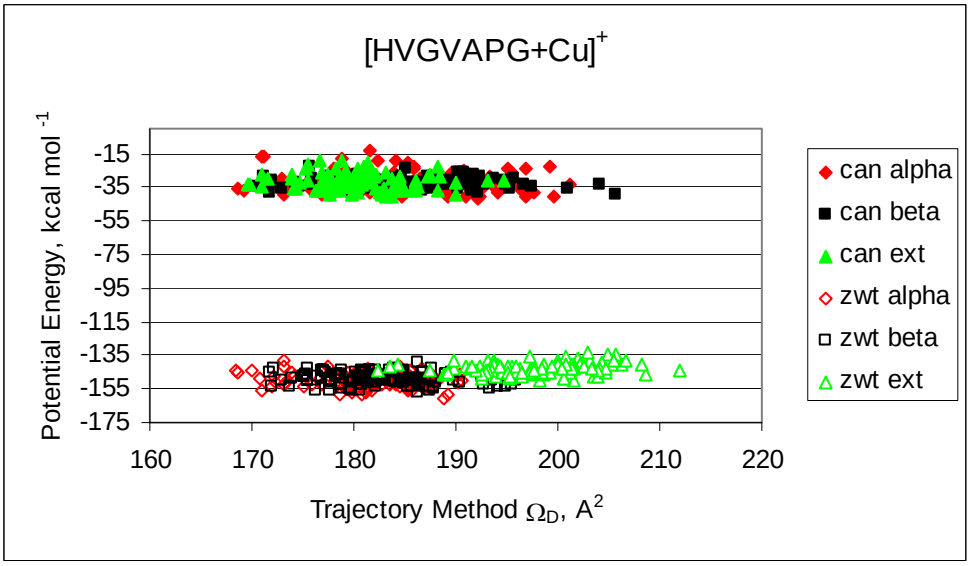
[HVGVAPG+Cu]+
Potential Energy, kcal mol -1
-15
-35
-55
-75
-95
-115
-135
-155
-175
160
170
180
190
200
210
220
Trajectory Method ΩD, A2
can alpha
can beta
can ext
zwt alpha
zwt beta
zwt ext

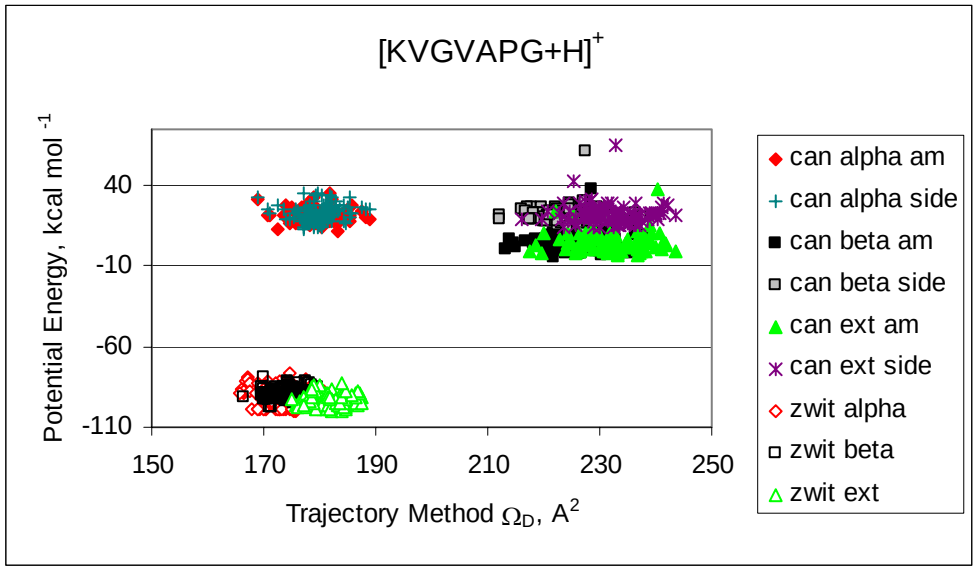
[KVGVAPG+H]+
Potential Energy, kcal mol -1
40
-10
-60
-110
150
170
190
210
230
250
Trajectory Method ΩD, A2
can alpha am
can alpha side
can beta am
can beta side
can ext am
can ext side
zwit alpha
zwit beta
zwit ext

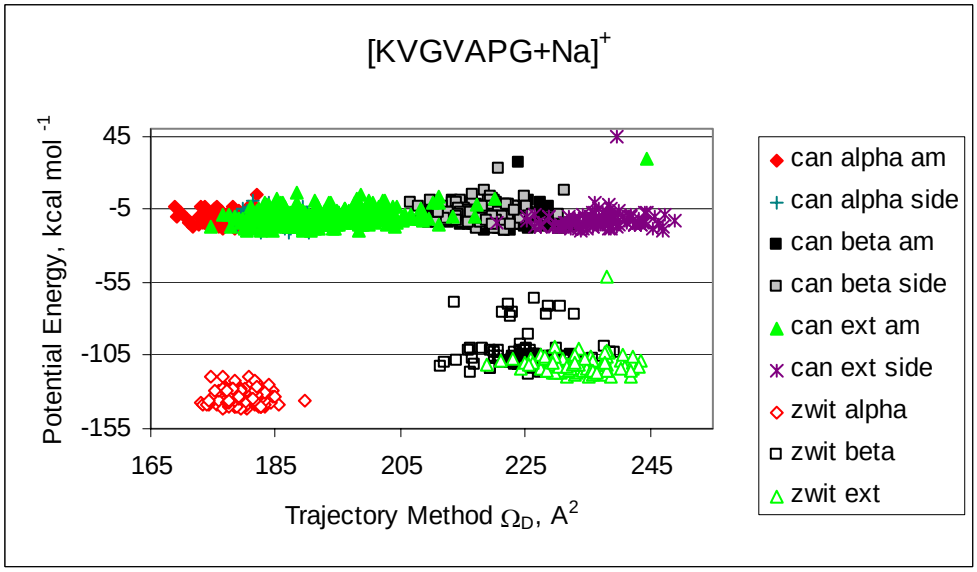
[KVGVAPG+Na]+
Potential Energy, kcal mol -1
45
-5
-55
-105
-155
165
185
205
225
245
Trajectory Method ΩD, A2
can alpha am
can alpha side
can beta am
can beta side
can ext am
can ext side
zwit alpha
zwit beta
zwit ext

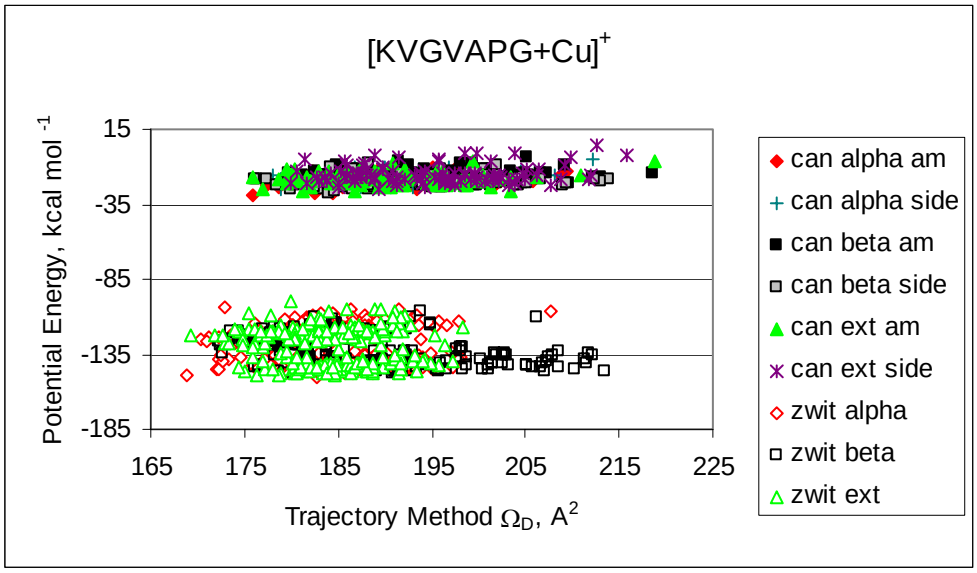
[KVGVAPG+Cu]+
Potential Energy, kcal mol -1
15
-35
-85
-135
-185
165
175
185
195
205
215
225
Trajectory Method ΩD, A2
can alpha am
can alpha side
can beta am
can beta side
can ext am
can ext side
zwit alpha
zwit beta
zwit ext

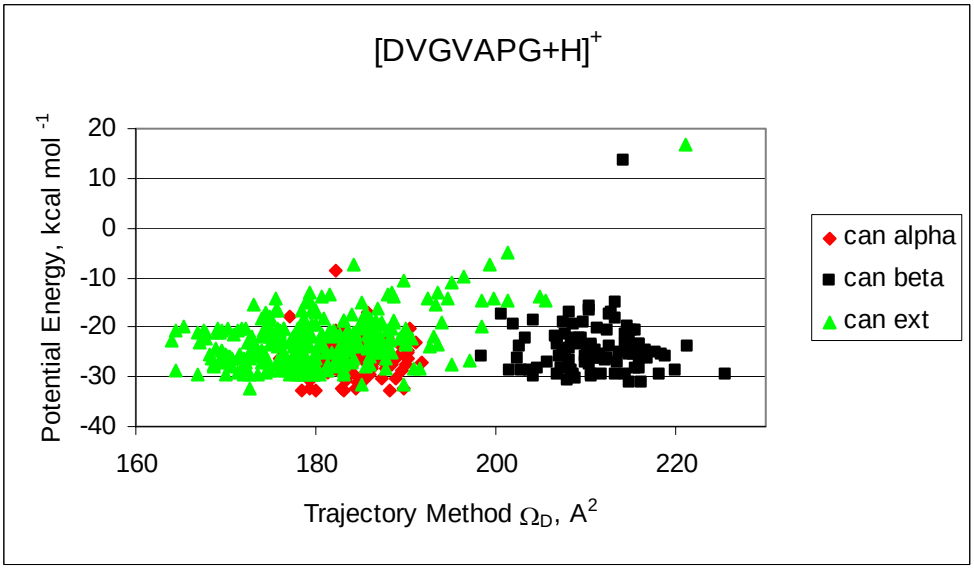
[DVGVAPG+H]+
Potential Energy, kcal mol -1
20
10
0
-10
-20
-30
-40
160
180
200
220
Trajectory Method ΩD, A2
can alpha
can beta
can ext

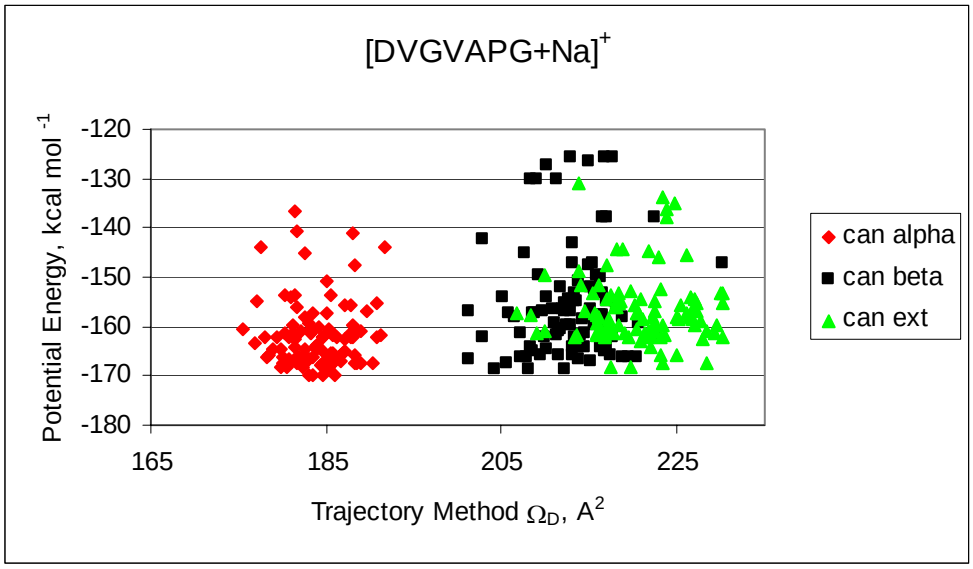
[DVGVAPG+Na]+
Potential Energy, kcal mol -1
-120
-130
-140
-150
-160
-170
-180
165
185
205
225
Trajectory Method ΩD, A2
can alpha
can beta
can ext

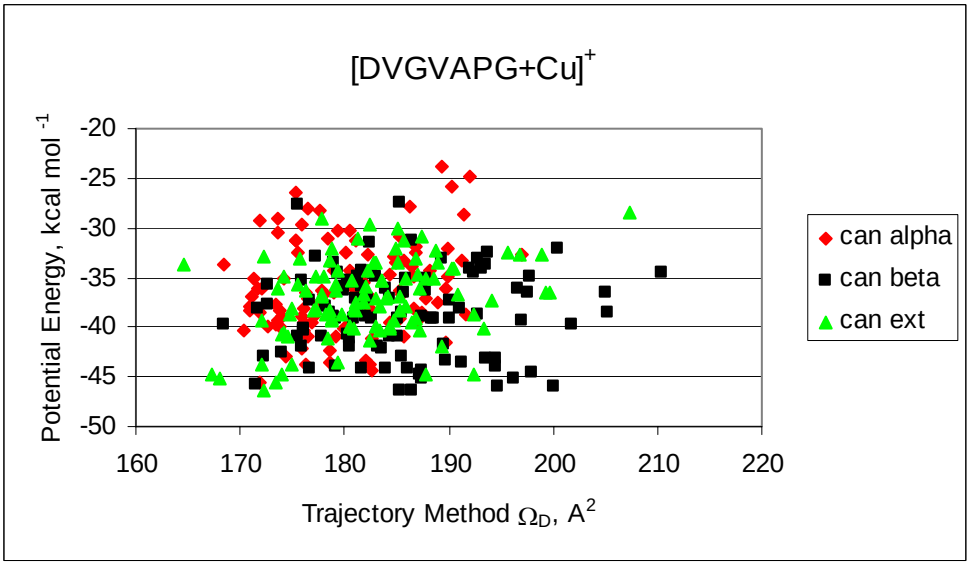
[DVGVAPG+Cu]+
Potential Energy, kcal mol -1
-20
-25
-30
-35
-40
-45
-50
160
170
180
190
200
210
220
Trajectory Method ΩD, A2
can alpha
can beta
can ext

# VITA

James Garrett Slaton received his Bachelor of Science Degree in chemistry from Truman State University in Kirksville, MO, in 1998. He entered the Chemistry program at Texas A&M University in September, 1999. His research interests include tandem mass spectrometry of peptides, ion mobility spectrometry, and photodissociation.

Dr. Slaton may be reached by email at garrett.slaton@gmail.com.